

Structures, charge distributions, and dynamical properties of weakly bound complexes of aromatic molecules in their ground and electronically excited states.

by

Cheolhwa Kang

B.S., Korea University, 1991

M.S., Korea University, 1993

Submitted to the Graduate Faculty of

Arts and Science in partial fulfillment

of the requirements for the degree of

Doctor of Philosophy

University of Pittsburgh

2005

UNIVERSITY OF PITTSBURGH
FACULTY OF ARTS AND SCIENCES

This dissertation was presented

by

Cheolhwa Kang

It was defended on

25th March 2005

and approved by

Kenneth Jordan, Professor, Department of Chemistry

Hrvoje Petek, Professor, Department of Physics and Astronomy

Sunil Saxena, Assistant Professor, Department of Chemistry

Dissertation Director: David W. Pratt, Professor, Department of Chemistry

Dedicated to My Parents
Kyung-Joong Kang, Kyung-Ok Jung
And Parents-in-Law
Deok-Hee Nam, Sang-Geum Lee

And
My Wife Sung-Hwa Nam,
Son Jeff DongHyun Kang

Copy right by Cheolhwa Kang

2005

Structures, charge distributions, and dynamical properties of weakly bound complexes of aromatic molecules in their ground and electronically excited states.

Cheolhwa Kang, Ph. D.

University of Pittsburgh, 2005

Abstract.

Complexes or clusters are non-covalently bound assemblies of two or more molecules that are held together by hydrogen bonding, van der Waals interactions, and other weak forces. The derived values of the rotational constants can be used to determine the structures of such species, in both their ground and electronically excited states. Some species exhibit different structures in the two states, owing to photon-induced changes in their electronic distributions. Evidence for the motion of one species relative to another along some intermolecular coordinate also is observed in some cases. We describe the application of these techniques to nitrogen and water complexes of *p*-difluorobenzene and Ar and water complexes of indole and azaindole, as models of hydrophobic and hydrophilic interactions. These studies have provided detailed information about how the electronic charge distributions of the species interact, how the structures of the individual species are modified when they interact, and how the properties of the complex are different from its component parts.

TABLE OF CONTENTS

PREFACE.....	x
1. Introduction.....	1
1.1. References.....	4
2. High resolution electronic spectrum of the N ₂ van der Waals complex of <i>p</i> -difluorobenzene. Structure and internal motion.....	5
2.1. Abstract.....	5
2.2. Introduction.....	6
2.3. Experimental.....	7
2.4. Results.....	8
2.4.1. Geometry of the complex.....	10
2.4.2. Barriers to internal rotation.....	20
2.5. Discussion.....	22
2.6. Acknowledgments.....	27
2.7. References.....	28
3. High resolution electronic spectrum of the <i>p</i> -difluorobenzene-water complex: Structure and internal rotation dynamics.....	31
3.1. Abstract.....	31
3.2. Introduction.....	32
3.3. Experimental.....	34
3.4. Results.....	34
3.5. Discussion.....	38
3.5.1. Structure of <i>p</i> DFB and its water complex.....	38
3.5.2. Nuclear spin statistical weights.....	43
3.5.3. Analysis of internal motion.....	45
3.6. Summary.....	51
3.7. Acknowledgements.....	51
3.8. References.....	52
4. High resolution electronic spectra of 7-azaindole and its Ar van der Waals complex.....	55
4.1. Abstract.....	55
4.2. Introduction.....	56
4.3. Experimental.....	57
4.4. Results.....	58
4.5. Discussion.....	64
4.5.1. Nature of the <i>S</i> ₁ electronic state of 7-azaindole.....	64
4.5.2. Structure of 7-azaindole- Ar.....	72
4.6. Summary.....	79
4.7. Acknowledgments.....	80
4.8. References.....	81
5. Experimental measurement of the induced dipole moment of an isolated molecule in its ground and electronically excited states. Indole and indole-H ₂ O.....	83
5.1. Abstract.....	83

5.2.	Introduction.....	84
5.3.	Experimental	87
5.4.	Results and Interpretation.....	88
5.4.1.	Indole.....	88
5.4.2.	Indole-water.....	93
5.5.	Discussion.....	99
5.5.1.	Indole.....	99
5.5.2.	Indole-water.....	101
5.6.	Summary.....	109
5.7.	Acknowledgements.....	111
5.8.	References.....	112
	APPENDIX A.....	116
	BIBLIOGRAPHY.....	185

LIST OF TABLES

Table 1. Rotational constants of <i>p</i> -difluorobenzene and <i>p</i> -difluorobenzene-nitrogen in their S_0 and S_1 electronic states. ^a	12
Table 2. Moments of inertia <i>I</i> and planar moments of inertia <i>P</i> of <i>para</i> -difluorobenzene (<i>p</i> DFB) and its nitrogen complex, and differences between the moments of inertia of the complex and the monomer. ^a	14
Table 3. Mean square displacements of the nitrogen molecule in the center-of-mass (COM) coordinate system of <i>p</i> DFB-N ₂ in its S_0 and S_1 electronic states. ^a	17
Table 4. Quadrupole moments of <i>p</i> -difluorobenzene in its S_0 and S_1 electronic states, according to theory (MP2/CIS 6-31G**).	26
Table 5. Inertial parameters of <i>p</i> DFB and its water complex in the zero-point vibrational levels of their S_0 and S_1 electronic states.	40
Table 6. COM coordinates of the water molecule in the principal axis frames of the bare <i>p</i> DFB molecule and of the <i>p</i> DFB-H ₂ O complex.	42
Table 7. Character table of the molecular symmetry group G_8 of <i>p</i> -difluorobenzene-water	44
Table 8. Inertial parameters of 7-azaindole and indole in its ground and excited electronic states.	69
Table 9. Inertial parameters of 7-azaindole in its ground and excited electronic states	71
Table 10. Inertial parameters of 7-azaindole and its Ar complex in the zero-point vibrational levels of their S_0 and S_1 electronic states.	74
Table 11. Comparison of center-of-mass (COM) coordinates of the Ar atom in the principal axis frame of 7-azaindole in 7-azaindole-Ar, and of indole in the indole-Ar complex, as determined from a Kraitchman analysis.	76
Table 12. Experimental and theoretical rotational constants and electric dipole moments of indole in its ground S_0 and excited S_1 electronic states.	95
Table 13. Experimental and theoretical rotational constants and electric dipole moments of indole-H ₂ O in its ground S_0 and excited S_1 electronic states.	98
Table 14. Electrostatic properties of water and indole in its S_0 and S_1 states.	107
Table 15. Observed and calculated dipole moments (in Debye) of indole and indole-H ₂ O in their S_0 and S_1 electronic states.	108

LIST OF FIGURES

- Figure 1. Rotationally resolved fluorescence excitation spectrum of the 0_0^0 band of the $S_1 \leftarrow S_0$ transition of *para*-difluorobenzene-nitrogen (*p*DFB- N_2). Below the experimental spectrum (top), the simulated spectrum of the stronger sub-band (bottom) and a simulation using the semirigid internal rotation model (middle trace) are shown. 9
- Figure 2. Portion of the fluorescence excitation spectrum of *p*DFB- N_2 near the origin of the weaker sub-band. Below the experimental spectrum (top), the simulated spectrum of the stronger sub-band (bottom) and a simulation using the semirigid internal rotation model (middle trace) are shown. Only the Q branch with $K_c' = K_c'' = J$ marked in the spectrum is well reproduced by the calculation. 11
- Figure 3. Geometry of the *p*DFB- N_2 complex. The position of the center of mass of N_2 is defined in the inertial coordinates (a , b , c) of the complex; the orientation of N_2 is defined by ρ (angle between the molecular axis of N_2 and the b axis) and τ (angle of rotation of N_2 around the b axis). 16
- Figure 4. Electron density difference map for the $S_1 \leftarrow S_0$ transition of *p*DFB. Red (dark) contours indicate regions of electron gain, and green (light) contours indicate regions of electron loss. 25
- Figure 5. Rotationally resolved fluorescence excitation spectrum of the origin band of the $S_1 \leftarrow S_0$ transition of *p*DFB- H_2O , shifted 168.1 cm^{-1} to the blue of the $S_1 \leftarrow S_0$ origin band of *p*DFB. The origin band of the complex is a superposition of two subbands which are separated by 0.121 cm^{-1} . The top trace is the experimental spectrum. The second and third traces are the calculated B and A subbands, respectively. 36
- Figure 6. Approximate structure of the doubly hydrogen-bonded complex of *p*-difluorobenzene with a single water molecule. a and b denote its in-plane inertial axes. 37
- Figure 7. Portion of the high resolution spectrum of *p*DFB- H_2O at full experimental resolution, extracted from the R branch of the stronger subband. The top trace is the experimental spectrum. The second and third traces show the separate calculated contributions of the two subbands in this region. 39
- Figure 8. Combined inversion and restricted internal rotation of the water molecule in *p*DFB- H_2O 49
- Figure 9. Light-induced changes in the electron distribution of *p*DFB are responsible for the differences in the intermolecular potentials of *p*DFB- H_2O in its ground and electronically excited states. 50
- Figure 10. Rotationally resolved fluorescence excitation spectrum of the origin band of 7-azaindole. The top trace shows the overall experimental spectrum. The bottom traces show a $\sim 0.2 \text{ cm}^{-1}$ portion of the R branch at full experimental resolution and two simulated spectra, with and without a superimposed lineshape function. 60
- Figure 11. Two possible orientations of the $S_1 \leftarrow S_0$ electronic transition moment (TM) vector in 7-azaindole. Only $\theta = -14.2^\circ$ is consistent with the results of the isotopomer experiments. 61
- Figure 12. Rotationally resolved fluorescence excitation spectra of the origin bands of three different isotopomers of 7-azaindole. The top trace shows the overall experimental

spectrum. The bottom traces show a $\sim 0.2 \text{ cm}^{-1}$ portion of the top trace at full experimental resolution and the contributions to this portion from the three different isotopomers.	62
Figure 13. Rotationally resolved fluorescence excitation spectrum of the $+ 280 \text{ cm}^{-1}$ vibronic band of 7AI. The top trace shows the overall experimental spectrum, an <i>ab</i> -hybrid band. The bottom traces show “stick” spectra of the <i>a</i> - and <i>b</i> -type contributions to the observed spectrum.....	65
Figure 14. Rotationally resolved fluorescence excitation spectrum of the 7-azaindole-Ar complex. The top trace shows the overall experimental spectrum. The bottom traces show a $\sim 0.1 \text{ cm}^{-1}$ portion of the experimental spectrum and two simulations, with and without a superimposed lineshape function. The individual <i>a</i> -, <i>b</i> -, and <i>c</i> -type contributions are also shown.....	66
Figure 15. Three-dimensional structures of 7AI and the 7AI-Ar complex, showing the inertial axis reorientation on complex formation.....	67
Figure 16. Potential profile of the intermolecular PES in the S_0 state of indole-Ar along the minimum energy path.....	77
Figure 17. Potential profile of the intermolecular PES in its S_0 state of azaindole-Ar along the minimum energy path.....	78
Figure 18. Rotationally resolved fluorescence excitation spectra near 284 nm of the origin bands in the $S_1 \leftarrow S_0$ transitions of (a) bare indole at 35231 cm^{-1} and (b) the indole-water complex at 35099.5 cm^{-1} . A and B indicate the origins of the $A' \leftarrow A''$ and $B' \leftarrow B''$ subtorsional bands, respectively, in the complex spectrum.....	89
Figure 19. The Stark effect in indole. Portion of the rotationally resolved spectrum of indole extracted from near the band origin (see Fig.18) showing the large perturbations in the spectrum due to an applied electric field.....	91
Figure 20. Illustration of indole showing its in-plane inertial axes and the orientations of its permanent electric dipole moments in the two electronic states.....	94
Figure 21. The Stark effect in indole- H_2O . Portion of the rotationally resolved spectrum of indole- H_2O extracted from near the origin (see Fig.18) of the $B' \leftarrow B''$ subtorsional band showing the influence of the applied electric field.....	97
Figure 22. Electron density difference map for the $S_1 \leftarrow S_0$ transition of indole. Dark contours indicate regions of electron gain, and light contours indicate regions of electron loss.....	102
Figure 23. Illustration of indole-water showing its in-plane inertial axes and the orientations of its permanent electric dipole moments in the two electronic states.....	104
Figure 24. Vector diagram showing the total dipole moments of indole-water in both electronic states and their component parts.....	110

PREFACE

Professor David W. Pratt has taught me a lot of chemistry and about getting experiments to work. Working for him has been a challenge - I could never keep up with the constant supply of new ideas for analyzing our results. Dr. Pratt led by example of his hard work, creativity, persistence and drive would be difficult to match. Whenever I was in trouble, he showed me patience and never made me hurry up in my research. Under such wonderful circumstances, I could have enough time in solving the problems and come true my imagination into a good result. I was really lucky to get the chance of working with him.

My colleagues in the Pratt group are also extremely talented, and it has been a privilege to work with them. I hope that they achieve the success in later life that they all deserve. I am grateful to Tri Nguyen for his ability to explain difficult concepts and his amazing good humor. John Yi deserves many thanks for his help with experiments; unequalled mechanical ability. Since 1998, Dr. Ribblett, Dr. Borst, Dr. Korter, Dr. Schaefer, Alexei Nikolaev, Rob Roscioli, Jennifer Reese, Seung-Hoon Hong, Leonardo Alvarez, Diane Mitchell, Philip Morgan, and Jessica Thomas have all helped my experimental and theoretical work and the writing of my thesis, and I thank them.

I owe thanks to several professors for their help: Professors Eric Borguet, Sanford Asher, Ken Jordan, Dave Waldeck, Gilbert Walker, Sunil Saxena, and Hrvoje Petek at Pittsburgh, Jon Hougren at NIST, and Keon Kim at Seoul, Korea.

None of experiments would have been possible without the skill and dedication of the machine and electronic shop staff at Pittsburgh. I am grateful to all of them, and especially to Jeff Sicher, Jim Mcnerney and Bob Muha. Many other staff members in the department went beyond the call of duty to help us, and they deserve thanks.

My family deserves special thanks. My parents and parents-in-law showed me how much could be accomplished through hard work, and those lessons have been very important. And my brothers, sister, brothers-in-law, and sisters-in-law have helped probably more than they know, by phoning and writing and being their wonderful selves.

Although it was a nice experience at chevron, I was not a good husband and dad. My wife, Sung-Hwa Nam, was always patient and has provided encouragement, support, love, and

help when I needed them. I have great debt to her. It is not possible to thank her enough. My son, Dong-Hyun, is the reason of my existence. Without their love and smile, my life could not be the proper one.

Most of all, my parents, through the whole my life, always give me endless support and encouragement. Definitely it will not be possible for me to compensate for a bit of their love. Still I can not imagine my life without them. They are something beyond expression. I devote all my work here, although small and unnoticeable, to them. God bless whole my family.

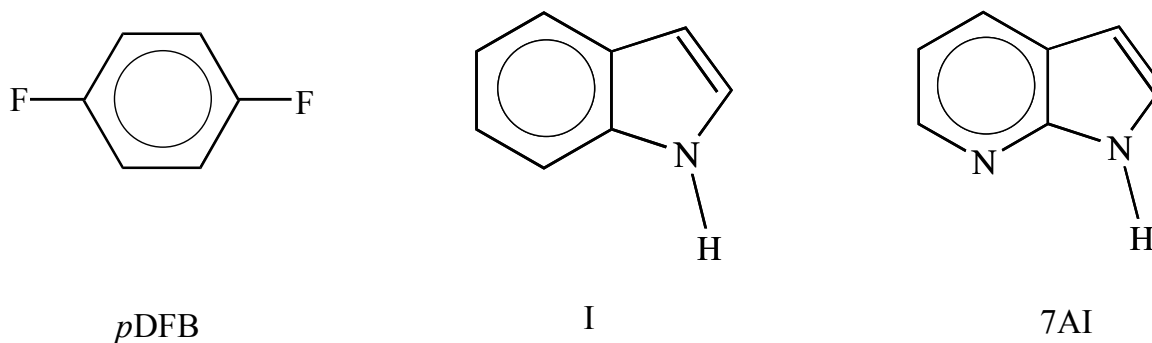
1. Introduction.

Advances in science are often driven by advances in instrumentation. Our developing understanding of the forces between molecules is no exception. The pioneering work in this field was done by Levy and co-workers [1], who demonstrated that the use of supersonic jets to simplify the electronic spectra of large molecules led to the “adventitious” formation of a wide variety of complexes held together by weak van der Waals forces and somewhat stronger hydrogen bonds. Performing these experiments with vibrational and rotational resolution, and at other frequencies (*e.g.*, IR and microwave), gave exciting new information about the equilibrium geometries and dynamical properties of many new molecules whose existence in nature was demonstrated for the first time. Water aggregates like $(\text{H}_2\text{O})_2$, $(\text{H}_2\text{O})_3$, \dots $(\text{H}_2\text{O})_n$ come to mind, but there are many other beautiful examples [2-5]. This information, in turn, has fueled the development of powerful new theoretical tools for calculating intermolecular potentials [6]. Predictions based on these calculations are likely to stimulate many further experiments, thereby “completing” the scientific cycle of experiment, theory, and hypothesis in this new field.

Understanding the factors that contribute to the potential energy of interaction between two or more species is an important research objective. All encounters between atoms and molecules, whether reactive or nonreactive, are (at least in the beginning) governed by such potentials. Of particular interest are the changes in the potentials that occur where two species approach each other, and how these changes depend upon angular coordinates. The “induced fit” that characterizes the behavior of many enzyme-substrate complexes in biology is a particular example. Beyond such molecular assemblies, properties of collections of molecules in liquids,

solutions, and solids also depend on their interactions at long range, and how the interaction between two species is affected by the presence of others (*i.e.*, many-body effects).

Described here are the results of recent high resolution electronic spectroscopy experiments on several weakly bound complexes of organic molecules. The substrates include *p*-difluorobenzene (*p*DFB), indole (I), and 7-azaindole (7AI), see below:



The complexing “agents” include argon (Ar), nitrogen (N₂), and water (H₂O). We thus explore the properties of atomic, diatomic, and triatomic complexes of increasingly complex host molecules. Our experiments are rotationally resolved. Hence, we determine the equilibrium geometries of each complex in its electronic ground state. A particular focus is on how these geometries change when the substrate to which the atom or molecule is attached became more asymmetric. Similar information is obtained about the electronically excited state. In many cases, the geometry of the excited state is different from that of the ground state, owing to changes in the electron distribution of the substrate when it absorbs light. Van der Waals “bonding” is entirely the result of electron correlation; such correlation, in turn, is significantly enhanced in excited states, compared to ground state.

The second focus of this thesis is on the permanent electric dipole moments of these complexes in their ground and electronically excited states. These have been measured for the first time using a newly developed Stark cell in our high resolution apparatus, by means of which homogeneous electric fields may be applied to the sample. Two such studies will be described here, on 7AI-Ar and $\text{I-H}_2\text{O}$. These studies give quantitative information about the changes in the charge distribution that are produced when a molecule absorbs light, thereby accounting for differences in the structures of the different complexes in their ground and electronically excited states. In the case of $\text{I-H}_2\text{O}$, the Stark measurements also give information about induced dipole moments; *i.e.*, the changes in the charge distributions of a substrate molecule that are produced when the complex is formed, a precursor to induced fits.

The third and final focus of this thesis is on the dynamical properties of weakly bound complexes in their ground and electronically excited states. The relatively weak interactions between closed shell molecules that are the hallmarks of such species gives rise to intermolecular bonds that are not rigid. As a result, Ar , N_2 , and H_2O all undergo large amplitude motions when they are attached to $p\text{DFB}$, I , or 7AI . Additionally, in the case of N_2 or H_2O , the attached molecule undergoes other internal motions such as hindered rotation and inversion. Surprisingly, the observed high resolution spectra are extraordinary sensitive to these dynamics. Thus, properly interpreted, one can derive “complete” intermolecular potentials in both ground and electronically excited state from such data.

1.1. References.

- [1] D. H. Levy, NATO Advanced Study Institutes Series, Series B: Physics B57 (Quantum Dyn. Mol.), 115-42 (1980).
- [2] C.-J. Tsai and K. D. Jordan, Chem. Phys. Lett. **213**, 181 (1993).
- [3] J. G. Gregory and D. C. Clary, J. Chem. Phys. **105**, 6626 (1996).
- [4] J. B. Paul, R. A. Provencal, C. Chapo, A. Petterson, and R. J. Saykally, J. Chem. Phys. **109**, 10201 (1998).
- [5] R. S. Fellers, L. B. Braly, R. J. Saykally, and C. Leforestier, J. Chem. Phys. **110**, 6306 (1999).
- [6] J. M. Hutson, A. Ernesti, M. M. Law, C. F. Roche, and R. J. Wheatley, J. Chem. Phys. **105**, 9130 (1996).

2. High resolution electronic spectrum of the N₂ van der Waals complex of *p*-difluorobenzene. Structure and internal motion.

Martin Schäfer

Laboratorium für Physikalische Chemie, Eidgenössische Technische Hochschule Zürich,
CH-8093 Zürich, Switzerland

Cheolhwa Kang and David W. Pratt

Department of Chemistry, University of Pittsburgh,
Pittsburgh, Pennsylvania 15260, USA

2.1. Abstract.

Rotationally resolved fluorescence excitation spectra of the N₂ van der Waals complex of *p*-difluorobenzene (*p*-DFB-N₂) have been recorded in the collision-free environment of a molecular beam. The data obtained provide information about the structure and internal motion of *p*DFB-N₂ in its ground (S₀) and excited (S₁) electronic states. In the ground state, the N₂ molecule sits at R ~ 3.5 Å above the ring plane, is parallel to the short axis of the ring, and undergoes hindered internal rotation about the axis perpendicular to the ring with an apparent two-fold barrier of ~ 10 cm⁻¹. Excitation to the S₁ state decreases R by ~ 0.1 Å and reduces the barrier to ~ 2 cm⁻¹. The N₂ molecule appears to have no preferred orientation in the S₁ state. The S₁ - S₀ transition moment orientation in *p*DFB is unaffected by complex formation.

Published in the *J. Phys. Chem. A*, **107**, 10753 (2003)

2.2. Introduction.

Weakly bound van der Waals (vdW) complexes between aromatic molecules and rare gases or small molecules have been the focus of much recent attention, for many reasons. One reason is that such complexes are unique chemical species, with their large vdW bond distances of 3-5 Å, their low bond energies of only a few hundred wavenumbers, and their large amplitude, low frequency vibrational motions. Another reason is that the properties of such species reveal information about solvent-solute interactions in cases where dispersion forces are dominant. And another reason is that the dynamic process of vibrational predissociation (VP) of vdW complexes also provides a testing ground for theories of collision dynamics, intramolecular vibrational redistribution (IVR), and dissociation dynamics. All are fundamental to chemical reactivity.

We focus in this report on one such species, the vdW complex of N₂ and *p*-difluorobenzene (*p*DFB-N₂). Our attention was drawn to this complex when it was reported, based on a study of the rotational contour of the 6₀¹ band in its S₁-S₀ electronic spectrum, that the electronic transition moment (TM) was rotated by about 30° towards the F-F axis, from its position normal to that axis in the bare molecule [1]. Conformationally-induced changes in the orientation of an electronic TM have been observed, especially in substituted benzenes [2]. But such a large, *complex*-induced change in the orientation of an electronic TM would be unprecedented.

Molecular nitrogen complexes of several aromatic molecules have been studied before, including benzene-N₂ [3-5], *p*DFB-N₂ [6-8], *m*DFB-N₂ [8], *o*DFB-N₂ [8], C₆H₅X-N₂ (X=F, Cl, Br) [9], phenol-N₂ [10], aniline-N₂ [11, 12], benzyl-N₂ [13], and cyclopentadienyl-N₂ [14]. These studies focused on structures, on vdW modes, and on the barriers to internal rotation of N₂

in different symmetry environments. N_2 forms an in-plane, hydrogen bonded complex with phenol [10], but π hydrogen bonded complexes with the remaining molecules. Evidence for a nearly free internal rotation of the attached N_2 has been provided in most cases.

Here, we present a study of the fully resolved S_1 - S_0 electronic spectrum of p DFB- N_2 in the collision-free environment of a molecular beam. Two bands are observed in the vicinity of the electronic origin and assigned as the two lowest energy, symmetry-distinguishable transitions involving N_2 internal rotation. Analysis of these two bands provides information about the structures and internal motions of p DFB- N_2 in both electronic states. No complex-induced change in the TM orientation is observed. However, there is a significant change in the intermolecular potential energy surface when the photon is absorbed.

2.3. Experimental.

para-Difluorobenzene (p DFB) was purchased from Aldrich (99%) and used without further purification. Dry helium (99.9%) and nitrogen (99.9%) gas were used in all experiments. High resolution data were obtained using the CW molecular beam laser spectrometer described in detail elsewhere [15]. p DFB was heated to about 300 K, seeded in a mixture of 10-15% N_2 in He at a backing pressure of about 0.5 bar, expanded through a 280 μ m quartz nozzle, skimmed once, and probed 15 cm downstream of the nozzle by a frequency doubled, single-frequency, tunable ring dye laser operating with rhodamine 110, yielding about 200 μ W of ultraviolet radiation. Fluorescence was collected using spatially selective optics, detected by a photomultiplier tube and photon counting system, and processed by a computerized data acquisition system. Relative frequency calibrations of the spectra were performed using a near-confocal interferometer having a mode-matched FSR of 299.7520 ± 0.0005 MHz at the

fundamental frequency of the dye laser. Absolute frequencies in the spectra were determined by comparison to transition frequencies in the electronic absorption spectrum of I₂ [16].

2.4. Results.

Figure 1 shows the rotationally resolved S₁←S₀ fluorescence excitation spectrum of the N₂ van der Waals complex of *p*DFB. This spectrum differs from that of the bare molecule in three ways. First, the origin band is shifted by -26.6 cm⁻¹ with respect to that of the bare molecule. Second, the band types of the two spectra differ. Whereas the bare molecule exhibits a pure *b*-type spectrum, showing no central Q branch [17], the spectrum of *p*DFB-N₂ exhibits an obvious Q branch and follows *c*-type selection rules. Third, the origin band of the complex is split into two torsional sub-bands, separated by 0.71 cm⁻¹, with significantly different relative intensities. The electronic origin of the bare molecule consists of only a single strong band.

Fits of the stronger sub-band spectrum in Fig. 1 were initiated by constructing the rotational energy level diagrams of *p*DFB-N₂ in its S₀ and S₁ electronic states, applying the appropriate selection rules, and calculating the frequencies of the allowed rovibronic transitions, for comparison with experiment. The calculated rotational constants were obtained from an optimized geometric structure, based in part on *ab initio* calculations. Both states were initially assumed to be rigid, asymmetric tops. The simulated spectrum was then compared with the experimental spectrum and several transitions were assigned. These assignments were iteratively optimized by a least-squares analysis. This analysis, while satisfactory in some respects, gave a standard deviation of the fit that was unusually high (observed minus calculated (OMC) = 9.0 MHz). An inspection of this fit revealed that high J (J ≥ 10) transitions were shifted by as much as 100 MHz with respect to their calculated positions. Therefore, Watson's quartic distortion

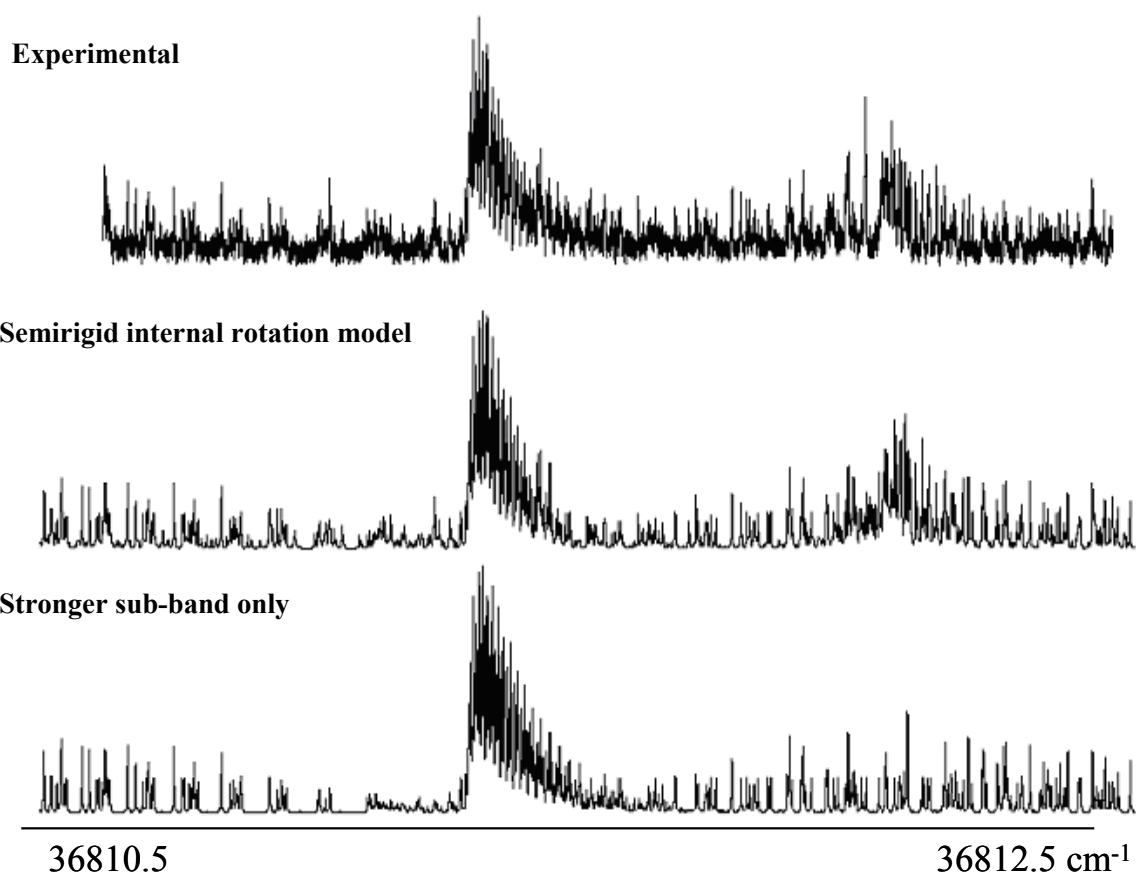


Figure 1. Rotationally resolved fluorescence excitation spectrum of the 0_0^0 band of the $S_1 \leftarrow S_0$ transition of *para*-difluorobenzene-nitrogen (*p*DFB-N₂). Below the experimental spectrum (top), the simulated spectrum of the stronger sub-band (bottom) and a simulation using the semirigid internal rotation model (middle trace) are shown.

terms [18] were added to the Hamiltonians of both electronic states. This modification led to an improved OMC of 4.4 MHz, when 200 lines were included in the fit. Unfortunately, the weaker sub-band in Fig. 1 could not be fit by either of these procedures, as shown in Fig. 2.

From the stronger sub-band fit, we determined the origin band frequency and the inertial constants of the two electronic states. These are listed in Table 1. The relative intensities of the transitions could be fit to a rotational temperature of about 5 K. The Lorentzian linewidth is about 15 MHz in the bare molecule and about 40 MHz in the complex. Thus, the weakly bound N₂ molecule reduces the fluorescence lifetime of *p*DFB from about 11 to 4 nsec. Incipient VP and/or IVR may be responsible for this behavior.

2.4.1. Geometry of the complex.

Information about the geometry of the complex can be obtained from its planar moments of inertia (P). These are related to the ordinary moments of inertia (I) by $P_a = (I_b + I_c - I_a)/2$, etc. Values of these for both *p*DFB and *p*DFB-N₂ are listed in Table 2.

In the bare molecule, the c inertial axis is perpendicular to the ring plane and the a inertial axis lies in the plane, passing through the fluorine atoms. Examining the data in Table 2, we see that P_a (*p*DFB-N₂) ($=P_a$) $\approx P_a$ (*p*DFB) ($=P_a^m$). This means that the orientation of the a axis in *p*DFB is unchanged on complexation. We also see that $P_c \approx P_b^m$. This means that the orientations of the b and c axes are exchanged when the N₂ is attached, thus explaining why the 0₀⁰ band of *p*DFB-N₂ is c -axis polarized. The S₁-S₀ transition moment of the complex still lies in the plane of *p*DFB, roughly perpendicular to a .

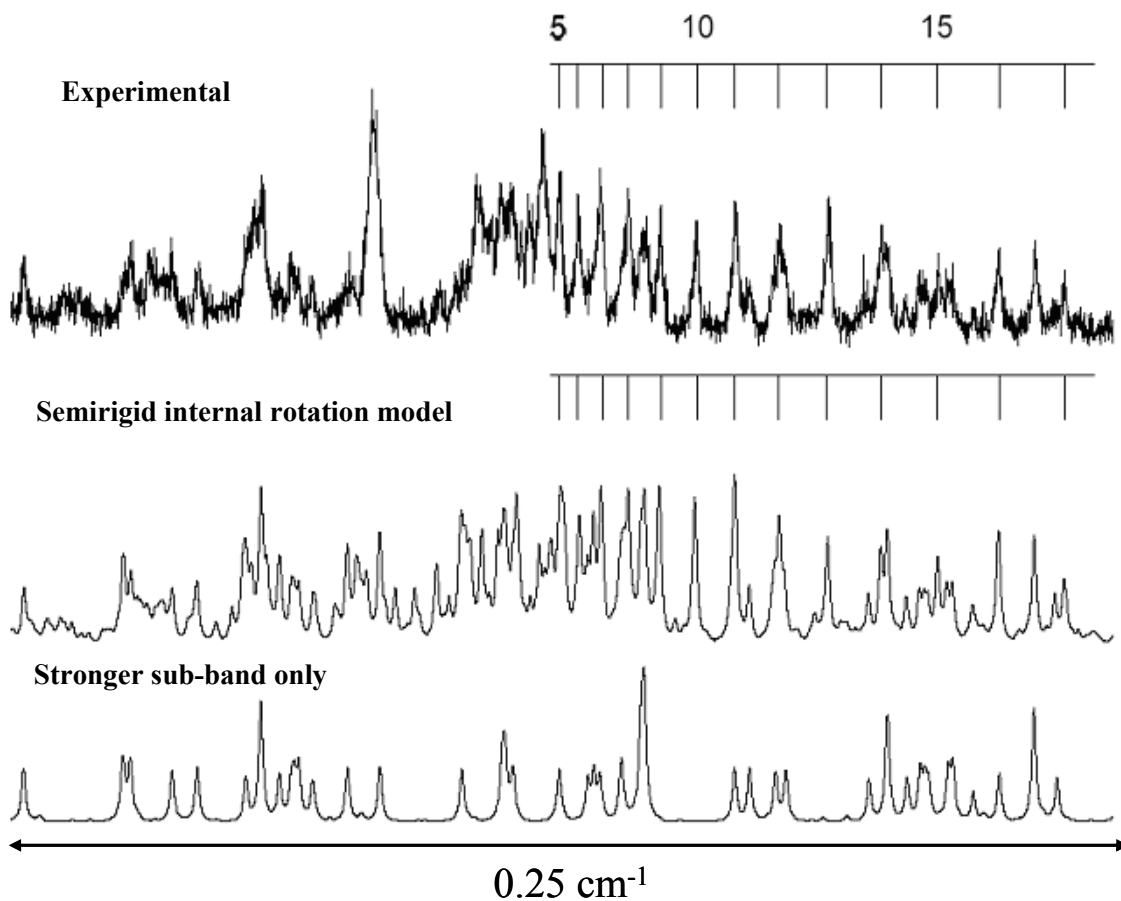


Figure 2. Portion of the fluorescence excitation spectrum of *p*DFB-N₂ near the origin of the weaker sub-band. Below the experimental spectrum (top), the simulated spectrum of the stronger sub-band (bottom) and a simulation using the semirigid internal rotation model (middle trace) are shown. Only the Q branch with $K_c' = K_c'' = J$ marked in the spectrum is well reproduced by the calculation.

Table 1. Rotational constants of *p*-difluorobenzene and *p*-difluorobenzene-nitrogen in their S₀ and S₁ electronic states.^a

Parameter	Ground State		Excited State	
	Monomer ^b	N ₂ Complex	Monomer	N ₂ Complex
<i>A</i> /MHz	5637.6(2)	1364.8(4)	5283.2(2)	1391.8(3)
<i>B</i> /MHz	1428.0(1)	1128.3(4)	1434.2(1)	1126.1(3)
<i>C</i> /MHz	1139.4(1)	803.9(2.5)	1128.5(1)	818.1(2.5)
Δ _K /MHz		0.034(48)		0.026(47)
Δ _{JK} /MHz		-0.062(71)		-0.052(70)
Δ _J /MHz		0.029(22)		0.029(22)
δ _K /MHz		0.056(35)		0.064(37)
δ _J /MHz		-0.019(11)		-0.019(12)
κ/MHz	-0.872	0.153	-0.853	0.072
N ^c (OMC/MHz ^d)	350(3.0)	167(4.4)		
ν ₀ /cm ⁻¹ ^e	36837.84	36811.25		

^a Uncertainties of the last digits are given in parentheses.

^b Our values, which compare favorably to literature values (17).

^c Number of single transitions included in the fit.

^d Standard deviation of the fit.

^e Origin frequencies. Precision 0.01 cm⁻¹.

Table 2 also lists values of the differences in the relevant planar moments of p DFB-N₂, from which more structural information can be obtained. Thus, among the differences $P_a - P_a^m$, $P_b - P_b^m$, and $P_c - P_b^m$, $P_b - P_c^m$ is by far the largest. A large $P_b - P_c^m$ ($P_c^m \approx 0$) requires that the N₂ molecule lies on top (or the bottom) of the benzene ring (in both electronic states). A complex configuration with the N₂ molecule lying in or near the plane of p DFB would require $P_b \approx 0$ and a - and/or b -type selection rules.

Of further interest are the values of $P_a - P_a^m$ and $P_c - P_b^m$. While small, neither of these planar moment differences is zero. This means that the N₂ molecule cannot be attached to p DFB “end-on”, perpendicular to the ac plane. Instead, the N₂ molecule must lie more or less in a plane parallel to the ac plane. The value of the moment of inertia of the N₂ molecule is $8.5 \text{ u } \text{Å}^2$ (19). Neither planar moment difference in p DFB-N₂ is as large as this, but $P_c - P_b^m = 5.1 \text{ u } \text{Å}^2$ and $P_a - P_a^m = -0.8 \text{ u } \text{Å}^2$ in the S₀ state. This suggests that the N≡N axis is roughly parallel to c in this state. $P_c - P_b^m$ is significantly smaller in the S₁ state, being approximately equal (in magnitude) to $P_a - P_a^m$. This suggests that the preferred orientation of the N≡N axis changes when the photon is absorbed.

A more rigorous treatment of this problem requires that the effects of large amplitude motion be taken into account. Two types of motion would seem to be important, “radial” motions and “angular” ones. Radial motions result in displacements of the N₂ molecule’s center of mass (COM) from its equilibrium position. Angular motions result in tilts of the N₂ molecule’s N≡N bond axis with respect to its equilibrium position. Both types of motion should be fast on the time scale of overall molecular rotation. Thus, the measured rotational constants are vibrationally averaged values over both kinds of coordinates.

Table 2. Moments of inertia I and planar moments of inertia P of *para*-difluorobenzene (*p*DFB) and its nitrogen complex, and differences between the moments of inertia of the complex and the monomer.^a

	Parameter	<i>p</i> DFB		<i>p</i> DFB-N ₂	
		I^m	P^m	I	P
Ground State	<i>a</i>	89.64(1)	353.91(2)	370.3(1)	353.1(10)
	<i>b</i>	353.91 (2)	89.64(2)	447.9(2)	275.5(10)
	<i>c</i>	443.55(4)	0.00(2)	628.7(20)	94.8(10)
	$a - a^m$			280.8(1)	-0.8(7)
	$b - c^m$			4.5(2)	275.5(11)
	$c - b^m$			274.7(20)	5.1(10)
Excited State	<i>a</i>	95.66(1)	352.28(2)	363.1(1)	351.7(10)
	<i>b</i>	352.38(2)	95.56(2)	448.8(1)	266.0(10)
	<i>c</i>	447.83(4)	0.10(2)	617.8(19)	97.1(10)
	$a - a^m$			267.5(1)	-0.6(10)
	$b - c^m$			1.0(1)	265.9(11)
	$c - b^m$			265.4(19)	1.5(10)

^a All values in uÅ². Uncertainties in the last digits are given in parentheses.

Previous studies of the dynamical properties of similar complexes in the gas phase [20] suggest that the intermolecular potential energy surface is relatively steep along the radial coordinate, and relatively flat along the angular ones. Therefore, radial motions are ignored in what follows. Angular motions are taken into account by defining the coordinates ρ and τ shown in Fig. 3. ρ is a “tilt” angle that describes the orientation of the N≡N axis in the ab plane ($\rho = 90^\circ$ in the parallel configuration), and τ is a “torsional” angle that describes the orientation of the N≡N axis in the ac plane ($\tau = 0^\circ$ when the N≡N axis is parallel to the a axis). Using these coordinates, a set of equations can be written that describe the relations between the moments and products of inertia of the complex $I_{\alpha\alpha'}$ ($\alpha, \alpha' = a, b, c$) and those of the bare molecule I_a^m . These are [21]

$$I_a = I_a^m + (\sin^2 \tau \sin^2 \rho + \cos^2 \rho) I_{N_2} + \mu(b^2 + c^2) \quad (1)$$

$$I_b = I_c^m + \sin^2 \rho I_{N_2} + \mu(a^2 + c^2) \quad (2)$$

$$I_c = I_b^m + (\cos^2 \tau \sin^2 \rho + \cos^2 \rho) I_{N_2} + \mu(a^2 + b^2) \quad (3)$$

$$I_{ab} = -\cos \tau \sin \rho \cos \rho I_{N_2} - \mu ab \quad (4)$$

$$I_{ac} = -\sin \tau \cos \tau \sin^2 \rho I_{N_2} - \mu ac \quad (5)$$

$$I_{bc} = -\sin \tau \sin \rho \cos \rho I_{N_2} - \mu bc \quad (6)$$

Here, $\mu = m_{N_2} m_{\text{DFB}} / (m_{N_2} + m_{\text{DFB}}) = 22.4839$ u is the reduced mass of the complex, and a , b , and c are the COM coordinates of the attached N_2 molecule in the complex coordinate system. The potential $V(\tau)$ should be two-fold symmetric, given the likely electronic distribution of p DFB in

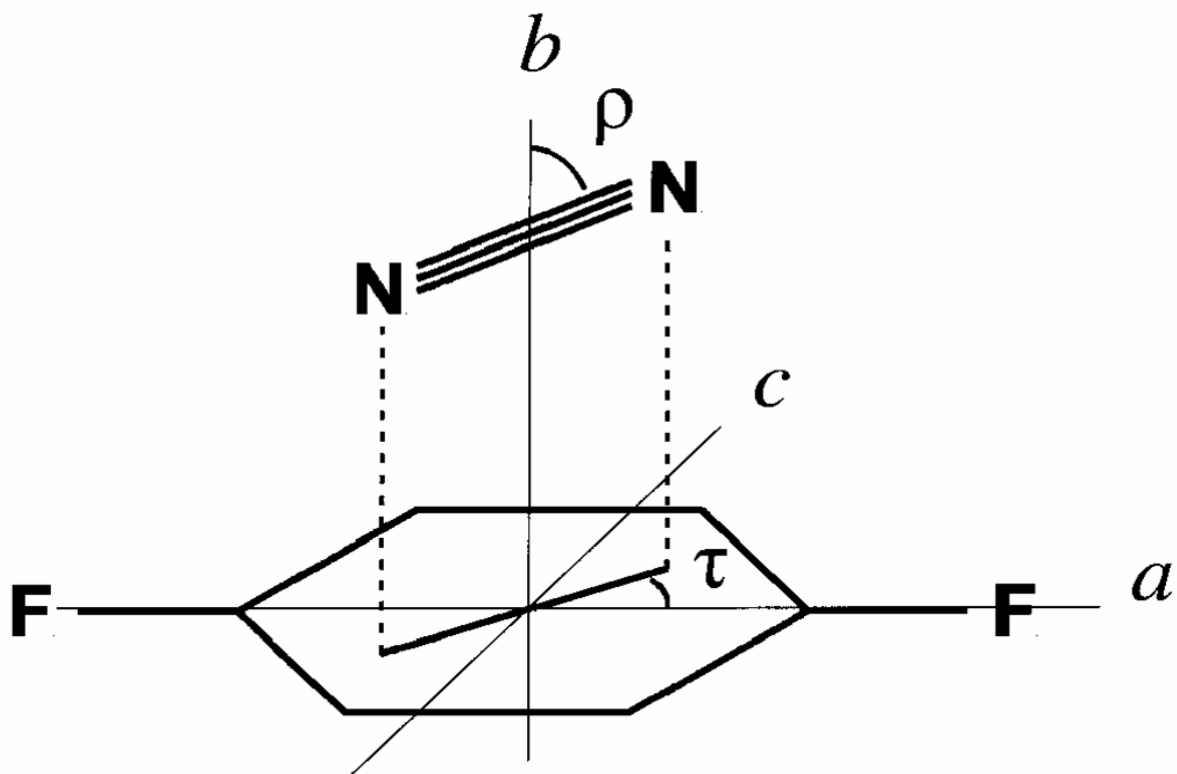


Figure 3. Geometry of the *p*DFB-N₂ complex. The position of the center of mass of N₂ is defined in the inertial coordinates (*a*, *b*, *c*) of the complex; the orientation of N₂ is defined by ρ (angle between the molecular axis of N₂ and the *b* axis) and τ (angle of rotation of N₂ around the *b* axis).

Table 3. Mean square displacements of the nitrogen molecule in the center-of-mass (COM) coordinate system of *p*DFB-N₂ in its S₀ and S₁ electronic states.^a

Parameter	Ground (S₀) State	Excited (S₁) State
$\langle a^2 \rangle^{1/2}/\text{\AA}$	0.09(2)	0.08(2)
$\langle b^2 \rangle^{1/2}/\text{\AA}$	3.53(1)	3.45(1)
$\langle c^2 \rangle^{1/2}/\text{\AA}$	0.69(2)	0.35(2)

^a Uncertainties in parentheses.

both states. (Only a motion that interchanges the nitrogen nuclei can explain the observed 2:1 intensity ratio between the two sub-bands in the UV spectrum). Hence, averaging over τ should result in zero values for $\langle a \rangle$ and $\langle c \rangle$; the COM of the attached N₂ should lie on b . Similarly, the average values of $\langle \sin \tau \rangle$ and $\langle \cos \tau \rangle$ also should be zero. Thus, since I_{ab} , I_{ac} , and I_{bc} (Eqs. (4) - (6)) are zero, \mathbf{I} is diagonal.

We now use Eqs. (1) - (3) to obtain estimates of the vibrationally averaged values of ρ and τ in both electronic states. First, we compare the experimental values of the moments I_a , *etc.* of the complex with the corresponding moments I_a^m of the bare molecule in a Kraitchman-type analysis [21]. This yields estimates of the mean square displacements $\langle a^2 \rangle$, $\langle b^2 \rangle$, and $\langle c^2 \rangle$ of the COM of the attached N₂ in both electronic states; these are listed in Table 3. Examining these data, we see that $\langle b^2 \rangle^{1/2} = 3.53 \text{ \AA}$ in the S₀ state and $\langle b^2 \rangle^{1/2} = 3.45 \text{ \AA}$ in the S₁ state. The decrease in $\langle b^2 \rangle^{1/2}$ in the S₁ state is consistent with the red shift of the S₁-S₀ origin band of *p*DFB-N₂ relative to the bare molecule. The values of $\langle a^2 \rangle^{1/2}$ are relatively small and the values of $\langle c^2 \rangle^{1/2}$ are relatively large, in both electronic states. Previous studies of rare gas complexes of aromatic molecules have yielded vibrationally averaged in-plane coordinates that are more nearly equal, as in 1-fluoronaphthalene-Ar and 2-fluoronaphthalene-Ar [20]. In contrast, *p*DFB-N₂ exhibits very different values of the two, $\langle a^2 \rangle^{1/2} = 0.09 \text{ \AA}$ and $\langle c^2 \rangle^{1/2} = 0.69 \text{ \AA}$ in the S₀ state. These data suggest that the N₂ molecule moves with significantly larger amplitude (or has significantly greater spatial extent) along c than along a , which again supports the idea that it is preferentially oriented along c , rather than a . The value of $\langle c^2 \rangle^{1/2}$ is much smaller in the S₁ state. All of these values are subject to some uncertainty, given the poorly defined potentials along the intermolecular coordinates. But they have at least some quantitative significance.

Next, we re-express Eqs. (1) - (3) in terms of the planar moment differences $P_a - P_a^m$, $P_b - P_b^m$, and $P_c - P_b^m$, obtaining Eqs. (7) - (9):

$$P_a - P_a^m = \frac{1}{2}(1 + \langle \cos 2\tau \rangle) \sin^2 \rho I_{N_2} + \mu \langle a^2 \rangle \quad (7)$$

$$P_b - P_c^m = \cos^2 \rho I_{N_2} + \mu \langle b^2 \rangle \quad (8)$$

$$P_c - P_b^m = \frac{1}{2}(1 - \langle \cos 2\tau \rangle) \sin^2 \rho I_{N_2} + \mu \langle c^2 \rangle \quad (9)$$

Finally, we compare the experimental values of $P_a - P_a^m$, $\langle a^2 \rangle$, etc. (Tables 2 and 3) with Eqs. (7) - (9), thereby obtaining estimates of $\langle \rho \rangle$ and $\langle \tau \rangle$. Eq. (8) yields $\langle \rho \rangle = 45 \pm 10^\circ$ in the S_0 state and $\langle \rho \rangle = 65 \pm 15^\circ$ in the S_1 state. Apparently, the N_2 molecule spends a significant amount of time in near-perpendicular orientations, especially in the ground state. Eqs. (7) and (9) yield $\langle \tau \rangle = 70 \pm 10^\circ$ in the S_0 state. The corresponding value in the S_1 state is not well determined. Eq. (7) gives a similar value, but Eq. (8) gives a value much less than this, $\langle \tau \rangle = 15 \pm 10^\circ$. We conclude, then, that the N_2 molecule lies mainly in the plane, parallel to the c axis in the S_0 state, but rotates more freely in the S_1 state.

Mean torsional amplitudes $\overline{\Delta\tau} = (\Delta\tau^2)^{1/2}$ can be obtained by expanding $\langle \cos 2\tau \rangle = \langle \cos 2(\tau_e + \Delta\tau) \rangle$ as a Taylor series, which yields for $\tau_e = 0$ or 90°

$$\langle \cos 2\tau \rangle_{\tau_e=0} = -\langle \cos 2\tau \rangle_{\tau_e=90} = \langle \cos 2\Delta\tau \rangle \approx \cos 2\overline{\Delta\tau} \quad (10)$$

where $\langle \Delta\tau^{2n} \rangle \approx \langle \Delta\tau^2 \rangle^n$ has been used in the approximation of Eq. (10). With this approximation, 33° and 42° were obtained for $\overline{\Delta\tau}$ in S_0 and S_1 , respectively. Such large amplitudes clearly indicate that the barriers hindering internal motion are quite low in both electronic states.

2.4.2. Barriers to internal rotation.

Estimates of the barriers to internal motion in *p*DFB-N₂ may be obtained in the following way. First, we assume that the N₂ molecule is rigidly attached to *p*DFB with its N≡N axis lying in a plane parallel to the *ac* plane. We further assume the N₂ exhibits a hindered rotation about the *b* axis which is governed by a two-fold potential, $V_2(\tau)$. In that event, $\rho = 90^\circ$, $\langle a^2 \rangle = \langle c^2 \rangle = 0$, and $B_{\text{rigid}} = \hbar^2 / (2h[I_c^m + I_{\text{N}_2}])$, from Eq. (2). The difference between this “rigid-body” value of B and the observed B_{eff} can then be used to estimate V_2 via the relation [22]

$$B_{\text{eff}} - B_{\text{rigid}} = FW_{\text{A}}^{(2)} \left(\frac{I_{\text{N}_2}}{I_c^m + I_{\text{N}_2}} \right)^2 \quad (11)$$

where F is the internal rotor constant

$$F = \frac{\hbar^2}{2hI_{\text{N}_2}} \left(\frac{I_c^m + I_{\text{N}_2}}{I_c^m} \right) = 60.78 \text{ GHz} \quad (12)$$

and $W_{\text{A}}^{(2)}$ is a second-order perturbation coefficient. In the high barrier approximation, this coefficient can be related to the energy difference between the two lowest torsional states, ΔE [22]

$$W_{\text{A}}^{(2)} = -\frac{1}{2}\pi^2 w_1 \approx \frac{1}{4}\pi^2 (b_2 - b_1) = \frac{1}{4}\pi^2 \frac{\Delta E}{F} \quad (13)$$

from which the reduced barrier height,

$$s = 4V_{\text{N}} / (N^2 F) \quad (14)$$

can be derived. This simple model yields $s = 6.10$ and $V_2 = 12.4 \text{ cm}^{-1}$ for the S₀ state, and $s = 3.77$ and $V_2 = 7.6 \text{ cm}^{-1}$ for the S₁ state.

The difference between the calculated torsional splittings in the two states ($\Delta E = 12.1$ GHz in S_0 and $\Delta E = 22.3$ GHz in S_1) is too small to explain the observed separation of the two sub-bands in the spectrum, 21.3 GHz. Thus, the actual barriers are likely to be smaller than the above estimates. (In agreement with this, the simple model (Eq. (11)) gives only an upper limit to V_2). V_2 barriers of about 10 and 2.5 cm^{-1} in the two states yield values of $\langle \cos 2\tau \rangle$ that are similar to the observed ones, based on simulations using an effective Hamiltonian for the large amplitude motion [23]. With such small barriers, the high barrier approximation may be unreliable.

More rigorously, the spectrum was analyzed with the aid of the semirigid internal rotor model described elsewhere [24]. Torsional levels ($J = 0$) were calculated for different potentials $V_2(\tau)$. Taking the distance between the two Q branches in the spectrum (21.3 GHz) as the difference $\Delta E' - \Delta E''$, it was evident that $|V_2'| < |V_2''|$ and that $|V_2'| < 7.5 \text{ cm}^{-1}$. A comparison of these results with the frequencies of the torsional sidebands observed in the REMPI spectrum of *p*DFB-N₂ [8] suggests $V_2' \approx 2 \text{ cm}^{-1}$.

Next, attempts were made to least-squares fit the rotational structure of both sub-bands simultaneously, by varying both the moments of inertia of the complex and the potential energy terms, in both states. Initially, rigid rotor Hamiltonians and potentials containing only V_2 terms were employed. Later, centrifugal distortion and structural relaxation terms [21] were included in the rotational Hamiltonians, and V_4 terms were added to the potential. The best fits were obtained when the N₂ molecule was oriented parallel to *c* in the S_0 state, in accord with the previous conclusion. No obvious preference was detected for the S_1 state.

Despite these attempts, it was not possible to fully reproduce the observed spectrum of the weaker sub-band. Fig. 2 shows a typical example. Here, $V_2'' = 7.2 \text{ cm}^{-1}$, $V_2' = 2.2 \text{ cm}^{-1}$, and V_4''

$= V_4' = 0$; yielding a predicted sub-band splitting of 22.4 GHz, in approximate agreement with experiment (21.3 GHz). Including modest centrifugal distortion and structural relaxation terms leads to a fit of 224 single transitions with an OMC of 7.3 MHz. Still, principally due to spectral overlap, only the Q branch with $K_c' = K_c'' = J$ and some P branch transitions could be fit, as shown in Fig. 2. A possible explanation for this behavior is that the second lowest torsional level in S_1 , in which the weaker sub-band likely terminates, is just above the barrier, and is likely perturbed by torsion-rotation interactions. A similar problem exists for benzene- N_2 , which also has very small torsional barriers. Only the high resolution spectra of the lowest $m=0$ torsional state have been successfully analyzed to date [3, 4].

Most models developed by us to interpret the high resolution spectra of $pDFB-N_2$ reproduce well the splittings observed in the low resolution spectrum of the Parmenter group [1]. These splittings are thus attributed to the contributions of torsional side bands to the spectrum, rather than hybrid band character. Both of the bands studied in this work are pure b -type bands.

2.5. Discussion.

Apart from this negative result, that there is no *complex*-induced electronic TM rotation in $pDFB-N_2$, the most interesting finding in this work is that there is a substantial change in the barrier to internal rotation of the attached N_2 when the complex absorbs light, from $V_2 \sim 10 \text{ cm}^{-1}$ in the S_0 state to $V_2 \sim 2 \text{ cm}^{-1}$ in the S_1 state. The $N\equiv N$ bond axis is more or less uniquely oriented along the short in-plane axis in the ground S_0 state, but essentially free to assume any orientation parallel to the aromatic plane in the excited S_1 state. This result is, at first glance, even more surprising when one realizes that the binding energy of the complex must *increase* on electronic excitation, since the S_1-S_0 origin of $pDFB-N_2$ is shifted to the red of the corresponding origin of

the bare molecule by $\sim 27 \text{ cm}^{-1}$. A stronger vdW bond is also indicated by the observed decrease in R (Table 3) on S_1 excitation.

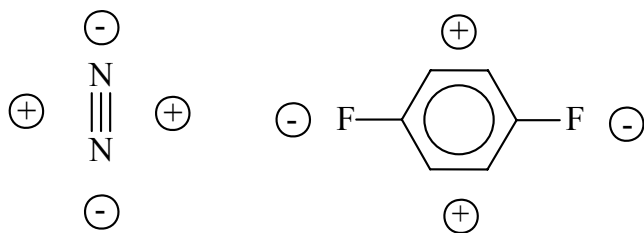
This apparent dilemma is resolved when one realizes that V_2 barriers are measures of the *anisotropy* of the potential in the aromatic plane, not of its average values. Large differences in either the attractive or the repulsive terms in orientations parallel to a and parallel to c will give rise to large barriers. Conversely, if there are only small differences in these terms, and V_2 is more isotropic, the internal rotation will be nearly free. Seemingly, this is the case in the S_1 state of $p\text{DFB-N}_2$.

Probing this issue further, we have performed *ab initio* calculations on $p\text{DFB}$ in its S_0 and S_1 electronic states using the Gaussian 98 suite of programs [25]. A 6-31G** basis set was employed; the MP2 method was used for the S_0 state, and the CIS method was used for the S_1 state. These calculations qualitatively reproduce the changes in the rotational constants that occur when the molecule absorbs light; *i.e.*, a large decrease in A , and smaller changes in B and C (*cf.* Table 1). As is well known, these changes are a consequence of a quinoidal distortion of the ring. The S_1 state has significantly shorter parallel ring C-C bonds than “perpendicular” ones.

If there are significant differences in the geometries of the two states of $p\text{DFB}$, then there must also be significant differences in their electron distributions. Figure 4 shows an electron density difference map for $p\text{DFB}$, illustrating clearly that the absorption of light produces a large change in the distribution of π electrons around the ring. In particular, π -electron density shifts from regions parallel to the C-F bonds (along the long axis) to regions perpendicular to these bonds (along the short axis). It is thus reasonable to suggest that these changes in electron

distribution are primarily responsible for the significant differences in the barrier heights in S_0 and S_1 p DFB- N_2 .

p DFB and N_2 are both quadrupolar molecules; owing to their high symmetry, their first nonvanishing multipole moments are the quadrupole moments, as shown below:



Clearly, the stable configuration of the S_0 state of p DFB- N_2 should be one in which the N_2 is attached to the top (or bottom) of the aromatic plane, perpendicular to the two C-F bonds. This is exactly what is observed. But excitation of p DFB by light changes its “in-plane” electron distribution, and could therefore change both the preferred orientation of the $N\equiv N$ bond axis and the barrier opposing its motion. Table 4 lists the quadrupole moments of p DFB in its S_0 and S_1 electronic states, according to theory. As expected, the quadrupole tensor of S_0 p DFB is nearly axially symmetric about c ; it is large and negative along a , and equally large and positive along b . The predicted anisotropy is $\sim 38 D \text{ \AA}$. The corresponding tensor of S_1 p DFB is significantly different; it is both less symmetric, and less anisotropic. $Q_b - Q_a$ is $\sim 22 D \text{ \AA}$, a 40% reduction compared to the ground state. The larger value of Q_c no doubt is partially responsible for increasing the binding energy of the attached N_2 . More importantly, the decrease in $Q_b - Q_a$ clearly indicates that the “in-plane” π -electron distribution is more isotropic in the S_1 state, and thus explains the large decrease in V_2 in this state.

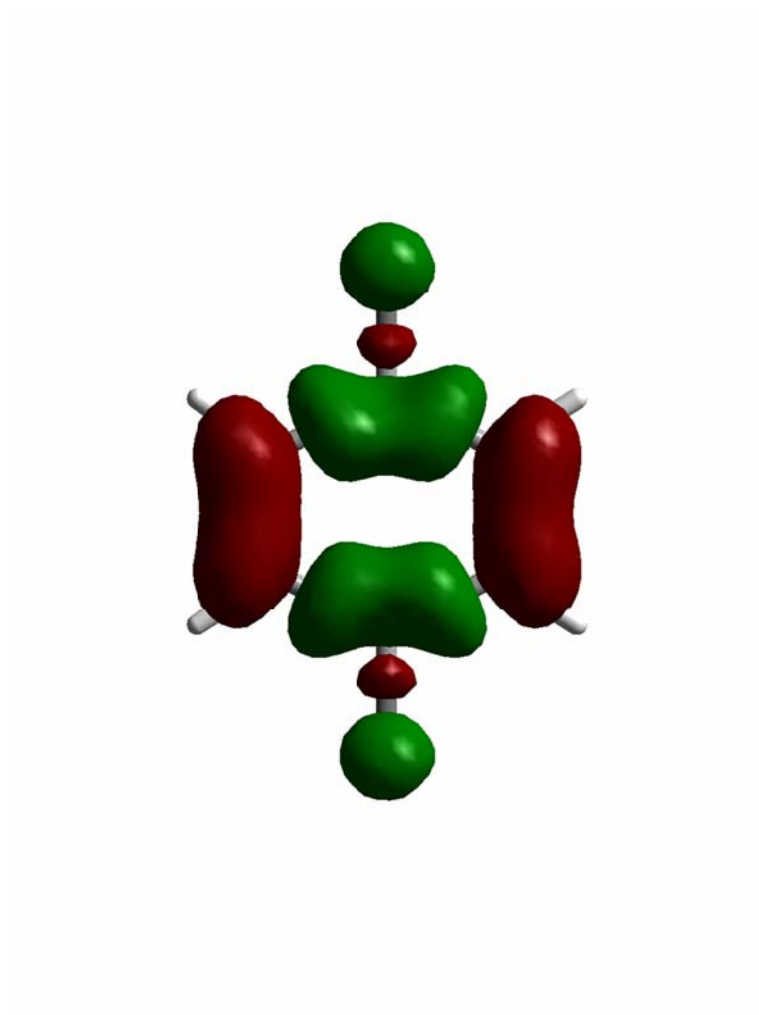


Figure 4. Electron density difference map for the $S_1 \leftarrow S_0$ transition of *p*DFB. Red (dark) contours indicate regions of electron gain, and green (light) contours indicate regions of electron loss.

Table 4. Quadrupole moments of *p*-difluorobenzene in its S₀ and S₁ electronic states, according to theory (MP2/CIS 6-31G**).

Parameter^a	S₀	S₁
<i>Q</i> _a	-19.27	-9.64
<i>Q</i> _b	+19.18	+12.62
<i>Q</i> _c	+0.10	-2.97

^a In units of Debye Ångstroms, in the inertial coordinate system of *p*DFB.

This situation stands in sharp contrast to that in aniline-N₂ [12]. Here, a large increase in barrier height is observed on S₁-S₀ excitation, from $\sim 25 \text{ cm}^{-1}$ in the S₀ state to $\sim 65 \text{ cm}^{-1}$ in the S₁ state. But N₂ is bound by a dipole-induced dipole interaction in aniline-N₂, leading to an equilibrium geometry (in both states) in which the N≡N bond axis is parallel to the *long* axis of the ring. And excitation of aniline to its S₁ state leads to a large increase in its dipole moment along this axis [26], thus explaining the large increase in V_2 in this system.

Future studies of this type will provide valuable data that may be used to benchmark intermolecular potentials, so important in both *intra* and *intermolecular* dynamics.

2.6. Acknowledgments.

This work was supported by NSF (CHE-9987048). M. Schäfer thanks the Schweizerischer Nationalfonds for a postdoctoral fellowship.

2.7. References.

- [1] Q. Ju and C. S. Parmenter, Abstract MH07, 53rd International Symposium on Molecular Spectroscopy, Columbus, OH, 1998. See also Q. Ju, Ph.D. Thesis, Indiana University, December 1998.
- [2] P. W. Joireman, R. T. Kroemer, D. W. Pratt, and J. P. Simons, *J. Chem. Phys.* **105**, 6075 (1996).
- [3] Th. Weber, A. M. Smith, E. Riedle, H. J. Neusser, and E. W. Schlag, *Chem. Phys. Lett.* **175**, 79 (1990).
- [4] Y. Ohshima, H. Kohguchi, and Y. Endo, *Chem. Phys. Lett.* **184**, 21 (1991).
- [5] H. J. Neusser, R. Sussman, A. M. Smith, E. Riedle, and Th. Weber, *Ber. Bunsenges. Phys. Chem.* **96**, 1252 (1992).
- [6] B. D. Gilbert, C. S. Parmenter, M.-C. Su, H.-K. Oh, and Z.-Q. Zhao, *Appl. Phys.* **B59**, 397 (1994).
- [7] B. D. Gilbert, C. S. Parmenter, and H.-K. Oh, *J. Phys. Chem.* **99**, 2444 (1995).
- [8] Y. Hu, W. Lu, and S. Yang, *J. Photochem. Photobiol.* **A106**, 91 (1997).
- [9] Y. Hu, W. Lu, and S. Yang, *J. Chem. Phys.* **105**, 5305 (1996).
- [10] M. S. Ford, S. R. Haines, I. Pugliesi, C. E. H. Dessent, and K. Müller-Dethlefs, *J. Electron Spectrosc.* **112**, 231 (2000).
- [11] K. Yamanouchi, S. Isogai, and S. Tsuchiya, *J. Mol. Struct.* **146**, 349 (1986).
- [12] M. Schäfer and D. W. Pratt, *J. Chem. Phys.* **115**, 11147 (2001).
- [13] R. Disselkamp and E. R. Bernstein, *J. Chem. Phys.* **98**, 4339 (1993).
- [14] S. Sun and E. R. Bernstein, *J. Chem. Phys.* **103**, 4447 (1995).

- [15] W. A. Majewski, J. F. Pfanstiel, D. F. Plusquellic, and D. W. Pratt, in *Laser Techniques in Chemistry*, ed. A. B. Myers and T. R. Rizzo (Wiley, New York, 1995), pp. 101-148.
- [16] S. Gerstenkorn and P. Luc, *Atlas du spectre d'absorption de la molécule d'iode* (CNRS, Paris, 1978).
- [17] R. Sussman, R. Neuhauser, and H. J. Neusser, *Can. J. Phys.* **72**, 1179 (1994).
- [18] J. K. G. Watson in *Vibrational Spectra and Structure*, ed. by J. R. Durig (Elsevier, Amsterdam, 1977), Vol. 6, p.1, and references therein.
- [19] A. Lofthus and P. H. Krupenie, *J. Phys. Chem. Ref. Data* **6**, 113 (1977).
- [20] See, for example, B. B. Champagne, J. F. Pfanstiel, D. W. Pratt, and R. C. Ulsh, *J. Chem. Phys.* **102**, 6432 (1995).
- [21] W. Gordy and R. L. Cook, *Microwave Molecular Spectra*, 3rd Ed. (Wiley Interscience, New York, 1984).
- [22] D. R. Herschbach, *J. Chem. Phys.* **31**, 91 (1959).
- [23] J. Makarewicz, *J. Mol. Spectrosc.* **176**, 169 (1996).
- [24] M. Schäfer, *J. Chem. Phys.* **115**, 11139 (2001).
- [25] M. J. Frisch, G. W. Trucks, H. B. Schlegel, G. E. Scuseria, M. A. Robb, J. R. Cheeseman, V. G. Zakrzewski, J. A. Montgomery, R. E. Stratmann, J. C. Burant, S. Dapprich, J. M. Millam, A. D. Daniels, K. N. Kudin, M. C. Strain, O. Farkas, J. Tomasi, V. Barone, M. Cossi, R. Cammi, B. Mennucci, C. Pomelli, C. Adamo, S. Clifford, J. Ochterski, G. A. Petersson, P. Y. Ayala, Q. Cui, K. Morokuma, D. K. Malick, A. D. Rabuck, K. Raghavachari, J. B. Foresman, J. Cioslowski, J. V. Ortiz, A. G. Baboul, B. B. Stefanov, G. Liu, A. Liashenko, P. Piskorz, I. Komaromi, R. Gomperts, R. L. Martin, D. J. Fox, T. Keith, M. A. Al-Laham, C. Y. Peng, A. Nanayakkara, M. Challacombe, P. M. W. Gill, B. G. Johnson, W. Chen, M. W. Wong, J. L.

Andres, C. Gonzalez, M. Head-Gordon, E. S. Replogle and J. A. Pople, *Gaussian 98 (Revision A.9)*, Gaussian, Inc., Pittsburgh, PA, 1998.

[26] T. M. Korter, D. R. Borst, C. J. Butler, and D. W. Pratt, *J. Am. Chem. Soc.* **123**, 96 (2001).

3. High resolution electronic spectrum of the *p*-difluorobenzene-water complex: Structure and internal rotation dynamics.

Cheolhwa Kang and David W. Pratt*
Department of Chemistry, University of Pittsburgh,
Pittsburgh, Pennsylvania 15260, USA

Martin Schäfer
Laboratorium für Physikalische Chemie,
Eidgenössische Technische Hochschule Zürich,
ETH Hönggerberg - HCI, CH-8093 Zürich, Switzerland

3.1. Abstract.

The rotationally resolved $S_1 \leftarrow S_0$ electronic spectrum of the water complex of *p*-difluorobenzene (*p*DFB) has been observed in the collision-free environment of a molecular beam. Analyses of these data show that water forms a planar σ -bonded complex with *p*DFB via two points of attachment, a stronger F---H-O hydrogen bond and weaker H---O-H hydrogen bond, involving an *ortho* hydrogen atom of the ring. Despite the apparent rigidity of this structure, the water molecule also is observed to move within the complex, leading to a splitting of the spectrum into two tunneling subbands. Analyses of these data show that this motion is a combined inversion-internal rotation of the attached water, analogous to the “acceptor switching” motion in the water dimer. The barriers to this motion are found to be significantly different in the two electronic states owing to changes in the relative strengths of the two hydrogen bonds that hold the complex together.

Published in the *J. Phys. Chem. A*, **109**, 767 (2005)

3.2. Introduction.

Due to the important role of water as a solvent and its ability to form hydrogen bonds with other molecules, either as a proton donor or acceptor, water-containing complexes have attracted a lot of attention in recent years, especially water complexes of aromatic molecules [1, 2]. If the aromatic molecule contains a functional group with oxygen or nitrogen, it normally forms a water complex with a σ hydrogen bond. In phenol-water [3-5], the water binds as a proton acceptor to the hydroxy group, whereas it binds as a proton donor to the oxygen of the methoxy group in anisole-water [6-8]. In aniline-water, the water acts as a proton donor to the amino group with a hydrogen bond almost perpendicular to the ring plane [9], whereas in the nitrogen-containing heterocycles pyrrole-water [10] and indole-water [11,12], the water forms a N-H---OH₂ hydrogen bond as a proton acceptor.

Other water binding motifs exist in aromatic molecules. In the water complex of the nonpolar, hydrophobic benzene molecule, water binds with its hydrogens pointing towards the π electron system, although large amplitude motions make the elucidation of the exact structure difficult [13-17]. In complexes with more than one water molecule, the water molecules form a cluster that is hydrogen bonded to the π electron system of benzene [6, 13, 18, 19]. And in the benzene-water cation, the oxygen atom of the water molecule approaches the C₆H₆⁺ cation in the aromatic plane, an arrangement that is about 160 cm⁻¹ lower in energy than the “a-top” geometry [20].

Using IR depletion R2PI spectroscopy, Brutschy and coworkers found similar complex formation patterns for substituted benzene-water clusters [6]. According to their initial interpretation, water binds to the π electron system in 1:1 complexes with fluorobenzene or *p*-

difluorobenzene (*p*DFB). But rotational contours in REMPI spectra and *ab initio* calculations later showed that a planar configuration where the water forms two hydrogen bonds (F---H-O and *ortho*-H---O-H) is slightly or significantly more stable than a π bonded structure in fluorobenzene-water or *p*DFB-water, respectively [21, 22]. Moreover, there are still ambiguities concerning the proper interpretation of C-F---H-O interactions. Caminati, *et al.* [23] analyzed the F---H-O hydrogen bond in difluoromethane-water using free jet millimeter wave absorption spectroscopy. None of the observed transitions were split, suggesting that water is rigidly attached to the CH₂F₂. From the stretching force constant, it was concluded that the F---H-O interaction appears to be rather strong, almost as strong as the O-H ---O internal hydrogen bond in the water dimer [24]. The binding energy was estimated to be $\sim 700 \text{ cm}^{-1}$ by assuming a Lennard-Jones potential function. However, Thalladi, *et al.* [25] reported that the C-F group in crystalline fluorobenzenes is a very poor proton acceptor, having the characteristics of weak hydrogen bonds. Only in the absence of competing interactions is the true nature of the C-F---H-O interaction ever likely to be revealed.

Rotationally resolved electronic spectroscopy is a powerful tool for studying such phenomena because it is sensitive to both the equilibrium geometry of the complex as well as to its feasible motions. In this report, a study of the rotationally resolved UV spectrum of the complex between *p*DFB and water is presented. From analyses of the moments of inertia, the structures of the complex in its S₀ and S₁ states were determined. And from analyses of splittings that appear in the spectra, motions of the attached water molecule are revealed, from which information about the relative strengths of the two hydrogen bonds that hold the complex together may be deduced.

3.3. Experimental.

High resolution data were obtained using the CW molecular beam laser spectrometer described in detail elsewhere [26]. *p*DFB was seeded in helium at a backing pressure of about 1 bar (monomer) or 2.7 bar (complex). For the water complex, helium was enriched with water vapor by passing the gas through a container holding water at room temperature. The gas mixture was expanded through a 280 μm quartz nozzle, skimmed once, and probed 15 cm downstream of the nozzle by a frequency doubled, single frequency, tunable ring dye laser operating with Rhodamine 110, yielding about 200 μW (150 μW for the monomer) of ultraviolet radiation. Fluorescence was collected using spatially selective optics, detected by a photomultiplier tube and photon counting system, and processed by a computerized data acquisition system. Relative frequency calibrations of the spectra were performed using a near-confocal interferometer having a mode-matched FSR of 299.7520 ± 0.0005 MHz at the fundamental frequency of the dye laser. Absolute frequencies in the spectra were determined by comparison to transition frequencies in the I_2 spectrum [27].

3.4. Results.

Figure 5 shows the high resolution spectrum of the origin band of the $S_1 \leftarrow S_0$ transition of the *p*DFB-water complex. The origin of the complex is shifted by $+168.1 \text{ cm}^{-1}$ with respect to that of the bare molecule [28]. To determine whether or not the spectrum contains an underlying subband structure, an autocorrelation analysis was performed to see if multiple overlapping subbands were present. This analysis revealed that there are two overlapping bands in the spectrum, separated by 3.63 GHz with significantly different relative intensities.

We initially worked to fit the stronger of these two subbands. The fitting procedure began with the simulation of a spectrum using assumed geometries of the complex. We assumed that the water lies in the plane of *p*DFB and that one O-H bond of the water is involved in the formation of a six-membered ring system with the F-C-C-H fragment of *p*DFB, as shown in Figure 6. The simulated spectrum was compared with the experimental spectrum and several transitions were assigned. An effective way to fit the spectrum is using the “selected quantum number” feature of *jb95* [29]. Each of the resolved lines was first assigned with $K_a = 0$ and subsequently followed by $K_a = 1, 2, 3, \dots$ because the intensity significantly decreases as K_a increases. A least-squares fit of assigned quantum numbers to the spectrum with the procedure outlined above was used to modify the assumed rotational constants. This procedure was repeated iteratively until all stronger lines were accounted for. To fit the weaker band, a second spectrum was generated using the rotational constants of the stronger subband and moved along the frequency axis based on the autocorrelation results. A selected quantum number assignment was carried out in the manner described above and optimized by a least-squares fit. This fit reveals that the origin of the weaker subband is positioned at -3.63 GHz with respect to that of the stronger one, in excellent agreement with the results of the autocorrelation analysis.

A portion of the experimental spectrum, expanded to full experimental resolution from the R branch of the stronger subband, is shown in Figure 7 together with the separate calculated contributions of the two subbands in this region. Whereas the monomer exhibits a pure *b*-type spectrum [28], the spectrum of the water complex consists of two subbands with intensity ratio 1:3 and *a/b* hybrid band type (about 15% *a*, 85% *b*). The rotational temperature of the complex was estimated to be about 2.5 K, and the linewidths were about 30 MHz in the monomer and 40

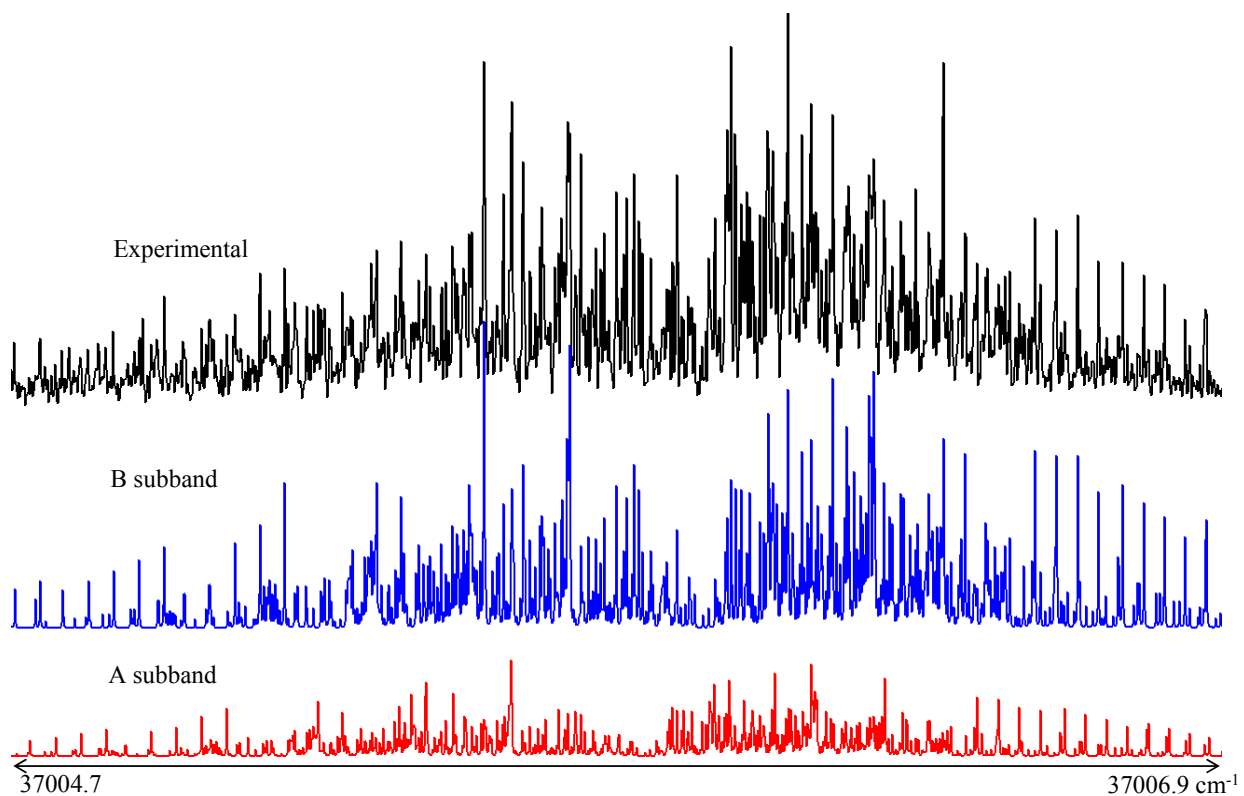


Figure 5. Rotationally resolved fluorescence excitation spectrum of the origin band of the $S_1 \leftarrow S_0$ transition of $p\text{DFB-H}_2\text{O}$, shifted 168.1 cm^{-1} to the blue of the $S_1 \leftarrow S_0$ origin band of $p\text{DFB}$. The origin band of the complex is a superposition of two subbands which are separated by 0.121 cm^{-1} . The top trace is the experimental spectrum. The second and third traces are the calculated B and A subbands, respectively.

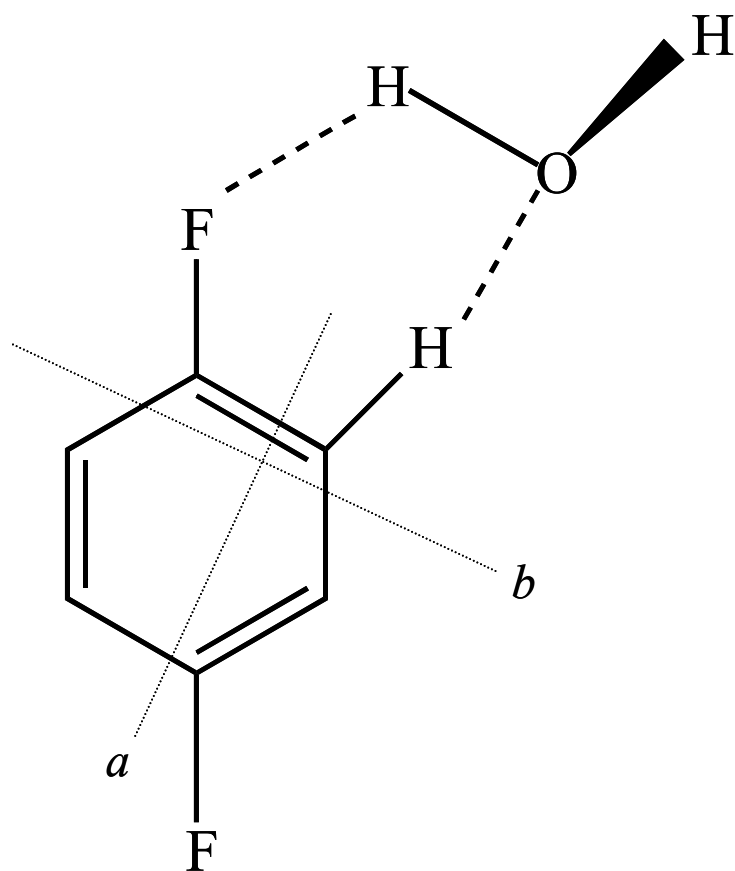


Figure 6. Approximate structure of the doubly hydrogen-bonded complex of *p*-difluorobenzene with a single water molecule. *a* and *b* denote its in-plane inertial axes.

MHz in the complex spectrum. An analysis using Voigt line shapes with a 26 MHz Gaussian component revealed Lorentzian linewidths of 15 and 25 MHz for the monomer and complex, respectively, corresponding to fluorescence lifetimes of 11.5 and 6.3 ns.

3.5. Discussion.

3.5.1. Structure of *p*DFB and its water complex.

Table 5 lists the inertial parameters of *p*DFB and its water complex. These data provide useful information about the structure of its ground electronic state and how this structure changes upon electronic excitation. First, in *p*DFB itself [28], there is a large decrease in the *A* rotational constant ($\Delta A = A' - A'' = -354.4$ MHz, - 6.3 %), reflecting an expansion of the ring perpendicular to the *a* inertial axis, and an increase in the *B* rotational constant ($\Delta B = 6.2$ MHz, 0.4 %), suggesting a contraction of the C–C bonds adjacent to the C-F bonds. Clearly, there is enhanced conjugation of the two groups in the electronically excited state which results in a considerable decrease in the electron density on the F atoms. More quantitatively, the excited state rotational constants can be interpreted in terms of a contraction of about 0.03 Å in the C-F bond lengths and an increase of about 2.4° in the C-C(F)-C angles.

Inertial defects (ΔI) often are used as measure of a molecule's planarity. For a rigid planar structure, ΔI is zero whereas for a rigid nonplanar structure, ΔI is negative. Concerning the *p*DFB-water complex, the magnitudes of its inertial defects are relatively small ($\Delta I'' = -0.68$ amu Å² in the ground state and $\Delta I' = -0.74$ amu Å² in the excited state), but significantly different from those of bare molecule ($\Delta I'' = 0.00(5)$ amu Å², $\Delta I' = -0.20(5)$ amu Å² [28]). The values

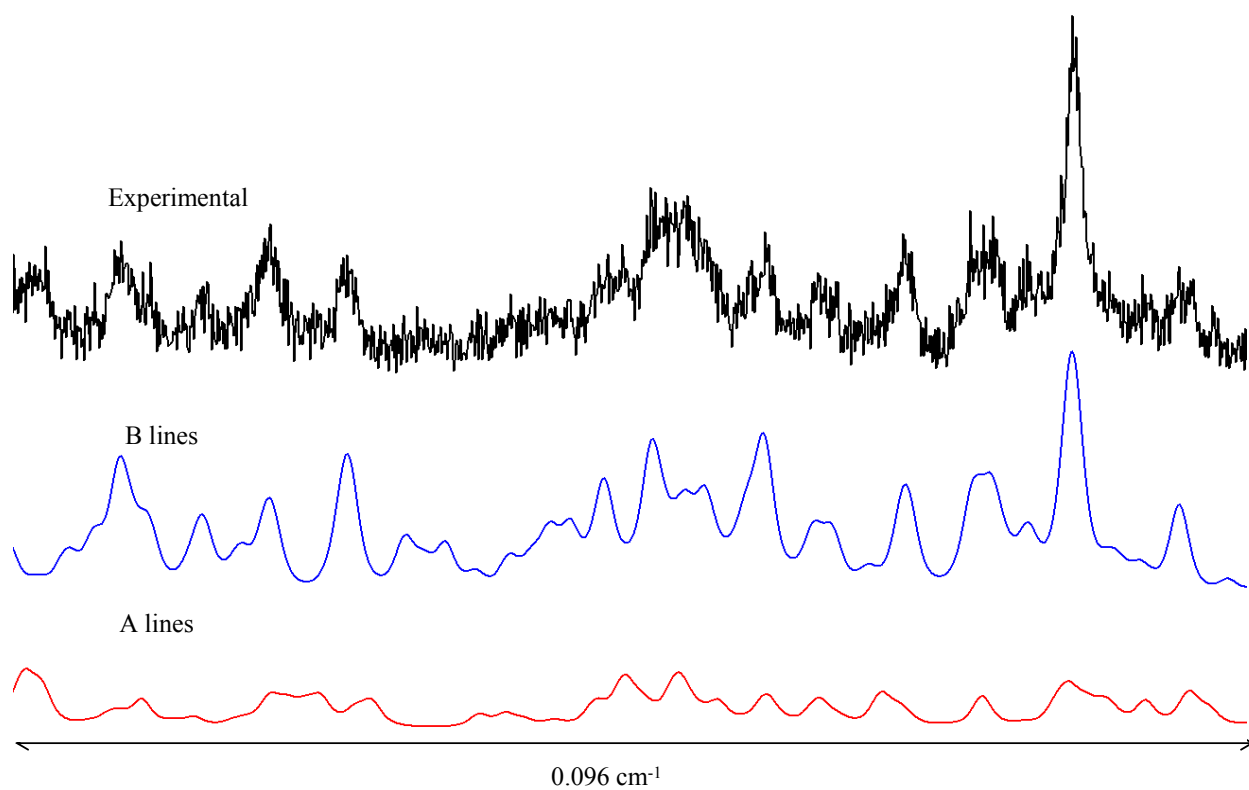


Figure 7. Portion of the high resolution spectrum of *p*DFB-H₂O at full experimental resolution, extracted from the R branch of the stronger subband. The top trace is the experimental spectrum. The second and third traces show the separate calculated contributions of the two subbands in this region.

Table 5. Inertial parameters of *p*DFB and its water complex in the zero-point vibrational levels of their S_0 and S_1 electronic states.

	<i>p</i> DFB	<i>p</i> DFB-H ₂ O		
		a subband	b subband	
S_0	A, MHz	5637.6 (2)	3310.0 (2)	3309.6 (2)
	B, MHz	1428.0 (1)	806.1 (1)	806.1 (1)
	C, MHz	1139.4 (1)	648.7 (1)	648.8 (1)
	ΔI , amu Å	-0.004	-0.68	-0.68
S_1	A, MHz	5283.2 (2)	3185.1 (2)	3184.6 (2)
	B, MHz	1434.2 (1)	795.4 (1)	795.5 (1)
	C, MHz	1128.5 (1)	637.1 (1)	637.1 (1)
	ΔI , amu Å	-0.020	-0.80	-0.74

for *p*DFB-water are smaller than that expected for two out-of-plane hydroxy hydrogen atoms. While it is difficult to reach structural conclusions based on the results for a single isotopomer, the data suggest that, on average, the oxygen atom and one hydrogen atom of the water molecule lie in the plane, and that the second hydrogen atom lies out of the plane. Both hydrogens undergo large amplitude motion along out-of-plane coordinates. For comparison, the indole-water complex [12] exhibits an inertial defect of $\Delta I'' = -1.41 \text{ amu \AA}^2$ in the ground state. This is about twice *p*DFB-water's value. The differences are mainly explained by out-of-plane vibrational motions of the two hydrogens in water. Indole itself is essentially planar in both electronic states, and both water hydrogens are out-of-plane in the complex. Therefore, we suggest that the inertial defect of about -0.7 amu \AA^2 in *p*DFB-water can be generated if, on average, one of the two water hydrogens points out-of-plane.

More information about the structure of the complex and the possible motions of water can be deduced from the Kraitchman analysis [30] shown in Table 6. This analysis gives the position of the center-of-mass (COM) of the attached molecule from a comparison of the moments of inertia of the bare molecule and the complex. The relatively small, non-zero $|c|$ values in both electronic states are due to the out-of-plane motions of the two hydroxy hydrogen atoms. The in-plane displacements $|a| = 3.605$ and $|b| = 2.85 \text{ \AA}$ in the ground state increase on electronic excitation by $0.05 - 0.10 \text{ \AA}$. An increase in these distances is consistent with decreasing the strength of the hydrogen bonding interactions, which is responsible for the blue shift of the origin band of the water complex relative to that of the bare molecule.

It is interesting to compare the results for *p*DFB-water to those for the analogous benzonitrile-water (BN-water) complex [31-34]. In both complexes, the oxygen is bound to an *ortho* hydrogen and one hydroxy hydrogen is bound to the fluorine or the cyano group. In the

Table 6. COM coordinates of the water molecule in the principal axis frames of the bare *p*DFB molecule and of the *p*DFB-H₂O complex.

State	coordinate	<i>p</i> DFB frame (Å)	complex frame (Å)
S ₀	<i>a</i>	3.605(5)	3.848(7)
	<i>b</i>	2.858(4)	1.132(3)
	<i>c</i>	0.23(3)	0.067(9)
	<i>r</i>	4.6545 (5)	4.012(6)
S ₁	<i>a</i>	3.703(5)	3.916(8)
	<i>b</i>	2.905(3)	1.107(2)
	<i>c</i>	0.24(3)	0.065(10)
	<i>r</i>	4.713(5)	4.070(6)

electronic ground state S_0 , the structures of these complexes are very similar. The water COM in BN-water is slightly further away from the aromatic ring (coordinates with respect to the ring center: 3.59/3.14/0.00 Å). However, *p*DFB-water and BN-water differ in their behavior upon excitation into S_1 . Whereas there is no significant change in the *a* and *b* COM coordinates in BN-water (they decrease by less than 0.01 Å), the coordinates increase by 0.05 - 0.10 Å in *p*DFB-water. The larger structural change in *p*DFB-water also is reflected in the larger blue shift of the origin of the complex with respect to that of the monomer; 168.1 cm^{-1} in *p*DFB. In contrast, BN-water exhibits a red shift of -69.8 cm^{-1} with respect to that of BN itself [34].

3.5.2. Nuclear spin statistical weights.

Due to the D_{2h} symmetry of *p*DFB and the C_{2v} symmetry of H_2O , the molecular symmetry (MS) group [35] of the complex is G_{16} . Assuming that only the two hydrogens of H_2O or the *a* inertial axis of *p*DFB are feasible tunneling paths connecting symmetrically equivalent configurations, the effective molecular symmetry group is G_8 which is isomorphic with D_{2h} (see Table 7). Exchanging the two hydrogens of H_2O corresponds to the permutation $P_1 = (ab)$, and rotating around the *a* inertial axis of *p*DFB corresponds to $P_2 = (26)(35)$. The full molecular symmetry group G_{16} can be obtained by $G_{16} = G_8 \otimes \{E, (14)(23)(56)\}$, where the permutation (14)(23)(56) corresponds to an internal rotation around the *b* inertial axis of *p*DFB.

In Table 7, classifications of the rovibronic wavefunctions according to the symmetry species of the molecular symmetry group G_8 are given (in G_{16} , add the superscript + to the symmetry labels of Γ_{el} and Γ_{rot}). According to the general selection rule for electric dipole transitions ($\Gamma'_{rve} \otimes \Gamma''_{rve} \supset \Gamma_2^{+(+)}$), electronic transitions within one tunneling state follow μ_b -type selection rules whereas μ_a -type transitions are possible between the different substates

Table 7. Character table of the molecular symmetry group G_8 of *p*-difluorobenzene-water

	E	P ₁	E*	P ₁ *	P ₂	P ₂ P ₁	P ₂ *	P ₂ P ₁ *		Ψ_{rot}	Ψ_e
Eq. rot	R ⁰	R ⁰	R _y ^π	R _y ^π	R _z ^π	R _z ^π	R _x ^π	R _x ^π	w ⁺ , w ^{-b}	K _a K _c	
Γ ₁ ⁺	1	1	1	1	1	1	1	1	16, 24	ee	S ₀
Γ ₂ ⁺	1	1	-1	-1	1	1	-1	-1	16, 24	eo	
Γ ₃ ⁺	1	-1	1	-1	1	-1	1	-1	48, 72		
Γ ₄ ⁺	1	-1	-1	1	1	-1	-1	1	48, 72		
Γ ₁ ⁻	1	1	1	1	-1	-1	-1	-1	12, 12	oe	S ₁
Γ ₂ ⁻	1	1	-1	-1	-1	-1	1	1	12, 12	oo	
Γ ₃ ⁻	1	-1	1	-1	-1	1	-1	1	36, 36		
Γ ₄ ⁻	1	-1	-1	1	-1	1	1	-1	36, 36		

^a P₁ = (*ab*) is the permutation of the water hydrogen nuclei, P₂ = (26)(35) is the permutation of the *p*DFB nuclei symmetric to its *a* axis. The molecule fixed axis system (*x,y,z*) is defined so that the carbon or fluorine nucleus labelled 1 of *p*DFB has a positive *z* coordinate and the carbon or hydrogen labelled 2 a positive *x* coordinate.

^b Nuclear spin statistical weight (the superscripts refer to G₁₆; weights for G₈: w = w⁺ + w⁻).

of an p DFB internal rotation around its a axis. Therefore, μ_a - type transitions are theoretically split, but the splitting is expected to be too small to be observed in the UV spectrum.

Nuclear spin statistical weights can be used to determine which nuclei are involved in the large amplitude motion producing the observed splitting. These weights are determined by the fact that rovibronic states having symmetry Γ_{rve} can only combine with a nuclear state having symmetry Γ_{nspin} in the molecular symmetry group if the product of these symmetries $\Gamma_{\text{rve}} \otimes \Gamma_{\text{nspin}}$ contains Γ_{int} [35]. Γ_{int} is the complete internal wavefunction and must be antisymmetric with respect to any odd permutation of fermions. Therefore, Γ_{int} is $\Gamma_3^{+(-)}$ or $\Gamma_4^{+(-)}$ as the parity is + or - (see Table 7). (The second superscript in parentheses describes the classification in G_{16} and can be dropped in G_8 .) In G_8 , the proton spin functions of p DFB generate the representation $\Gamma_{\text{nspin}}^{\text{H}} = 10 \Gamma_1^+ \oplus 6 \Gamma_1^-$, whereas in G_{16} the hydrogen and fluorine nuclei have to be considered, generating the representation $\Gamma_{\text{nspin}}^{\text{F,H}} = 24 \Gamma_1^{++} \oplus 16 \Gamma_1^{+-} \oplus 12 \Gamma_1^{-+} \oplus 12 \Gamma_1^{--}$. The H_2O hydrogen nuclei generate the representation $\Gamma_{\text{nspin}}^{\text{H}} = 3 \Gamma_1^{+(+) } \oplus \Gamma_3^{+(+) }$. The derived nuclear spin statistical weights w are given in Table 7. It can be easily seen that only a large amplitude motion which interchanges the water hydrogens leads to the observed 1:3 intensity ratio between the two subbands A and B in the UV spectrum. An internal rotation of p DFB around its a inertial axis would give a 10:6 ratio and a rotation around its b or c axes would give a 7:9 ratio. Other factors could contribute to these ratios, but these factors are expected to be small at the vibrational temperatures typically achieved in our apparatus.

3.5.3. Analysis of internal motion.

More specific information about the motion of the water molecule in the complex comes from an analysis of the observed tunneling splitting of 3.63 GHz and the relatively small but

significant differences in the rotational constants of the two subbands in both electronic states (*cf.*, Table 5). The 3.63 GHz splitting of the two subbands is equal to the difference in the subtorsional splittings in the two electronic states because the observed transitions obey the selection rule $\Delta\sigma = 0$. The two subbands have different intensities since $\sigma = 0$ and 1 levels have different nuclear spin statistical weights. Also, each of the subbands has different rotational constants due to the coupling between torsional motion of water and overall rotation. The differences between the rotational constants of two subbands are calculated from $\Delta A'' = A_{v_0''} - A_{v_1''}$, $\Delta A' = A_{v_0'} - A_{v_1'}$ and so forth [36]. According to Table 5, the rotational constants of the two subbands of the water complex are the same to within the error limits except for the A values; $\Delta A'' = 0.4$ MHz in the ground state and $\Delta A' = 0.5$ MHz in the excited state. This shows that the axis about which the motion of the water molecule is primarily occurring in the two states is approximately the same, and further that this axis is approximately parallel to the a principal inertial axis of the complex.

As discussed in the analysis of the tunneling splitting in BN-water [34], there exist several possible models for the motion of the attached water molecule. All require the breaking and remaking of at least one of the hydrogen bonds (F---H-O or H---O-H). One of the simplest models is an internal rotation of the H₂O about its C₂-(b -)axis within a planar equilibrium structure. The spectrum was analyzed with a semirigid internal rotor model consisting of a rigid frame with C_s symmetry and one rigid internal rotor of C_{2v} symmetry [37, 38]. For each electronic state, the molecule-fixed axis system (x, y, z) was rigidly attached to the frame with its origin at the COM of the whole molecule. The z axis was chosen to be parallel to the internal rotation axis, and the y axis was chosen to be parallel to the complex c principal axis, perpendicular to the symmetry plane of the frame. In a least-squares fit, the moments of inertia of

the complex I_{xx} , I_{yy} , I_{zz} , and the potential term V_2 of the potential $V(\tau) = V_2(1 - \cos 2\tau)/2$ for both states were determined. The planar moment of the H₂O internal rotor P_x was fixed to the value obtained from ground state rotational constant $B_0 = 435$ GHz [39]. This procedure yields upper limits for the V_2 potential barriers of $V_2'' = 450$ cm⁻¹ and $V_2' = 290$ cm⁻¹. The angle θ between the internal rotation axis and the a principal axis of the complex was estimated to be about 70° in S_1 whereas no preferred orientation was found for S_0 . This result leads to a predicted subband splitting of 3.6 GHz, in good agreement with the experimental value of 3.63 GHz. However, it is clear that the axis about which the water molecule is moving in the ground state cannot be its b axis. Such a motion would require a breaking of the hydrogen bond, a much higher energy process than 450 cm⁻¹. With the value $\theta=70^\circ$ in the excited state, since the internal rotation axis also has a component along the b axis, the rotational B constant of the complex also should be perturbed. But no difference in the B values of the two subbands was observed.

In a second model, the water molecule was assumed to rotate about an axis in its bc plane, 55 ° off its b axis ($F = 339$ GHz [39]), which corresponds to a rotation about one of the lone pairs of the oxygen atom. This motion [40] leads to a barrier estimate of $V_2'' = 330 \pm 20$ cm⁻¹ in the ground state and $V_2' = 230 \pm 30$ cm⁻¹ in the excited state, with a predicted subband splitting of 3.33 ± 0.9 GHz, in good agreement with the experimental value of 3.63 GHz. However, this simple motion does not provide for the equivalent exchange of the two hydrogens, which is needed to reproduce the observed 1:3 intensity ratio.

In the third, and preferred model, the observed tunneling splitting and differences in rotational constants are attributed to the combined effects of inversion and restricted internal rotation, as shown in Figure 8. While this process may be visualized as consisting of two separate steps, switching of the lone pairs and restricted internal rotation of the water molecule,

the net effect is a C_2 rotation of the water about its b symmetry axis. The two motions taken together are equivalent to the “acceptor switching” motion in the H_2O dimer [41]. Importantly, the combined motion renders the two hydroxyl hydrogens equivalent, explaining the observed 1:3 intensity ratio.

In this model, the determined values of V_2 ($V_2'' = 330$ and $V_2' = 230$ cm^{-1}) are the effective barrier heights for the combined inversion-torsional motion. But we imagine that the two steps make different contributions to V_2 . The barrier to water inversion in ground state $pDFB$ -water is likely to be relatively low, probably much less than the 130 cm^{-1} barrier in the water dimer [41]. In contrast, the barrier to the torsional motion of the attached H_2O in $pDFB$ -water is likely to be higher, owing to the stronger $C-F\cdots H-O$ interaction. The strength of this interaction is significantly decreased in the S_1 state; a principal reason for this decrease is the electron density redistribution shown in Figure 9. As we have seen, the fluorine lone pair electron density in the S_1 state of $pDFB$ -water is significantly reduced, compared to the ground state, leading to a significantly reduced value of V_2 in the excited state. MP2/6-31G** calculations confirm that, in the ground state, the $C-F\cdots H-O$ binding energy is about 300 cm^{-1} , whereas the $C-H\cdots O-H$ binding energy is much weaker, 30 cm^{-1} or so.

The geometry of the $C-F\cdots H-O$ intermolecular interaction is considerably different from those of $O-H\cdots O$ and $O-H\cdots N$ hydrogen bonds. Whereas the normal hydrogen bonding angle is almost linear, the angle $C-F\cdots H$ is significantly decreased to around 110° [22], making for weaker interactions. In comparison with CH_2F_2 -water (~ 700 cm^{-1}) [23], our $O-H\cdots F$ intermolecular interaction (~ 300 cm^{-1} , including the water inversion motion) appears to be significantly weaker. Arguably, the acceptor ability of $C(sp^2)-F$ is not as good as that of $C(sp^3)-F$.

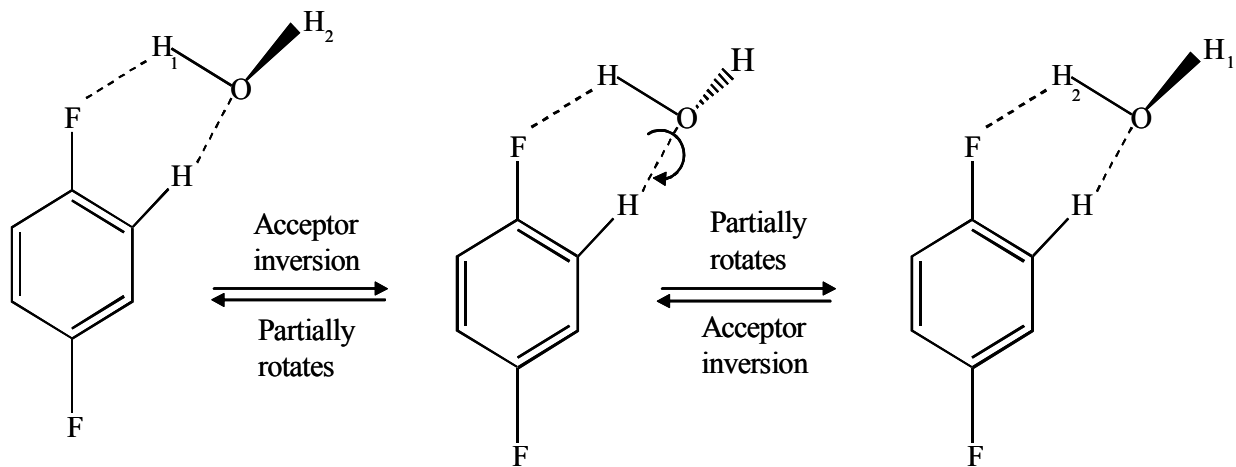


Figure 8. Combined inversion and restricted internal rotation of the water molecule in *p*DFB-H₂O.

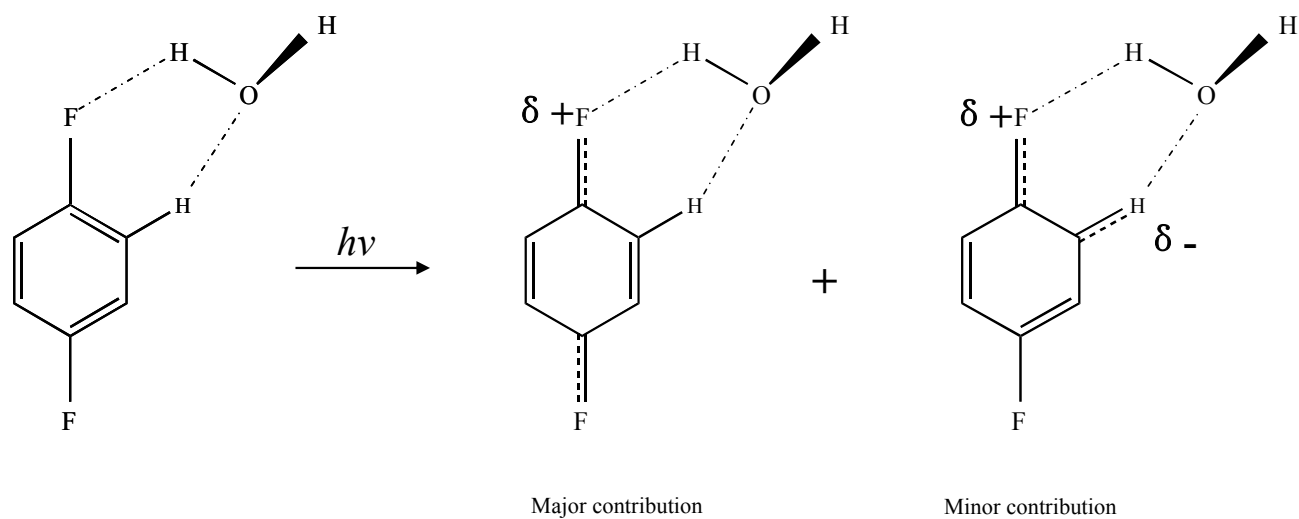


Figure 9. Light-induced changes in the electron distribution of *p*DFB are responsible for the differences in the intermolecular potentials of *p*DFB-H₂O in its ground and electronically excited states.

Still, the strength of any hydrogen bond depends more on donor acidity than on acceptor basicity, an effect that is nicely confirmed by comparisons of the properties of *p*DFB and BN water complexes. The V_2 barriers in the BN-water are nearly the same in both states [34]. There are obviously only very small changes in the electronic structure of BN upon excitation, which is also indicated by a small increase of its dipole moment (+0.09 D) [42].

3.6. Summary.

The structural and dynamical properties of a binary complex between *p*-difluorobenzene (*p*DFB) and water are revealed by studies of its high resolution electronic spectrum in the collision-free region of a molecular beam. The complex exhibits two hydrogen bonds, a stronger F---H-O bond in which the attached water molecule acts as a proton donor, and a weaker H---O-H bond in which the attached water molecule acts as a proton acceptor, resulting in a (heavy-atom) planar structure. The water molecule also is observed to move within the complex; the motion is a combined inversion-internal rotation; appeared by a barrier of $\sim 330 \text{ cm}^{-1}$ in the ground electronic state. Reduction of this barrier to $\sim 230 \text{ cm}^{-1}$ in the electronically excited state is attributed to light-induced changes in the π -electron distribution in the aromatic ring.

3.7. Acknowledgements.

We thank John T. Yi for helpful discussions. This work was supported by NSF (CHE-0315584).

3.8. References.

- [1] B. Brutschy, *Chem. Rev.* **100**, 3891 (2000)
- [2] K.S. Kim, P. Tarakeshwar, and Lee, J.Y., *Chem. Rev.* **100**, 4145 (2000)
- [3] M. Gerhards, M. Schmitt, K. Kleinermanns, and W. Stahl, *J. Chem. Phys.* **104**, 967 (1996)
- [4] G. Berden, W.L. Meerts, M. Schmitt, and K. Kleinermanns, *J. Chem. Phys.* **104**, 972 (1996)
- [5] S. Melandri, A. Maris, P.G. Favero, and W. Caminati, *Chem. Phys.* **283**, 185 (2002)
- [6] H.-D. Barth, K. Buchhold, S. Djafari, B. Reimann, U. Lommatzsch, and B.Brutschy, *Chem. Phys.* **239**, 49 (1998)
- [7] M. Becucci, G. Pietraperzia, M. Pasquini, G. Piani, A. Zoppi, R. Chelli, E. Castellucci, and W. Demtröder, *J. Chem. Phys.* **120**, 5601 (2004)
- [8] J.W. Ribblett, W. E. Sinclair, D. R. Borst, J.T. Yi, and D.W. Pratt, in press.
- [9] U. Spoerel, and W. Stahl, *J. Mol. Spectrosc.* **190**, 278 (1998)
- [10] M.J. Tubergen, A.M. Andrews, and R. L. Kuczkowski, *J. Phys. Chem.* **97**, 7451 (1993)
- [11] J.R. Carney, F.C. Hagemeister, and T.S. Zwier, *J. Chem. Phys.* **108**, 3379 (1998)
- [12] T.M. Korter, D.W. Pratt, and J. Küpper, *J. Phys. Chem. A.* **102**, 7211 (1998)
- [13] A.J. Gotch, and T.S. Zwier, *J. Chem. Phys.* **96**, 3388 (1992)
- [14] S. Suzuki, P.G. Green, R.E. Bumgarner, S. Dasgupta, W.A. Goddard, III, and G.A. Blake, *Science* **257**, 942 (1992)
- [15] H.S. Gutowsky, T. Emilsson, and E. Arunan, *J. Chem. Phys.* **99**, 4883 (1993)
- [16] R.N. Pribble, A.W. Garrett, K. Haber, and T.S. Zwier, *J. Chem. Phys.* **103**, 531 (1995)
- [17] T. Emilsson, H.S. Gutowsky, G. de Oliveira, and C.E. Dykstra, *J. Chem. Phys.* **112**, 1287 (2000)
- [18] A.W. Garrett, and T.S. Zwier, *J. Chem. Phys.* **96**, 3402 (1992)

- [19] R.N. Pribble, and T.S. Zwier, *Faraday Discuss. Chem. Soc.* **97**, 229 (1994)
- [20] N. Solcà, and O. Dopfer, *Chem. Phys. Lett.* **347**, 59 (2001)
- [21] V. Brenner, S. Martrenchard-Barra, P. Millie, C. Dedonder-Lardeux, C. Jouvet, and D. Solgadi, *J. Phys. Chem.* **99**, 5848 (1995)
- [22] P. Tarakeshwar, K.S. Kim, and B. Brutschy, *J. Chem. Phys.* **110**, 8501 (1999)
- [23] W. Caminati, S. Melandri, I. Rossi, and P.G. Favero, *J. Am. Chem. Soc.* **121**, 10098 (1999)
- [24] B.J. Smith, D.J. Swanton, J.A. Pople, H.F. Schaefer III, and L. Radom, *J. Chem. Phys.* **92**, 1240 (1990)
- [25] V.R. Thalladi, H.C. Weiss, D. Blaser, R. Boese, A. Nangia, and G.R. Desiraju, *J. Am. Chem. Soc.* **120**, 8702 (1998)
- [26] W.A. Majewski, J.F. Pfanstiel, D.F. Plusquellic, and D.W. Pratt, in *Laser Techniques in Chemistry*, edited by Myers A.B.; Rizzo, T., (Wiley, New York, **1995**), pp. 101-148.
- [27] S. Gerstenkorn, and P. Luc, Atlas du spectre d'absorption de la molecule d'iode (CNRS, Paris, **1978**).
- [28] R. Sussman, R. Neuhauser, and H.J. Neusser, *Can. J. Phys.* **72**, 1179 (1994) See also M. Schäfer, C.-H. Kang, and D. W. Pratt, *J. Phys. Chem. A.* **107**, 10753 (2003)
- [29] Described in D.F. Plusquellic, R.D. Suenram, B. Maté, J.O. Jensen, and A.C. Samuels, *J. Chem. Phys.* **115**, 3057 (2001)
- [30] J. Kraitchman, *Am. J. Phys.* **21**, 17 (1953)
- [31] R.M. Helm, H. Vogel, H.J. Neusser, V. Storm, D. Consalvo, and H. Dreizler, *Z. Naturforsch. Teil A* **52**, 655 (1997)
- [32] V. Storm, H. Dreizler, and D. Consalvo, *Chem. Phys.* **239**, 109 (1998)
- [33] S. Melandri, D. Consalvo, W. Caminati, and P.G. Favero, *J. Chem. Phys.* **111**, 3874 (1999)

- [34] M. Schäfer, D.R. Borst, D.W. Pratt, and K. Brendel, *Mol. Phys.* **100**, 3553 (2002)
- [35] P.R. Bunker, *Molecular Symmetry and Spectroscopy* (Academic Press, New York/San Francisco/London, **1979**).
- [36] X.Q. Tan, W.A. Majewski, D.F. Plusquellic, and D.W. Pratt, *J.Chem.Phys.* **94**, 7721 (1991)
- [37] A. Bauder, E. Mathier, R. Meyer, M. Ribeaud, and H.H. Günthard, *Mol. Phys.* **15**, 597 (1968)
- [38] M. Schäfer, *J. Chem. Phys.* **115**, 11139 (2001)
- [39] F.C. DeLucia, P. Helminger, R.L. Cook, and W. Gordy, *Phys. Rev.* **A5**, 487 (1972)
- [40] Actually, because of electron repulsion between the lone pairs of the fluorine and oxygen atoms, the water molecule does not freely rotate about the axis of the H---O-H hydrogen bond. The two hydroxyl hydrogens experience a simultaneous inversion in the course of its internal rotation motion.
- [41] R.S. Fellers, L.B. Braly, R.J. Saykally, and C. Leforestier, *J. Chem. Phys.* **110**, 6306 (1999) and references therein.
- [42] D.R. Borst, T.M. Korter, and D.W. Pratt, *Chem. Phys. Lett.* **350**, 485 (2001)

4. High resolution electronic spectra of 7-azaindole and its Ar van der Waals complex

Cheolhwa Kang, John T. Yi, and David W. Pratt*
Department of Chemistry, University of Pittsburgh,
Pittsburgh, Pennsylvania 15260, USA

4.1. Abstract.

Rotationally resolved fluorescence excitation spectra of the $S_1 \leftarrow S_0$ origin band of 7-azaindole (1H-pyrrolo (2,3-b) pyridine) and its argon atom van der Waals complex have been recorded and assigned. The derived rotational constants give information about the geometries of the two molecules in both electronic states. The equilibrium position of the argon atom in the azaindole complex is considerably different from its position in the corresponding indole complex. Further, the argon atom moves when the UV photon is absorbed. There are significant differences in the intermolecular potential energy surfaces in the two electronic states. A large, vibration-state dependent rotation of the $S_1 \leftarrow S_0$ electronic transition moment vector of 7-azaindole relative to that of indole suggests that these differences have their origin in S_1/S_2 electronic state mixing in the isolated molecule, a mixing that is enhanced by nitrogen substitution in the six-membered ring.

Accepted for publication in the *Journal of Chemical Physics*

4.2. Introduction.

The doubly hydrogen bonded dimer of 7-azaindole (7AI) has been extensively studied both in the gas phase and in the condensed phase [1-5]. This is because (7AI)₂ undergoes a double proton transfer reaction on excitation with light. Proton transfer (PT) reactions in electronically excited states are fundamentally important chemical reactions. They also play a crucial role in a large variety of photochemical and biological processes, such as DNA base-pair tautomerization.

The driving force for excited state PT in (7AI)₂ is the electronic rearrangement that occurs on excitation of its ground state (S₀) to the first $\pi\pi^*$ excited state (S₁). Studies of these two states of isolated 7AI and related molecules should aid in the elucidation of this dynamics and the tautomerization process. In the gas phase, the ¹L_b state is generally the lowest excited state in indole, with the ¹L_a – ¹L_b energy gap depending on attached substituents. In 7AI, a relatively small ¹L_a – ¹L_b gap has been reported.¹ Because the ¹L_a state is believed to be more polar than the ¹L_b state, it is preferentially stabilized by interaction with the environment, the result being that ¹L_a emission dominates in polar solvent and possibly also in (7AI)₂.

Kim and Bernstein [6] analyzed the nature of the first excited singlet states of 7AI and several of its complexes with rare gas atoms and other small molecules. Differences in their behavior compared that of indole were attributed to strong $\pi\pi^* - n\pi^*$ mixing and to the hydrogen atom attached to the pyrrole nitrogen of 7AI being out of the molecular plane in the S₁ state. Huang, *et al.* [7] also studied jet-cooled 7AI and 7AI clusters with polar solvent molecules. Their data suggest mixing with the ¹L_a (S₂) state rather than with an $n\pi^*$ state.

The character of an electronically excited state often is revealed by the orientation of its electronic transition moment (TM), in transitions from the ground state. The orientations of the TM's of the S₁ and S₂ states of 7AI have been determined both theoretically and experimentally. Catalan and Perez [8] predicted TM angles of +7.5° (S₁) and -13° (S₂) with respect to the *a*

inertial axis. Ilich [9] predicted TM angles of -0.8° (S_1) and -23° (S_2) using semiempirical INDO/S1-CI methods. From a CASSCF study, Borin and Serrano-Andres [10] suggested a value of $+27^\circ$ for the S_1 state. Experimentally, an evaluation of the S_1 - S_0 rotational contour by Hassan and Hollas [11] gave an *ab* hybrid band with 93 % *a*- and 7 % *b*-type character, resulting in an angle of $\pm 15^\circ$. Nakajima, *et al.* [12] obtained a value of $-16 \pm 5^\circ$ from studies of several azaindole-(H_2O)_{n, n=1,2,3} complexes in the gas phase. More recently, Meerts and co-workers [13] obtained the value -21° based on their analyses of the high resolution spectra of four different isotopomers of 7-azaindole. This study also provided accurate values of the rotational constants of both electronic states of the isolated molecule.

High resolution electronic spectroscopy is an extremely powerful tool for addressing such issues. Previously, we have used this method in a detailed study of indole and indole-Ar in their S_0 and S_1 electronic states [14]. Here, a comparable study of 7AI and its Ar complex is described that yields unique information about the position of attachment of the Ar atom to the 7AI frame, its large amplitude motions, and how these change when the photon is absorbed. These properties of 7AI are quite different from those of indole. The two molecules also have significantly differently oriented S_1 - S_0 TM's. Thus, their quite different properties appear to have their origin in differences in the electronic distributions of the two species, which may be traced to the single substitution of the nitrogen atom for the C7 carbon in the six-membered ring.

4.3. Experimental.

7AI (> 99.0 %) was purchased from Aldrich and used without further purification. N (and C)-Deuterated 7AI were prepared by dissolving 7AI in excess CH_3OD , stirring at room

temperature, and removing the solvent using a vacuum line. Dry argon gas (99.999 %) was used in all experiments.

High resolution data were obtained using a molecular beam laser spectrometer [15]. The molecular beam was formed by expansion of 7AI vapor (heated to ~ 350 K and seeded in Ar carrier gas) through a heated 240 μm quartz nozzle into a differentially pumped vacuum system. The expansion was skimmed 2 cm downstream of the nozzle with a 1 mm skimmer and crossed 13 cm further downstream by a CW ring dye laser operating with R590 and intracavity frequency doubled in BBO, yielding 100 – 200 μW of ultraviolet radiation. Fluorescence was collected using spatially selective optics, detected by a photomultiplier tube and photon counting system, and processed by a computerized data acquisition system. Relative frequency calibrations of the excitation spectra were performed using a near-confocal interferometer having a mode-matched FSR of 299.7520 ± 0.0005 MHz at the fundamental frequency of the dye laser. Absolute transition frequencies in the spectra were determined by comparison to transition frequencies in the iodine absorption spectrum [16] and are accurate to ± 30 MHz.

4.4. Results.

Figure 10 shows the rotationally resolved electronic spectrum of the origin band of 7AI. Since there is a strong central Q-branch ($\Delta J = 0$) as well as P- ($\Delta J = -1$) and R-branches ($\Delta J = +1$), we were able to simulate the spectrum using *a*-type selection rules with (ee) \leftrightarrow (eo) and (oe) \leftrightarrow (oo) for (K_a, K_c). About 250 resolved lines of the experimental spectrum were used for comparison with the simulated spectra. As initial estimates, we used microwave values [17] of the rotational constants for the ground state and theoretical (CIS/ 6-31G**) [18] values of the rotational constants for the excited state. These were varied in a least-squares fashion in the fit until the difference between the observed and calculated line positions was minimized. From the

fit, individual transitions could be identified in the spectrum. Analyses of these with Voigt profiles yielded Gaussian and Lorentzian linewidths of ~ 18 and ~ 35 MHz, respectively. The Lorentzian width corresponds to a lifetime of 4.3 ns.

A best fit of the observed intensities in the spectrum yields a band of $94.2 \pm 1\%$ *a*-type character and $5.8 \pm 0.4\%$ *b*-type character. From the relationship $\tan^2 \theta = I(b)/I(a)$, we calculate $|\theta| = 14.2 \pm 1.3^\circ$. Here, θ is the angle between the transition moment (TM) vector and the *a*-inertial axis (positive angles are measured in a counterclockwise fashion with respect to *a*, see Figure 11), and $I(b)/I(a)$ is the intensity ratio of the *a*- and *b*-type bands. The ratio of *a* and *b*-type band intensities gives us the magnitude of the TM orientation angle but not its sign.

Additional information is needed to determine the absolute orientation of the TM vector. We chose to study two isotopomers of 7AI to accomplish this objective. ND is the singly deuterated isotopomer in which hydrogen 1 is replaced by deuterium, and CD is the singly deuterated isotopomer in which hydrogen 3 is replaced by deuterium (*cf.* Fig. 11). Figure 12 shows their rotationally resolved electronic spectra. Each of these spectra is separated by less than 1 cm^{-1} owing to slight differences in the zero-point energies of the two electronic states. Despite the high density of lines, fits of each isotopomer in the S_1 - S_0 spectra of azaindole proved to be straightforward. The R branch of the bare molecule nearly overlaps with the P branch of ND, and the R branch of ND also overlaps with the P branch of CD.

We simulated the ND spectrum using microwave values of the rotational constants for the ground state [17] and the ΔA , ΔB and ΔC values of the unsubstituted molecule for the excited state. In the fit, unassigned lines in the portion of P branch of ND belonging to the R branch of 7AI and unassigned lines in the portion of the R branch of ND belonging to the P branch of the

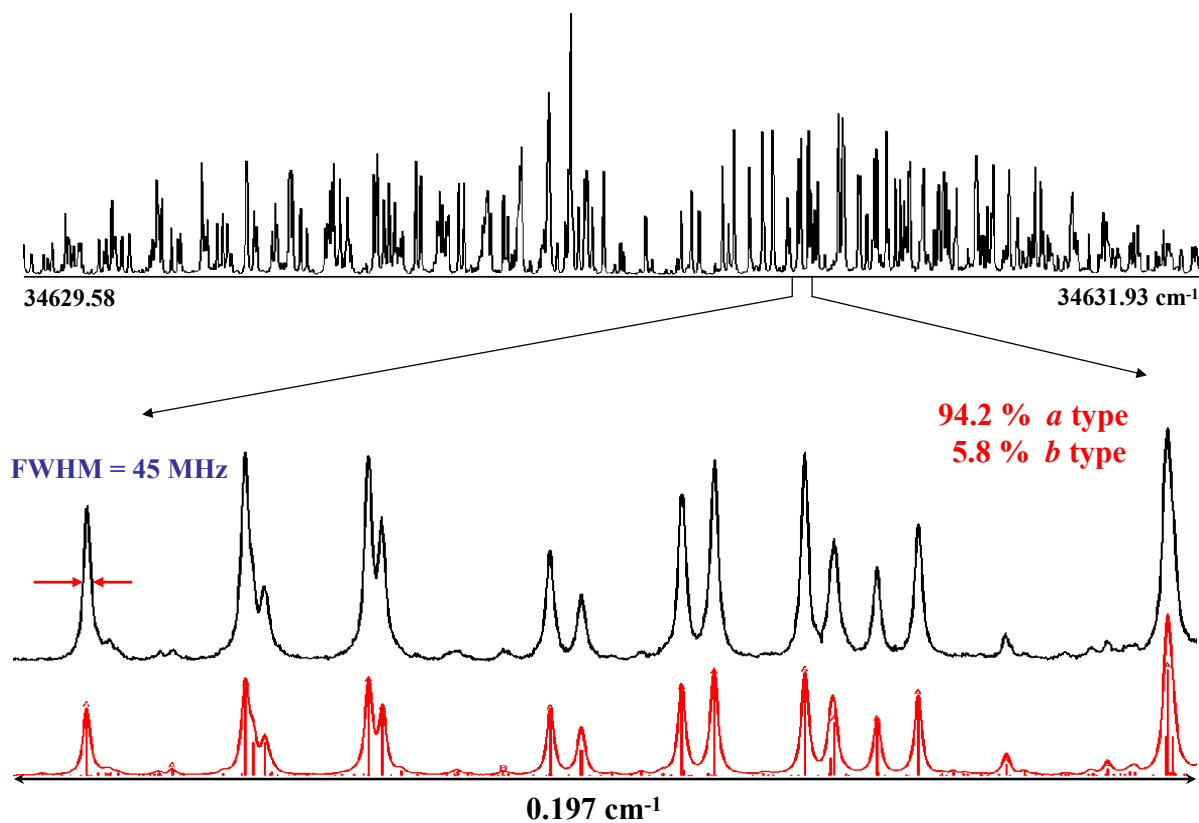
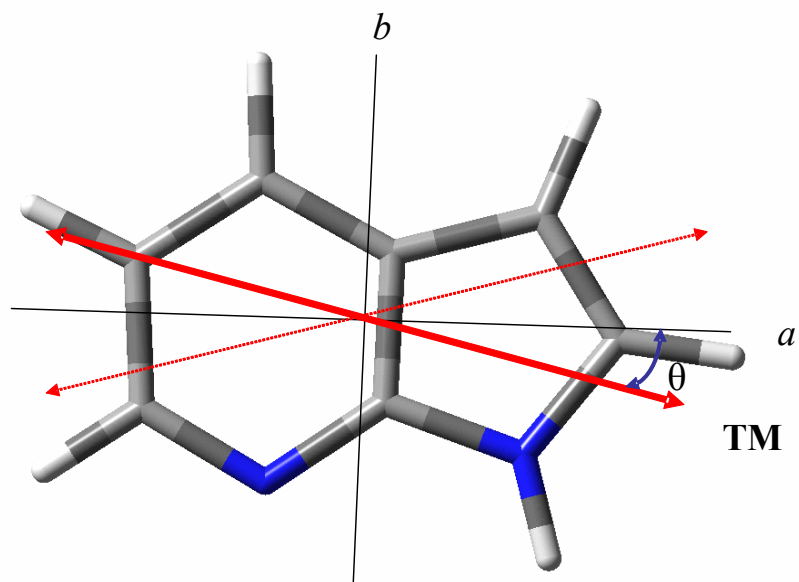


Figure 10. Rotationally resolved fluorescence excitation spectrum of the origin band of 7-azaindole. The top trace shows the overall experimental spectrum. The bottom traces show a $\sim 0.2 \text{ cm}^{-1}$ portion of the R branch at full experimental resolution and two simulated spectra, with and without a superimposed lineshape function.



$$\tan^2 \theta = I_b / I_a$$

$$\theta = -14.2 \pm 1.3^\circ$$

Figure 11. Two possible orientations of the $S_1 \leftarrow S_0$ electronic transition moment (TM) vector in 7-azaindole. Only $\theta = -14.2^\circ$ is consistent with the results of the isotopomer experiments.

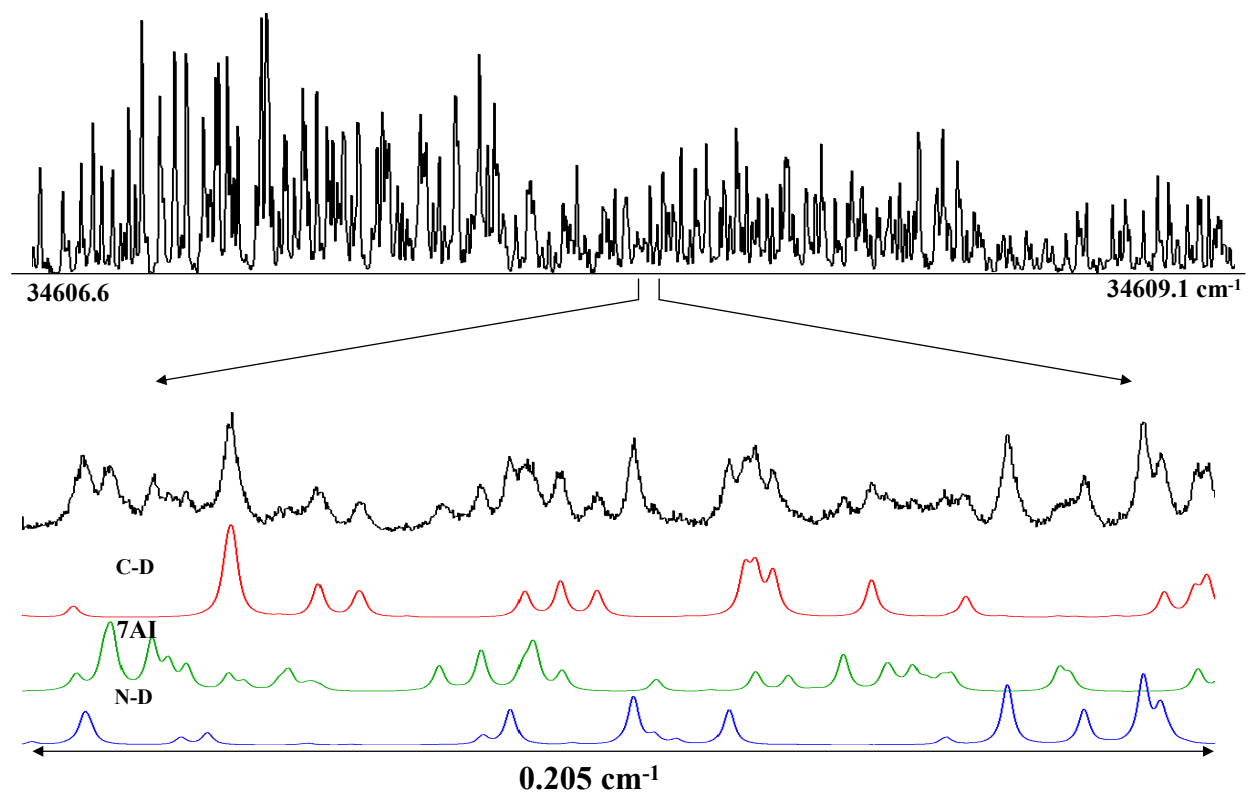


Figure 12. Rotationally resolved fluorescence excitation spectra of the origin bands of three different isotopomers of 7-azaindole. The top trace shows the overall experimental spectrum. The bottom traces show a $\sim 0.2 \text{ cm}^{-1}$ portion of the top trace at full experimental resolution and the contributions to this portion from the three different isotopomers.

CD isotopomer were identified. Then, the spectra of CD and 7AI itself were regenerated and moved along the frequency axis until all of resolved lines could be accounted for. The best fit simulated spectra of all isotopomers are shown in Figure 12. About 250 lines were fit for each of three isotopomers. And, most importantly, each spectrum exhibits a slightly different hybrid band character. ND has 96% *a* and 4% *b* character, and CD has 93% *a* and 7% *b* character.

The main idea behind this experiment is that the TM orientation is not influenced by deuterium substitution, but the *a* and *b* inertial axes are. By rotating these axes, we change the TM angle with respect to them, and change the relative intensities of *a*- and *b*-type transitions in the spectrum. If the angle is positive, *a*-type contributions should decrease in the ND isotopomer and increase in the CD isotopomer, as shown in Fig. 12. The opposite behavior is expected if the angle is negative. We find the latter behavior. Therefore, $\theta = -14.2 \pm 1.3^\circ$ in the parent molecule. Employing a similar strategy, but using GA methods to fit the spectra of four different isotopomers, Schmitt, *et al.* [13] found $\theta = -21^\circ$.

We also recorded high resolution spectra of some higher energy vibronic bands in 7AI. Figure 13 shows the results for the $+280\text{ cm}^{-1}$ band. The shape of this spectrum is quite different from that of the origin band. The relative intensity of the Q-branch is significantly decreased while that of the P- and R branches is increased, suggesting a significant rotation of the TM. To fit the spectrum, we independently simulated *a*-type and *b*-type bands and varied their relative intensities until they matched those that were experimentally observed. This spectrum was found to contain 36.8 % *a*-type character and 63.2 % *b*-type character, which yields a TM orientation of $|\theta| = 52.7 \pm 1.2^\circ$. This angle is significantly different from that of the origin band.

The rotationally resolved S_1 - S_0 electronic spectrum of the Ar complex of 7AI is shown in Figure 14. This band is red-shifted by 26 cm^{-1} compared to the origin of the bare molecule. The fitting procedure for this band began with the simulation of a spectrum using assumed geometries of the complex, with a single Ar atom attached on the top of the 7AI plane at a heavy atom separation of 3.5 \AA . This spectrum was then compared with the experimental one. This comparison reveals that the transitions involving high J ($J \geq 10$) are shifted from their predicted rigid rotor positions by as much as 100 MHz. Quartic distortion terms [19] were then included in the fit. When the Ar atom is attached, the inertial axes a , b , and c are reoriented. The orientations of all three inertial axes compared to those of the bare molecule were found to be significantly different; $\theta = 102.3^\circ$, $\varphi = 0.10^\circ$ and $\chi = 80.6^\circ$. This means that (approximately) the a inertial axis becomes the b inertial axis of the complex, b becomes c and c becomes a , respectively. This is shown in Figure 15. Also the center of mass coordinates were changed from (0,0,0) to (0.02, 0.12, 0.86 \AA) in the bare molecule coordinate system.

4.5. Discussion.

4.5.1. Nature of the S_1 electronic state of 7-azaindole.

Table 8 lists the rotational constants of the two electronic states of 7AI that were determined in this work and compares them with the corresponding values for indole.¹⁴ The rotational constants of the two molecules are qualitatively similar, with those of azaindole being slightly larger. The changes in these constants that occur when the photon is absorbed are also very similar. That the two sets of values for the two molecules are nearly the same is not surprising. Substitution of a CH group by a nitrogen atom should produce only small changes in

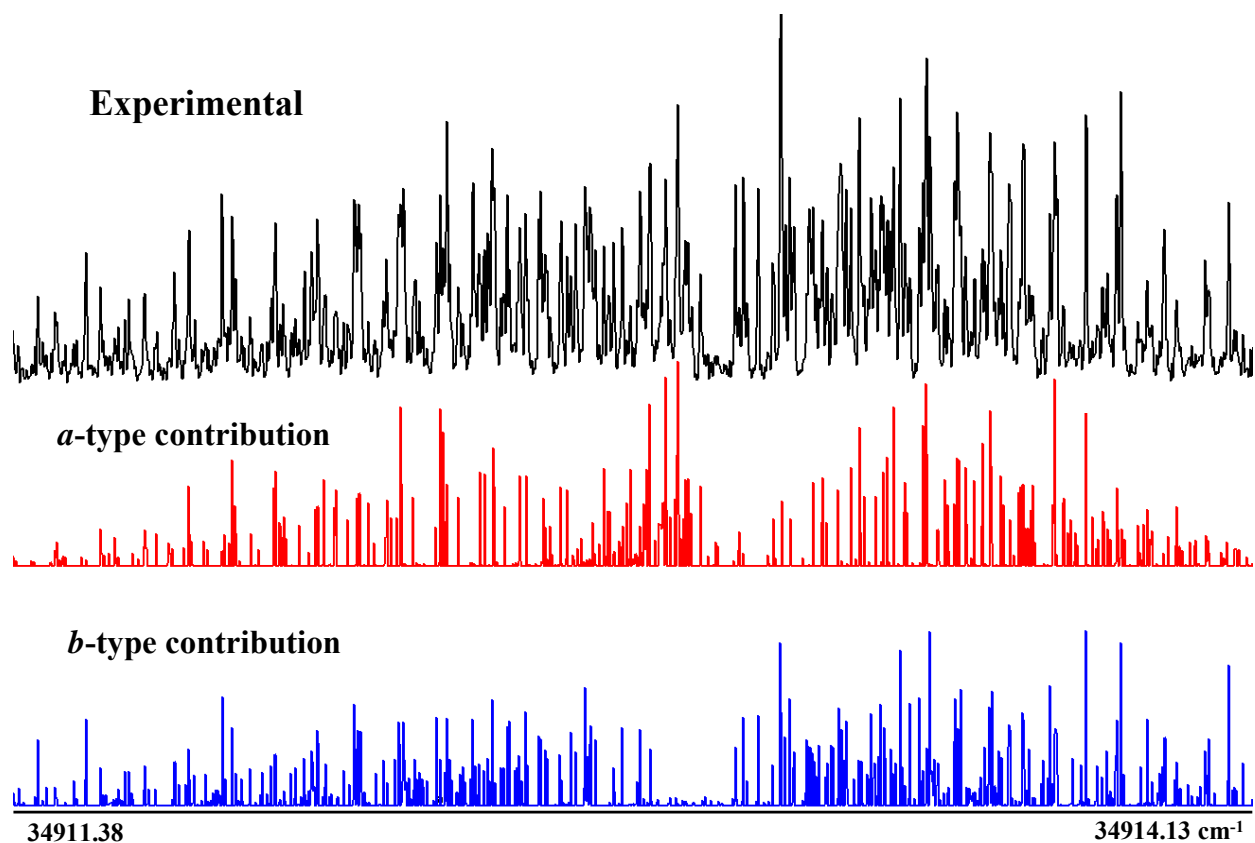


Figure 13. Rotationally resolved fluorescence excitation spectrum of the + 280 cm⁻¹ vibronic band of 7AI. The top trace shows the overall experimental spectrum, an *ab*-hybrid band. The bottom traces show “stick” spectra of the *a*- and *b*-type contributions to the observed spectrum.

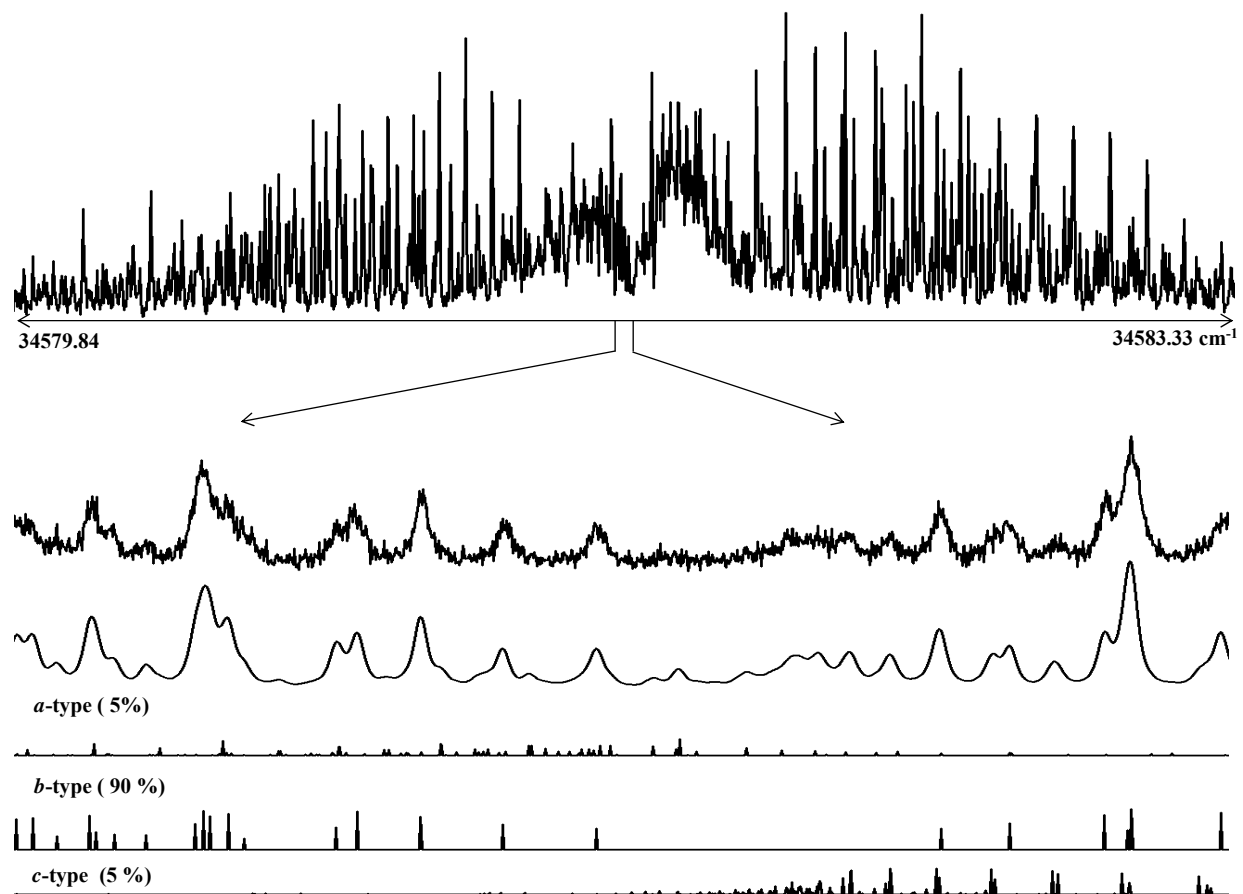


Figure 14. Rotationally resolved fluorescence excitation spectrum of the 7-azaindole-Ar complex. The top trace shows the overall experimental spectrum. The bottom traces show a $\sim 0.1 \text{ cm}^{-1}$ portion of the experimental spectrum and two simulations, with and without a superimposed lineshape function. The individual *a*-, *b*-, and *c*-type contributions are also shown.

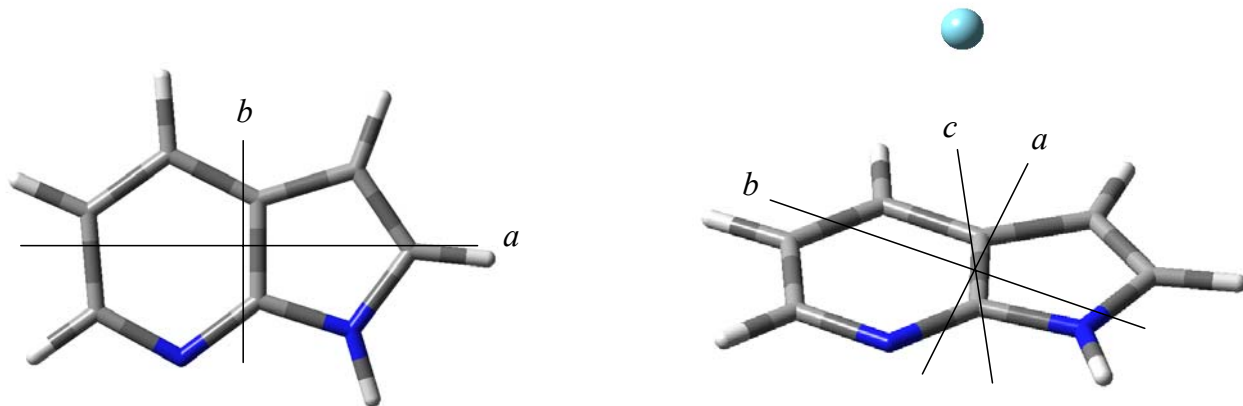


Figure 15. Three-dimensional structures of 7AI and the 7AI-Ar complex, showing the inertial axis reorientation on complex formation.

the moments of inertia about the three principal axes. In agreement with this, *ab initio* calculations (using the MP2/6-31G** method for the ground states and the CIS/6-31G** method for the excited states [18]) yield rotational constants for each state that are in excellent agreement with experiment ($\sim 0.2\%$ for the S_0 states and $\sim 2.5\%$ for the S_1 states).

Despite the similarities in their rotational constants, the S_1 - S_0 TM orientations of indole and azaindole are very different from each other. The S_1 origin band of indole is an *ab* hybrid band ($a/b = 61.6\% / 38.4\%$), with $\theta = +38.5^\circ$ [14]. The S_1 origin band of azaindole is a nearly pure *a*-type band, with $\theta = -13.9^\circ$. The distribution of electrons in S_1 azaindole must be very different from that in S_1 indole, despite the fact that the two states have very similar energies (35231.4 cm^{-1} for indole, 34630.7 cm^{-1} for azaindole). Unfortunately, equally reliable information about the origin of this effect cannot be obtained by the CIS method because the low-lying states of such molecules possess significant double excitation character [20].

Recent Stark-effect measurements on indole show that the lowest $\pi\pi^*$ transition in the isolated molecule is accompanied by a significant shift in electron density from the 5- to the 6-membered ring, resulting in a large change in the orientation of the electric dipole moment when the molecule absorbs light [21]. Similar effects have been observed in 7AI [22]. If there are differences in the orientations of the S_1 - S_0 TM's in the two molecules, these must be the result of differences in the electron distributions of the 6-membered rings, since the 5-membered rings in indole and 7AI are identical. Comparable 6-membered rings are found in aniline and 2-aminopyridine (2AP), respectively. Surprisingly, their S_1 - S_0 TM orientations also are very different from each other [23]. The 0_0^0 band of aniline is pure *b*-type, with $\theta(a) = -90^\circ$, whereas the 0_0^0 band of 2AP is an *ab*-hybrid type band, with $\theta(a) = -58^\circ$. 2AP and 7AI are N-heterocyclic

Table 8. Inertial parameters of 7-azaindole and indole in its ground and excited electronic states.

State	Parameter	7-azaindole	Indole
S_0	A, MHz	3928.3 (2)	3877.9 (1)
	B, MHz	1702.5 (1)	1636.1 (1)
	C, MHz	1188.2 (1)	1150.9 (1)
	$\Delta I, u \text{ \AA}^2$	-0.160	-0.099
S_1	A, MHz	3744.4 (3)	3743.2 (1)
	B, MHz	1701.7 (1)	1618.2 (1)
	C, MHz	1170.5 (1)	1130.2 (1)
	$\Delta I, u \text{ \AA}^2$	-0.210	-0.163

analogs of aniline and indole. Therefore, the aromatic nitrogen in the 6-membered ring (and, presumably, its lone pair of electrons) is responsible for the difference in the orientations of the S_1 - S_0 TM's in the two pairs of molecules. Each lone pair causes a rotation of the TM (and the nodal plane of the S_1 wavefunction) by more than 30° !

Next, we discuss the TM orientation in the $+280\text{ cm}^{-1}$ vibronic band of azaindole. In spite of its relatively low frequency, this band has a significantly rotated TM ($\theta = \pm 52.7^\circ$) compared to the origin band ($\theta = -13.9^\circ$). Table 9 lists the inertial parameters of $+280\text{ cm}^{-1}$ band compared to those of origin band. The two sets of ground state rotational constants are the same, showing that the two transitions originate in the same vibrational level. But, the A, B and C rotational constants of the corresponding S_1 vibrational levels are different. The inertial defect of the $+280\text{ cm}^{-1}$ level is significantly larger than that of the zero-point level of the S_1 state.

One explanation for this result is that the $+280\text{ cm}^{-1}$ band terminates in a vibrational level that is strongly coupled to the S_2 state, or perhaps is the origin of the S_2 - S_0 transition. The S_2 - S_0 TM is expected to be significantly rotated relative to the S_1 - S_0 TM, perhaps as much as 90° . And the $+280\text{ cm}^{-1}$ level appears to have out-of-plane character, based on its inertial defect. Fuke, *et al.*²⁴ carefully examined the $0 - 1050\text{ cm}^{-1}$ (280-289 nm) region of the absorption spectrum of jet-cooled 7AI and reported no $S_2 \leftarrow S_0$ vibronic bands. Sammeth, *et al.* [25] suggested that several high vibronic levels around 450 cm^{-1} above the L_b origin ($S_1 \leftarrow S_0$) in indole have $L_a(S_2 \leftarrow S_0)$ character by using polarized one-color two-photon fluorescence excitation techniques, both in the vapor phase and in a supersonic jet. The corresponding levels in 7AI might lie at lower energy.

Interestingly, our CIS/6-31G** calculations on 7AI give values of the TM angles that are in quite good agreement with experiment; $\theta = -23.4^\circ$ for the S_1 - S_0 transition and $\theta = +53.7^\circ$ for the

Table 9. Inertial parameters of 7-azaindole in its ground and excited electronic states

State	Parameter	Origin band	+280 cm ⁻¹ band
S_0	A, MHz	3928.3 (2)	3928.3 (2)
	B, MHz	1702.5 (1)	1702.5 (1)
	C, MHz	1188.2 (1)	1188.2 (1)
	$\Delta I, u \text{ \AA}^2$	-0.160	-0.160
S_1	A, MHz	3744.4 (3)	3818.0 (2)
	B, MHz	1701.7 (1)	1687.9 (1)
	C, MHz	1170.5 (1)	1171.2 (1)
	$\Delta I, u \text{ \AA}^2$	-0.210	-0.276

S₂-S₀ transition. It is possible that nitrogen atom substitution in the 6-membered ring reduces the contributions of double (and higher) excitations to the characters of the S₁ and S₂ states, making the CIS calculation more reliable in this case.

Another possible explanation for the “anomalous” polarization of the + 280 cm⁻¹ band is that it belongs to a tautomer of 7AI. 7AI has two hydrogen bonding sites, by donating the pyrrole proton and/or by accepting a proton at the pyridine nitrogen. Hydrogen bonding leads to self-association of 7AI in aprotic media; [1] 7AI also associates with various types of hydroxyl groups. If a simultaneous transfer of the two protons at these two sites occurs, the nitrogen in 7AI could undergo rehybridization and the 7AI tautomer (7H-Pyrrolo (2,3-b) pyridine) would be formed. The barrier to this process, prohibitive in the ground state, is reported to be reduced ten-fold in the excited state, to 600 ± 100 cm⁻¹ [2]. We calculated the S₁← S₀ transition of the 7 AI tautomer to be a weak transition, $f_{osc} = 0.05$, with its TM orientation collinear with the ring, making a large angle $\theta = +63.6^\circ$ with respect to the *a* inertial axis. This also is in good agreement with our experimental result. Stark experiments to determine the dipole moments of the two vibronic levels in question would help to determine which of these explanations is correct. The 7AI tautomer should have much larger dipole moments in both its ground and electronic excited states.

4.5.2. *Structure of 7-azaindole- Ar.*

Table 10 lists the inertial parameters of the Ar complex of 7AI and compares them with the corresponding values for the Ar complex of indole [14]. All three rotational constants of 7AI-Ar are different from those of 7AI itself. This indicates that the Ar atom is not attached to any of the bare molecule axes. Moreover, since the inertial defect ($\Delta I = I_c - I_a - I_b$) of complex is

significantly larger in magnitude ($\Delta I'' = -249.6$, $\Delta I' = -263.4 \text{ amu \AA}^2$), it is clear that the Ar atom lies above (or below) the bare molecule plane in both electronic states, as is also the case for indole-Ar [14].

More meaningful information about the position of the Ar atom in the 7AI frame can be determined using Kraitchman's equations [26]. In what follows, we use the differences in the rotational constants of 7AI and its Ar complex to determine the center-of-mass (COM) coordinates of the Ar atom in the principal axis frame of the bare molecule. The accuracy of this procedure depends on the reliability of the assumption that the attached mass does not change the inertial contributions of the mass centers that make up the original frame. Table 11 lists the results obtained, after a small correction of the rotational constants of the complex for centrifugal distortion effects. The out-of-plane coordinate ($|c| = 3.41 \text{ \AA}$) in the ground state of 7AI-Ar decreases on electronic excitation, to 3.38 \AA . This decrease is consistent with the observation that the origin band of complex is red-shifted relative to that of the bare molecule. The van der Waals interaction is stronger in the S_1 state of the Ar complex. The values of $|a|$ and $|b|$ in both states of complex are small, but not zero. The values are $|a| = 0.088$ and $|b| = 0.477 \text{ \AA}$ in the S_0 state and $|a| = 0.115$ and $|b| = 0.411 \text{ \AA}$ in the S_1 state. These non-zero values are most probably a consequence of displacements of the attached Ar atom from the COM, due to the anisotropic electron distribution of 7AI. The measured values represent vibrationally averaged displacements. They should be regarded as root-mean-square displacements averaged over the complete vibrational wavefunctions of the complex.

Table 11 also lists the COM coordinates of the Ar atom in indole-Ar, determined in the same way [14]. The out-of-plane $|c|$ coordinates in the two complexes in both states are essentially the same, consistent with their similar red shifts (-26 cm^{-1} in both species). The two

Table 10. Inertial parameters of 7-azaindole and its Ar complex in the zero-point vibrational levels of their S₀ and S₁ electronic states.

Parameter	7-Azaindole		7-Azaindole - Ar	
	S ₀	S ₁	S ₀	S ₁
A, MHz	3928.3 (3)	3744.4 (3)	1202.2 (1)	1185.1 (1)
B, MHz	1702.5 (1)	1701.7 (1)	1045.1 (1)	1044.8 (1)
C, MHz	1188.2 (1)	1170.5 (1)	772.3 (1)	781.5 (1)
$\Delta I, u \text{ \AA}^2$	-0.16	-0.21	-249.6	-263.4

sets of $|b|$ coordinates also are similar. But the two complexes have quite different $|a|$ displacement coordinates, $|a| = 0.088$ for 7AI-Ar and $|a| = 0.411 \text{ \AA}$ for indole-Ar in their ground electronic states. This comparison suggests that the intermolecular potentials of the two species are quite different, especially along the a axis. A similar situation occurs in the S_1 states of the two molecules (*cf.* Table 11).

Ab initio calculations [18] were performed on the ground states of the indole-Ar and 7AI-Ar complexes using the MP2/6-31G** method to explore this issue further. First, optimized geometries of indole and 7AI were determined using same basis set. Next, an Ar atom was attached perpendicular to the plane of the two molecules, fixed at the distance $|c| = 3.434 \text{ \AA}$ (3.408 \AA in 7AI-Ar). Then the Ar atom was moved along the a and b in-plane axes from -1 to $+1 \text{ \AA}$, in increments of 0.05 \AA . The origin $\{0,0\}$ lies at the COM of the bare molecule. The resulting potential energy surfaces of the two complexes are shown in Figures 16 and 17, as minimum energy paths along a . Both surfaces have two non-equivalent minima, at $\{-0.30, -0.45 \text{ \AA}\}$ and $\{0.85, -0.45 \text{ \AA}\}$ in indole, and at $\{-0.30, -0.45 \text{ \AA}\}$ and $\{0.45, -0.45 \text{ \AA}\}$ in 7AI. But the differences in energy between these two minima are very different in indole-Ar and in 7AI-Ar. The minimum with positive a is $\sim 50 \text{ cm}^{-1}$ lower in energy than the minimum with negative a in indole-Ar, giving a preferred binding site for the Ar atom that is shifted away from the center of ring and towards the nitrogen atom. This result has been confirmed by experiment [14]. In contrast, the energy difference between one side of the ring and the other side in 7AI-Ar is very small (Fig. 17). The barrier separating the two minima is very low, only $\sim 0.5 \text{ cm}^{-1}$, and is barely seen on the scale of figure, meaning that the Ar atom is not localized on one side or the other of the 7AI plane. Therefore, the vibrationally averaged probability density is spread out along a axis with maximum intensity near zero, in excellent agreement with our Kraitichman analysis result.

Table 11. Comparison of center-of-mass (COM) coordinates of the Ar atom in the principal axis frame of 7-azaindole in 7-azaindole-Ar, and of indole in the indole-Ar complex, as determined from a Kraitchman analysis.

State	Coordinate	7-Azaindole frame (Å)	Indole frame (Å)
S_0	$ a $	0.088(4)	0.411(1)
	$ b $	0.477(4)	0.4482(1)
	$ c $	3.4076(6)	3.434(4)
	$ r $	3.4420 (3)	3.4881(3)
S_1	$ a $	0.115(3)	0.3707(5)
	$ b $	0.411(4)	0.3727(5)
	$ c $	3.380(4)	3.400(4)
	$ r $	3.4069(3)	3.4410(3)

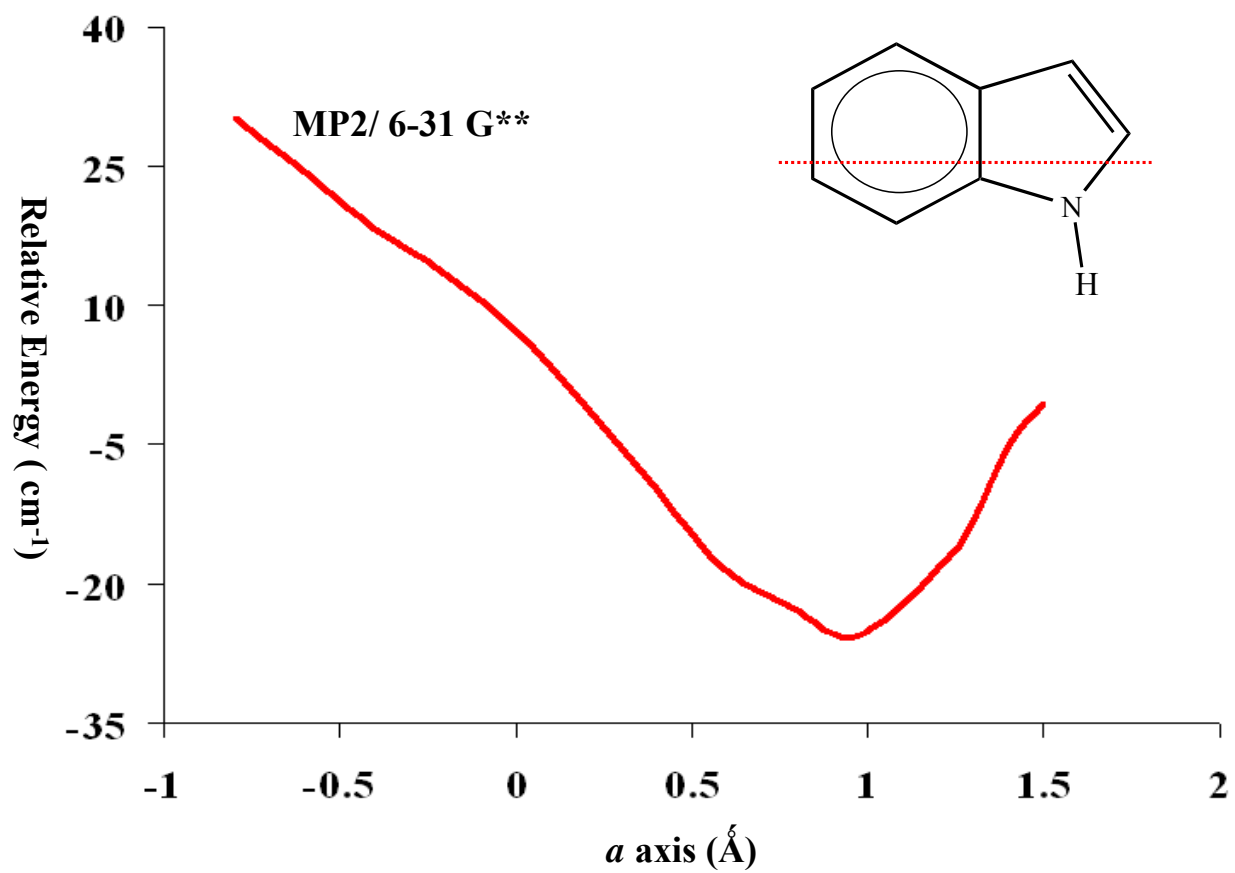


Figure 16. Potential profile of the intermolecular PES in the S_0 state of indole-Ar along the minimum energy path.

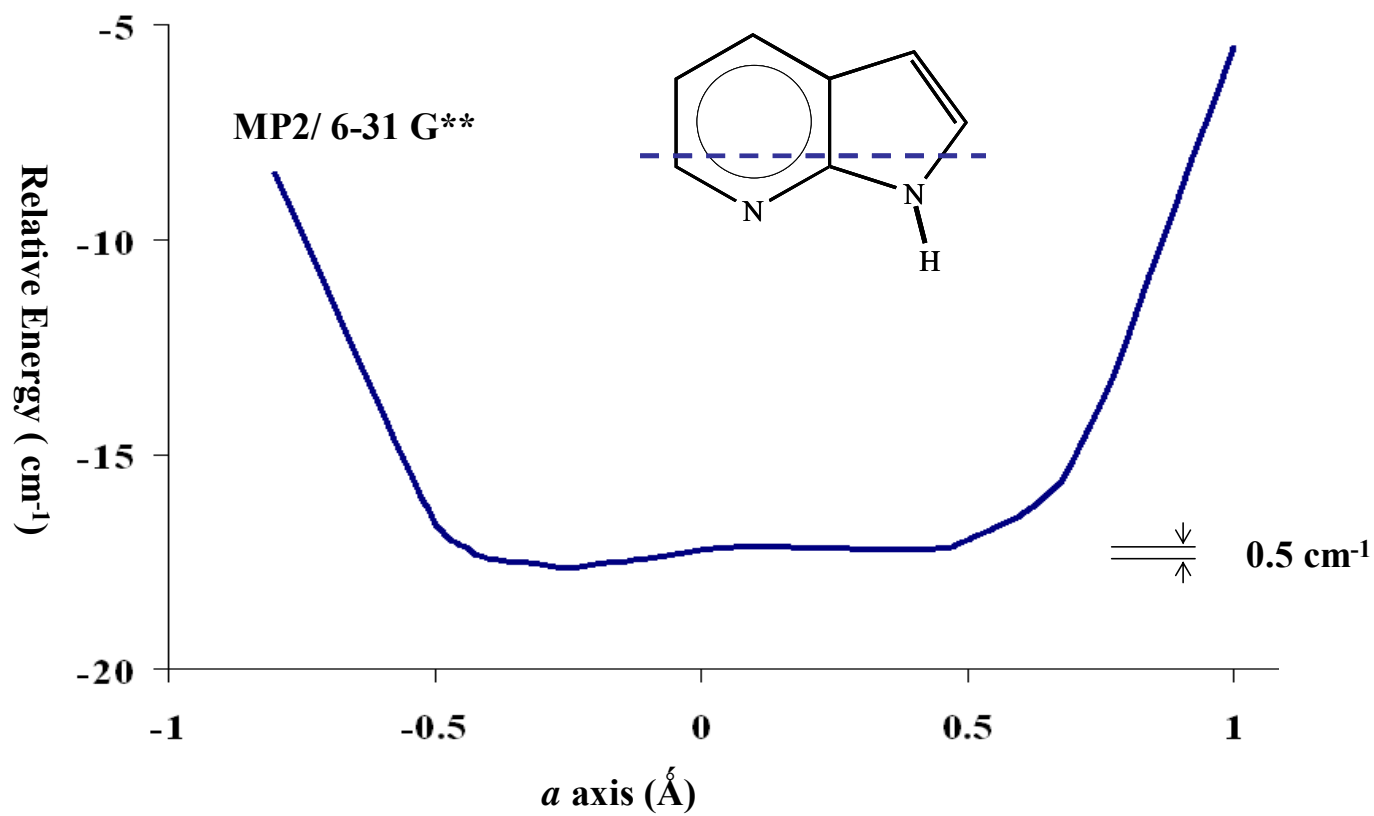


Figure 17. Potential profile of the intermolecular PES in its S_0 state of azaindole-Ar along the minimum energy path.

The main source of attraction that is responsible for the minima on these surfaces is likely to be a dipole-induced dipole interaction between the bare molecule and the Ar atom. Indole and 7AI are apparently very different in this respect. While the two host molecules have comparable dipole moments in their ground states, 1.963 D in indole [21] and 1.45 D in 7AI, [22] the orientations of these two dipoles are quite different. The dipole moment in indole is oriented along the N-C axis towards the benzene ring ($\theta_d = 45.5^\circ$) whereas the dipole moment in 7AI has a large component pointing towards the pyridine ring ($\theta_d = -24.1^\circ$). The (in-plane) nitrogen lone pair in 7AI makes a large contribution to this dipole. Thus, while there is only one attractive nitrogen atom in indole-Ar, there are two attractive nitrogen atoms in 7AI, which leads to a delocalization of the Ar atom. The Ar atom spends most of its time in between the two local minima. Recent Stark-effect measurements [22] have shown that electronic excitation of 7AI leads to large changes in both the magnitude and orientation of its dipole moment; μ_a increases by 53 % and μ_b decreases by 15 % in the S_1 state, compared to the ground state. The 0.03 Å (31 %) increase in $|a|$ and 0.07 Å (14 %) decrease in $|b|$ in the Ar complex of 7AI are likely consequences of this light-induced change in electronic distribution.

4.6. Summary.

We have observed and analyzed the rotationally resolved $S_1 \leftarrow S_0$ fluorescence excitation spectra of the origin and 280 cm^{-1} vibronic band of 7-azaindole (7AI), and of the single Ar atom van der Waals complex of 7AI, 7AI-Ar. The S_1 - S_0 transition moment orientation in 7AI has been determined to be -13.9° , very different from the corresponding TM of indole ($+38.5^\circ$). The corresponding TM of the $+280 \text{ cm}^{-1}$ band is significantly rotated relative to both of these values, owing either to strong S_1/S_2 mixing or to tautomerization of 7AI upon electronic

excitation. The vibrationally averaged position of the argon atom in 7AI is also very different from that in the analogous indole complex. All of these differences may be attributed to the changes in the electron distribution that are produced by the substitution of a nitrogen atom for the C7 carbon atom in the indole ring.

4.7. Acknowledgments.

This work has been supported by NSF (CHE-0315584).

4.8. References

- [1] C. A. Taylor, M. A. El-Bayoumi, and M. Kasha, *Proc. Natl. Acad. Sci. USA.* **63**, 253 (1969).
- [2] K. C. Ingham, and M. A. El-Bayoumi, *J. Am. Chem. Soc.* **96**, 167 (1974).
- [3] A. Douhal, S. K. Kim, and A. H. Zewail, *Nature.* **378**, 260 (1995).
- [4] K. Sakota, A. Hara, and H. Sekiya, *Phys. Chem. Chem. Phys.*, **6** 32 (2004)
- [5] S. K. Kim, E. R. Bernstein, *J. Phys. Chem.* **94** 3531 (1990)
- [6] Y. Huang, S. Arnold, M. Sulkes, *J. Phys. Chem.* **100**, 4734 (1996)
- [7] J. Caltalan, P. Perez, *J. Theor. Biol.* **81**, 213 (1979)
- [8] P. Ilich, *J. Mol. Struct.*, **354**, 37 (1995)
- [9] A. Nakajima, M. Hirano, R. Hasumi, K. Kaya, H. Watanabe, C. C. Carter, J. M. Williamson, T. A. Miller, , *J. Phys. Chem A*, **101**, 392 (1997)
- [10] A. C. Borin, L. Serrono-Andrés, *Chem. Phys* **262**, 253 (2000)
- [11] K. H. Hassan, J. M. Hollas, *J. Mol. Spec* **138**, 398 (1989)
- [12] M. Schmitt, C. Ratzler, K. Kleinermanns, W. L. Meerts, in press
- [13] W. A. Majewski, J. F. Pfanstiel, D. F. Plusquellic, and D. W. Pratt, in *Laser Techniques in Chemistry*, edited by A.B. Myers and T. R. Rizzo (Wiley, New York. 1995), pp.101
- [14] S. Gerstenkorn and P. Luc, Atlas du spectre d'absorption de la molécule d'iode (CNRS, Paris, 1978).
- [15] W. Caminati, S. D. Bernardo, A. Trombetti, *J. Mol. Struct.* **223**, 415 (1990)
- [16] M. J. Frisch, G. W. Trucks, H. B. Schlegel, P. M. W. Gill, B. G. Johnson, M. A. Robb, J.R.Cheeseman, T. Keith, G.A. Petersson, J.A. Montgomery, K. Raghavachari, M.A. Al-Laham, V.G. Zakrzewski, J.V. Ortiz, J.B. Foresman, J. Cioslowski, B. Stefanov, A. Nanyakkara,

M.Challacombe, C.Y. Peng, P.Y. Ayala, W.Chen, M.W. Wong, J.L. Andres, E.S. Replogle, R.Gomperts, R.L. Martin, D. J. Fox, J.S. Binkley, D.J. Defrees, J. Baker, J.P. Stewart, M. Head-Gordon, C. Gonzalez, and J.A. Pople, *Gaussian 98*, Revision A9; Gaussian, Inc.: Pittsburgh, PA, 1998..

[17] J. K. G. Watson, *Vibrational Spectra and Structure*; Durig, J. R., Ed.; Elsevier: Amsterdam, 1977; Vol. 6, pp. 1.

[18] C.-H. Kang, J. T. Yi, D. W. Pratt, in press

[19] D. M. Sammeth, S. Yan, L. H. Spangler, P.R. Callis, *J. Amer. Chem. Soc.*, **94**, 7340 (1990)

[20] K. Fuke, I. Yoshiuchi, K. Kaya, *J. Phys. Chem.* **88**, 5840 (1984)

[21] J. Kraitchman, *Am. J. Phys.* **21**, 17 (1953)

[22] T. M. Korter, J. Küpper, D.W. Pratt, *J. Chem. Phys.* **111**, 3946 (1999)

5. Experimental measurement of the induced dipole moment of an isolated molecule in its ground and electronically excited states. Indole and indole-H₂O.

Cheolhwa Kang, Timothy M. Korter[†] and David W. Pratt*
Department of Chemistry, University of Pittsburgh
Pittsburgh, Pennsylvania 15260 USA

5.1. Abstract.

Reported here are measurements of the magnitude and orientation of the induced dipole moment that is produced when an indole molecule in its ground S₀ and electronically excited S₁ states is polarized by the attachment of a hydrogen bonded water molecule in the gas phase complex indole-H₂O. We find the permanent dipole moment values $\mu_{IW}(S_0) = 4.4$ and $\mu_{IW}(S_1) = 4.0$ D, values that are substantially different from calculated values based on vector sums of the dipole moments of the component parts. From this result, we derive the induced dipole moment values $\mu^*_I(S_0) = 0.7$ and $\mu^*_I(S_1) = 0.5$ D. The orientation of the induced moment also is significantly different in the two electronic states. These results are quantitatively reproduced by a purely electrostatic calculation based on *ab initio* values of multipole moments.

[†]: *Department of Chemistry, Syracuse University*
Syracuse, New York 13244 USA

Published in the *J. Chem. Phys.* **122**, 174301 (2005).

5.2. Introduction.

A common method for measuring the ground state dipole moments of polyatomic molecules is through the Stark effect in microwave spectroscopy [1]. However, gas phase measurements of electronically excited states are not common. Freeman and Klemperer [2] were the first to determine the excited state dipole moment of an isolated polyatomic molecule, formaldehyde. Later, Lombardi [3] made important progress in the measurement of the excited state dipole moments of small aromatic molecules using the Stark effect on partially rotationally resolved electronic spectra. For example, a study of indole [4] indicated that excitation to S_1 produced a small change in the dipole moment of the molecule parallel to its long a -axis ($|\Delta\mu_a| = 0.14$ D, $\Delta\mu_b$ undetected). The introduction of the fully rotationally resolved electronic spectroscopy of large sized molecules in the early 1980s [5] allowed Hese and co-workers [6,7] to accurately measure the excited state dipole moments and polarizabilities of some naphthalenes. More recently, this technique has been applied to aniline, benzonitrile, aminobenzonitrile, and m -aminophenol as isolated molecules in the gas phase [8-10]. These measurements revealed that both the magnitude and the orientation of μ can change dramatically when a species absorbs light.

Here, we report an extension of this technique to the binary molecule complex indole- H_2O . Each of the component parts of this complex possesses permanent electric dipole moments; in fact, it is the mutual attraction of these two dipoles that leads to the formation of a strong hydrogen bond between them. But the primary focus in this project is the induced dipole moment in the complex; water with its dipole moment μ_W can induce a dipole μ_I^* in the neighboring polarizable indole molecule, and *vice versa*. Our hypothesis is that by measuring the permanent dipole moment μ_{IW} of indole- H_2O in both electronic states, we can estimate both the magnitude

and orientation of μ^*_I in both electronic states by comparing the values of μ_{IW} with the corresponding values of μ_I and μ_W of the component parts.

Dipole-induced dipole interactions are a subject of much modern research. One method of evaluating them is the method of distributed multipole analysis (DMA) and the related distributed polarizability analysis first introduced by Stone [11,12]. In this method, each atom of the molecule is polarized by the non-uniform (multipole) electric field of its partners. Thus, the response of the charge density to an external field or dipole is widely distributed over the molecule, rather than concentrated at a single center. The key feature of this model is the accurate calculation of the electrostatic energy from a set of point multipoles on each atom, which are determined by a DMA of an *ab initio* wavefunction. The distributed multipoles on each atom are a measure of the nonsphericity of the local charge distribution, and reflect the details of the charge distribution in accordance with simple bonding theory. This method has successfully predicted the structure of several hydrogen bonded complexes [13,14].

A second method that may be used to estimate induced dipole moment utilizes the first few molecular multipole moments and polarizabilities. For example, an induced dipole moment of a complex can be represented as the projection of the moments induced on each subunit by its partner, including up to the molecular quadrupole moment. Even in small complexes, there are substantial induced dipole moments; 0.482 D in OC-BF₃ [15], 0.388 D in OC-HCl [16], and 0.446 D in CO₂-HCl [17]. Despite concerns about the possible breakdown of this “purely electrostatic” approach at small intermolecular separations, reasonable agreements between the calculated and observed values were reported in all of these cases.

Indole was chosen as the first candidate for an application of this technique because it is the chromophore in tryptophan [18]. Tryptophan dominates the near UV absorption and emission

spectra of proteins [19]. The variable red shift of its fluorescence maximum from ~ 300 to ~ 350 nm is a useful diagnostic of protein structure [20]. The magnitude of this shift has been correlated with the local environment to which the tryptophan residues are exposed. This phenomenon is referred to as solvatochromism [21]. When a molecule is electronically excited, the solvation energies of the initial and final states are different, and the result is a shift of the emission maximum. The magnitude of the solvatochromic shift depends upon the nature of the local solvent environment, but more importantly upon changes in the electron distribution in the solute. These changes are revealed by differences in the values of the ground and excited state dipole moments.

A recent theoretical study by Callis and Burgess [22] shows that changes in the excited state dipole moment of the indole moiety can almost entirely account for the shifts in the fluorescence maxima of tryptophan in proteins. Theoretical studies have yielded an assortment of values for these dipole moments, ranging from 0.85 [23] to 2.83 D [24] for the 1L_b (S_1) state and 3.22 [25] to 5.87 D [24] for the 1L_a (S_2) state. However, the 1L_a state is consistently found to possess a significantly greater dipole moment than the ground state (1.86 [23] to 2.22 D [24]) while the dipole moment of 1L_b state exhibits little change upon excitation.

Experimental values of the dipole moments of the 1L_a and 1L_b electronic states are less common than their theoretical counterparts. Condensed phase measurements have yielded dipole moments of 5.44 D for the 1L_a state and 3.45 D for the 1L_b state [26]. These results are difficult to interpret due to the many, complicated interactions between the solute and the surrounding solvent [27]. These complications can be removed by performing the dipole moment measurements in the gas phase.

5.3. Experimental .

High resolution data were obtained using the molecular beam laser spectrometer described in detail elsewhere [28]. The apparatus has been modified to generate a homogeneous, static electric field in the laser/molecule interaction region for the Stark-effect measurements [8]. The molecular beam was formed by flowing Ar carrier gas (500 Torr) over indole (heated to ~ 375 K) and expanding the resulting mixture through a heated 280 μm quartz nozzle into a differentially pumped vacuum system. Indole ($> 99\%$) was purchased from Aldrich and used without further purification. For indole-water, Ar carrier gas was first flowed over room temperature water and then over indole before being introduced into the vacuum system. The expansion was skimmed 2 cm downstream with a 1 mm skimmer. It was then crossed 13 cm further downstream by a continuous-wave ring dye laser operating with R590 and intracavity frequency doubled in BBO (~ 400 μW of ultraviolet radiation). Two spherical mirrors are positioned one above and one below the intersection of the laser and molecular beams to collect the fluorescence. The top mirror has a focus at the intersection and the bottom mirror is focused at a hole (2 mm) drilled in the center of the top mirror. Using these spatially selective optics, the Doppler-limited spectral resolution is 18 MHz in the UV.

Inside the spherical collecting mirrors, two stainless steel wire grids were placed one above and one below the laser/molecular beam plane, separated by ~ 1 cm with ceramic spacers. Two power supplies were used to hold one grid at some positive voltage and the other at some negative voltage relative to a common ground. This experimental setup yields an electric field perpendicular to the polarization of the laser radiation and thus forces a selection rule of $\Delta M = \pm 1$. The collected fluorescence was detected with a photomultiplier tube and photon counting system, and processed by a computerized data acquisition system. Relative frequency calibrations of the spectra were performed using a near-confocal interferometer having a mode-

matched FSR of 299.7520 ± 0.0005 MHz at the fundamental frequency of the dye laser. Absolute frequencies in the spectra were determined by comparison to transition frequencies in the I_2 absorption spectrum and are accurate to ± 30 MHz [29]. Electric field strengths were calibrated using the known value of μ_a in the ground state of aniline [30] and the combination-difference method of spectral assignment. The aniline calibration yielded an effective electrode separation of 0.982 ± 0.004 cm.

5.4. Results and Interpretation.

Three steps are necessary to determine the induced dipole moment in indole- H_2O . First, we study the effect of an applied electric field on the fully resolved electronic spectrum of indole itself and use the results to determine the values of the permanent dipole moments of its S_0 and S_1 states. Next, we perform a similar study of the indole- H_2O complex. Finally, we compare the results of these two studies to extract the value of $\mu_{I_1}^*$, the induced dipole moment of an indole molecule that is polarized by the attached water molecule, in both electronic states.

5.4.1. Indole.

The zero-field rotationally resolved electronic spectrum of the 0_0^0 band of indole is shown in Figure 18a. It is similar in all respects to the spectrum recorded by Philips and Levy, [31] Berden, *et al.* [32] and Korter, *et al.* [33] The S_1 origin band of indole is an *ab*-hybrid band composed of 61.6% *a* type character and 38.4% *b* type character with $\theta_{TM} = + 38.3^\circ$. Thus established unambiguously is the 1L_b character of the S_1 state of the isolated molecule.

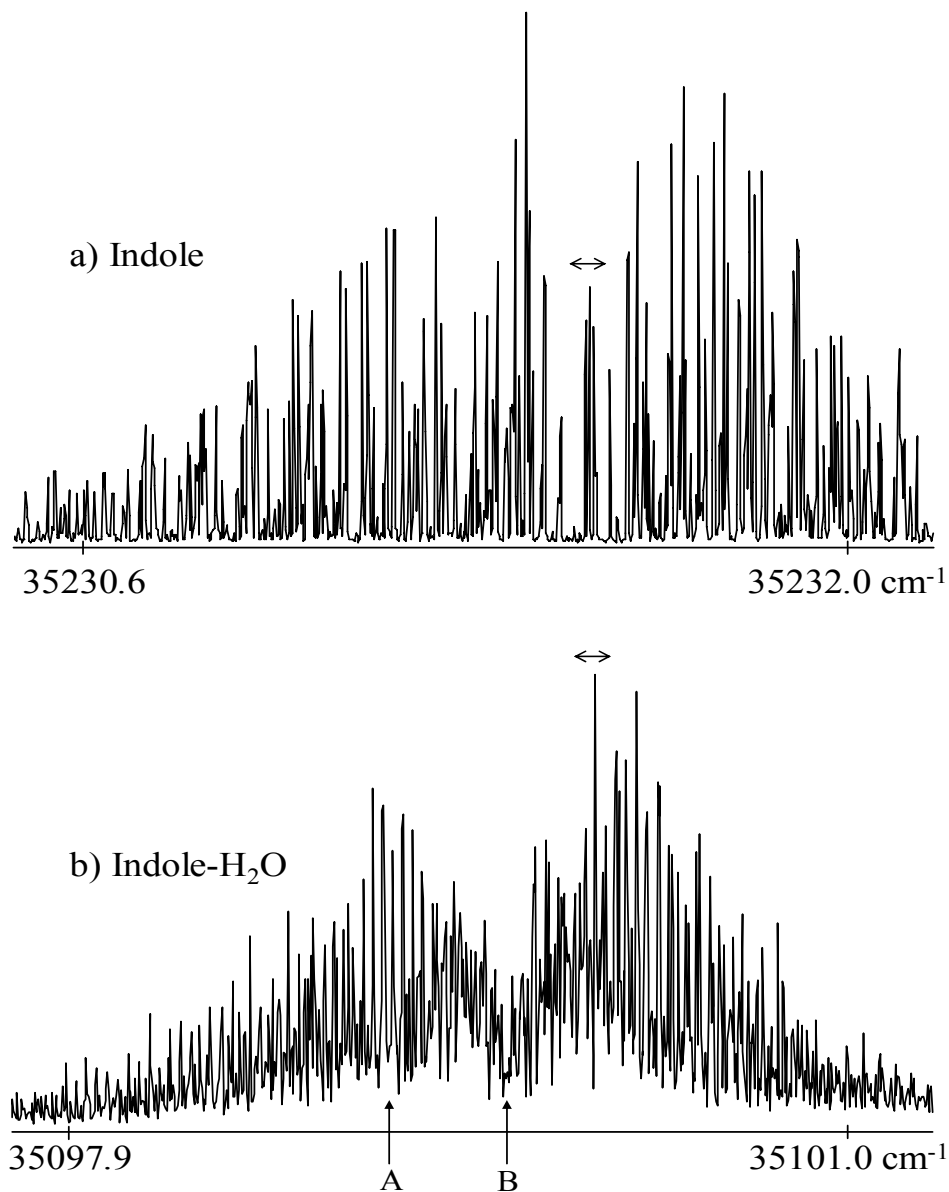


Figure 18. Rotationally resolved fluorescence excitation spectra near 284 nm of the origin bands in the $S_1 \leftarrow S_0$ transitions of (a) bare indole at 35231 cm^{-1} and (b) the indole-water complex at 35099.5 cm^{-1} . A and B indicate the origins of the $A' \leftarrow A''$ and $B' \leftarrow B''$ subtorsional bands, respectively, in the complex spectrum.

Figure 19 shows a small portion ($\sim 0.1 \text{ cm}^{-1}$) of the zero-field spectrum extracted from near the band center and how it is influenced by the application of a static electric field. Even at the smallest electric field value reported here (509 V/cm), there are detectable changes in the spectrum as the M degeneracy is lifted. The original zero-field transitions break apart into new $M' \leftarrow M''$ transitions and shift well beyond the experimental linewidth (FWHM) of 23 MHz (18 MHz Gaussian component and 10 MHz Lorentzian component).

Our first goal is to use these new, shifted transitions to experimentally determine the values of indole's permanent dipole moment in its S_0 and S_1 electronic states. Toward this end, we utilize all resolved lines to make a fit of the entire spectrum, not just fits of selected regions. These global fits are based upon assignments made of many different transitions with an assortment of quantum numbers and band types. The assignment of perhaps hundreds of transitions within a single spectrum enables us to accurately determine the different components of a molecule's dipole moment, and thus to also determine its orientation in the molecular frame.

To ensure accuracy over a wide range of transition types, we performed exact diagonalizations of truncated matrices to fit our spectra instead of using perturbation theory. The Hamiltonian is

$$\mathbf{H} = \mathbf{H}_r + \mathbf{H}_e \quad (1)$$

where \mathbf{H}_r is the rigid-rotor Hamiltonian,

$$\mathbf{H}_r = AJ_a^2 + BJ_b^2 + CJ_c^2 \quad (2)$$

and \mathbf{H}_e is the Stark Hamiltonian,

$$\mathbf{H}_e = -\underline{\mu} \cdot \underline{E} = -E_z \sum_{g=a,b,c} \mu_g \phi_{zg} \quad (3)$$

Here, A, B, and C are the rotational constants; J_a^2 , J_b^2 , and J_c^2 are the projections (squared) of the

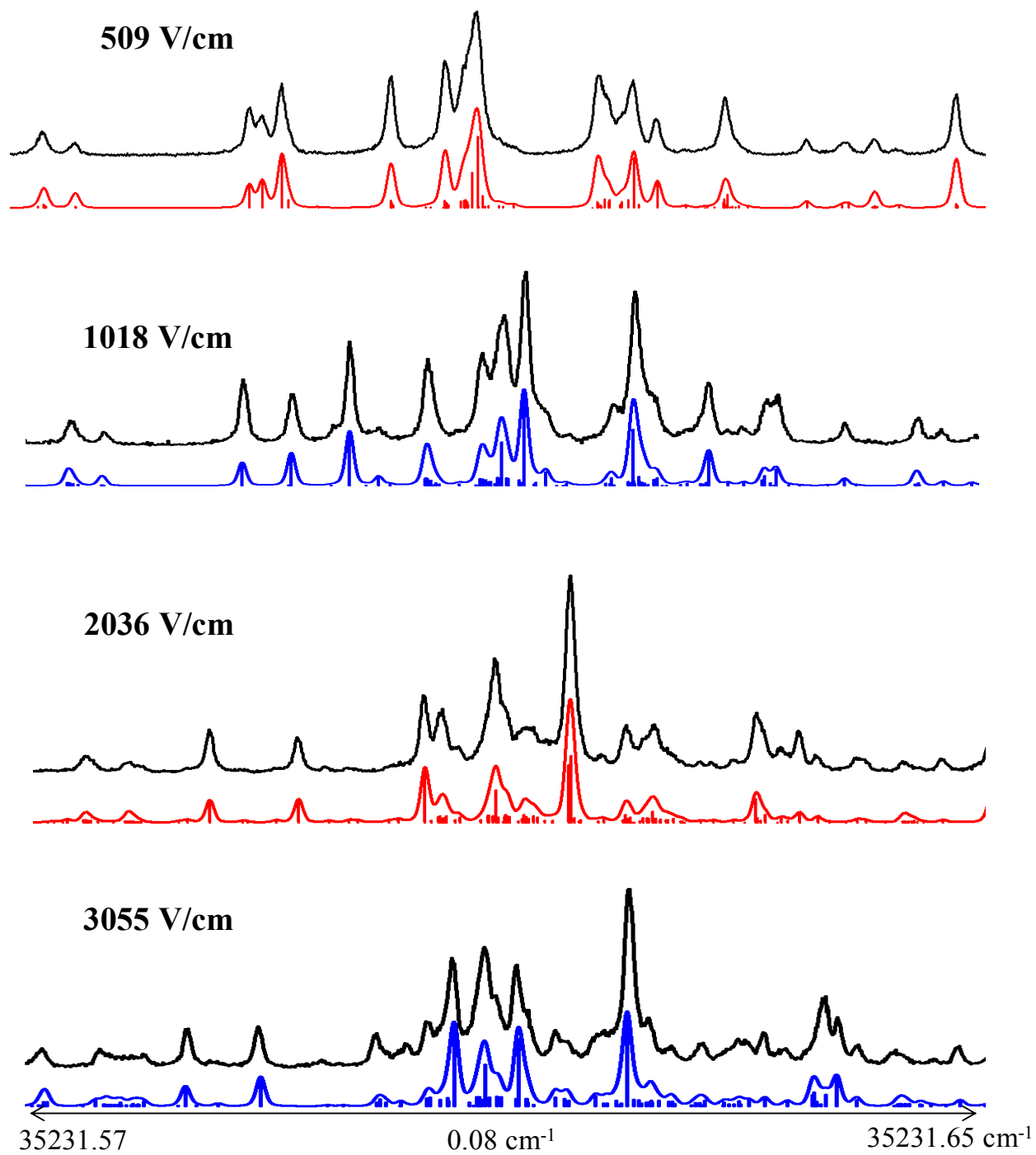


Figure 19. The Stark effect in indole. Portion of the rotationally resolved spectrum of indole extracted from near the band origin (see Fig.18) showing the large perturbations in the spectrum due to an applied electric field.

total rotational angular momentum on the inertial axes; E_Z is the applied electric field; μ_g ($g = a, b, c$) are the projections of μ on the inertial axes, and ϕ_{Zg} are the relevant direction cosines. In a basis of symmetric top functions $|JKM\rangle$, \mathbf{H}_r is diagonal in J and M but nondiagonal in K , making it easily separable into different matrices for each value of J , of size $2J + 1$. By choosing the space-fixed axis Z to be the electric field axis, \mathbf{H}_e is diagonal in M but nondiagonal in J and K ; a given J is connected to adjacent $J \pm 1$ blocks in the infinite energy matrix. Thus, to fit our spectra we diagonalized a matrix of elements for $J-1, J$, and $J + 1$ (of dimension $6J + 3$) for each value of J , extracted the relevant eigenvalues and eigenvectors, and discarded those corresponding to the $J-1$ and $J+1$ blocks, for each electronic state.

The computer program used for the simulating and fitting of Stark effect spectra in the UV is called DBSROT [34]. It has been designed to handle a wide range of problems that may be encountered in the analysis of high resolution spectra. The program utilizes Watson's Hamiltonian [35] for the distortable asymmetric rotor and the internal axis method [1,36] to describe the hindered torsional motions of methyl groups. It also includes Eulerian angles to treat the phenomenon of inertial axis-tilting [37].

The fit of the indole Stark effect spectra began by simulating spectra using known S_0 and S_1 rotational constants [32] as well as previously published values for the μ_a and μ_b components of μ in the ground state [38] and μ_a in the excited state [4]. The strength of the electric field is also a required parameter and is known from calibration experiments (*vide supra*). Initial work focused on the lowest electric field strength spectrum (509 V/cm) in order to better track the new transitions as they emerged from their original degenerate positions. After calculating the transition frequencies and intensities (assuming a - and b -type selection rules), the calculated spectra were then compared to those observed experimentally. The quantum numbers of the

observed transitions were then deduced from these comparisons and assignments were made. The values of the dipole moment components in the two electronic states were then determined from a linear least-squares fit of these assignments until a best set of values for the different dipole moment components was achieved.

Figure 19 also shows several examples of these fits. The dipole moment of indole was found to be 1.963 ± 0.013 (with $\mu_a = 1.376 \pm 0.008$ and $\mu_b = 1.40 \pm 0.01$ D) in the ground S_0 state, and 1.856 ± 0.013 (with $\mu_a = 1.556 \pm 0.008$ and $\mu_b = 1.01 \pm 0.01$ D) in the excited S_1 state. These results are summarized in Table 1 and shown schematically in Figure 20.

We have no information concerning the absolute orientation of μ_I . However, chemical intuition and *ab initio* calculations agree that the dipole moment points away from the nitrogen atom and towards the more negatively charged six-membered ring. (The direction of the dipole moment was confirmed unambiguously by the indole-water Stark experiments). The dipole moment values reported in Table 12 are based upon a fit of 162 assigned lines in the 2036 V/cm spectrum to a standard deviation of 3.09 MHz. Increasing the size of the energy matrix by inclusion of $J - 2$ and $J + 2$ terms did not improve the standard deviation of the fit. No field dependence of the data was detected [39]. All spectra examined yielded the same dipole moment values to within the standard deviation of the measurement. Axis tilting [32] has been ignored in the fits reported here.

5.4.2. Indole-water.

Figure 18b shows the rotationally resolved fluorescence excitation spectrum of the 0_0^0 band of indole-H₂O in the absence of an electric field. This band is shifted by 132 cm^{-1} to the red of the bare molecule. Its rotationally resolved spectrum was discussed earlier [33] and was

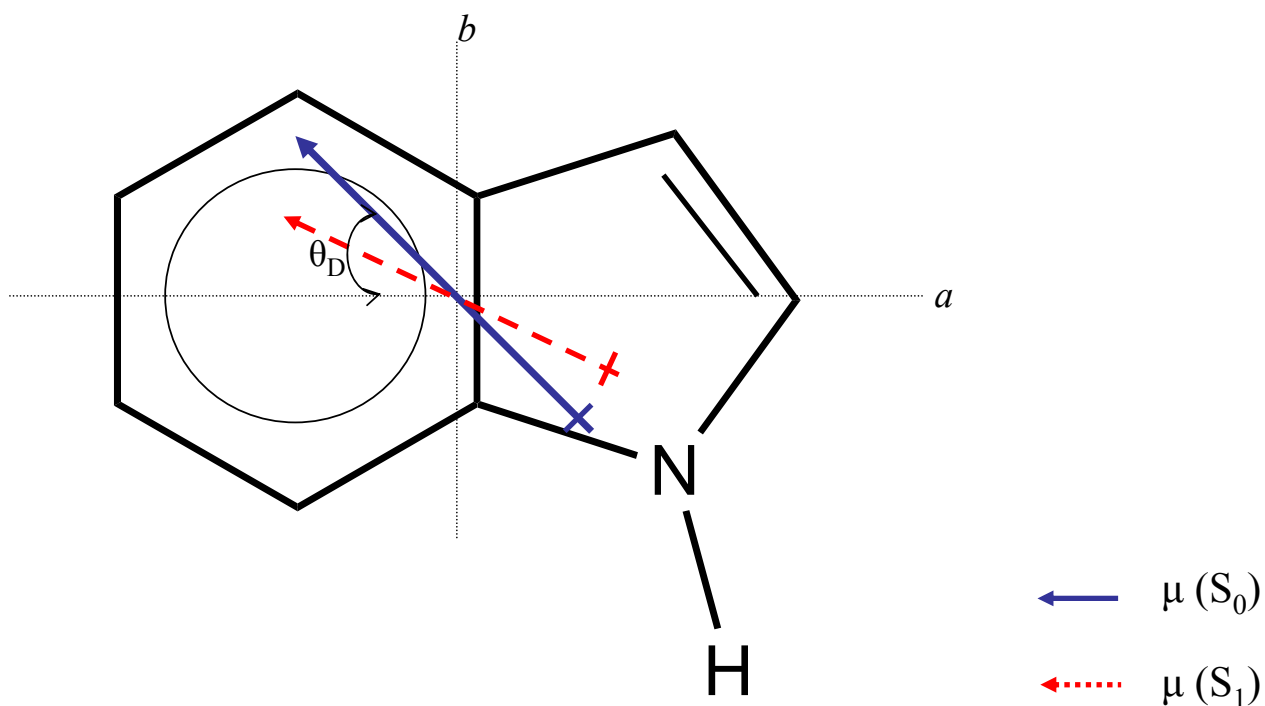


Figure 20. Illustration of indole showing its in-plane inertial axes and the orientations of its permanent electric dipole moments in the two electronic states.

Table 12. Experimental and theoretical rotational constants and electric dipole moments of indole in its ground S_0 and excited S_1 electronic states.

Method	State	A(MHz)	B(MHz)	C(MHz)	μ_a (D)	μ_b (D)	θ_D	μ (D)
Experiment	S_0	3877.9(1)	1636.1(1)	1150.9(1)	1.376(8)	1.40(1)	$\pm 45.5(4)$	1.963(13)
Experiment	S_1	3743.2(1)	1618.2(1)	1130.2(1)	1.556(8)	1.01(1)	$\pm 33.0(6)$	1.856(13)
MP2/6-31G**	S_0	3876.2	1637.2	1151.1	1.500	1.595	± 46.8	2.190

assigned to a 1:1 complex, with the water molecule linked to the indole frame *via* a quasi-linear N—H \cdots OH₂ σ hydrogen bond. Unlike the bare molecule, indole-water has a pure *b*-type S₁-S₀ spectrum. This is due to a rotation of the inertial frame by attachment of the water molecule so that the electronic transition moment now lies essentially parallel to the *b*-axis. Also readily apparent is the increased density of transitions in the spectrum of the complex compared to that of the monomer. This is a result of the larger moments of inertia of the complex, and of the overlapping torsional subbands (A' \leftarrow A'' and B' \leftarrow B'') arising from the hindered internal rotation of the water molecule [33].

Our next goal is to determine the values of the permanent electric dipole moments of indole-H₂O in its S₀ and S₁ electronic states. Figure 21 illustrates the Stark effect on a portion of the high resolution spectrum of the complex near the origin of the B' \leftarrow B'' band. The signal-to-noise ratio in this spectrum is significantly lower than that of the monomer, owing to the larger number of lines and to the smaller number of complexes in the molecular beam, compared to the bare molecule. An additional complicating factor is the significant overlap of the two torsional subbands. Despite these facts, clear Stark patterns emerge, and high quality fits of the B' \leftarrow B'' subband were obtained. These are also shown in Figure 21.

The fit of the indole-H₂O spectrum yielded the dipole moment components listed in Table 13. The dipole moment of indole-water was found to be 4.4 ± 0.3 (with $\mu_a = 4.20 \pm 0.06$ and $\mu_b = 1.2 \pm 0.3$ D) in the ground S₀ state, and 4.0 ± 0.3 (with $\mu_a = 3.90 \pm 0.06$, and $\mu_b = 0.9 \pm 0.3$ D) in the excited S₁ state. These values are based upon a fit of 52 assigned lines in the strong band of the 509 V/cm spectrum with a standard deviation of 5.23 MHz. Expanding the energy matrix to include J - 2 and J + 2 terms did not improve the standard deviation of the fit. All

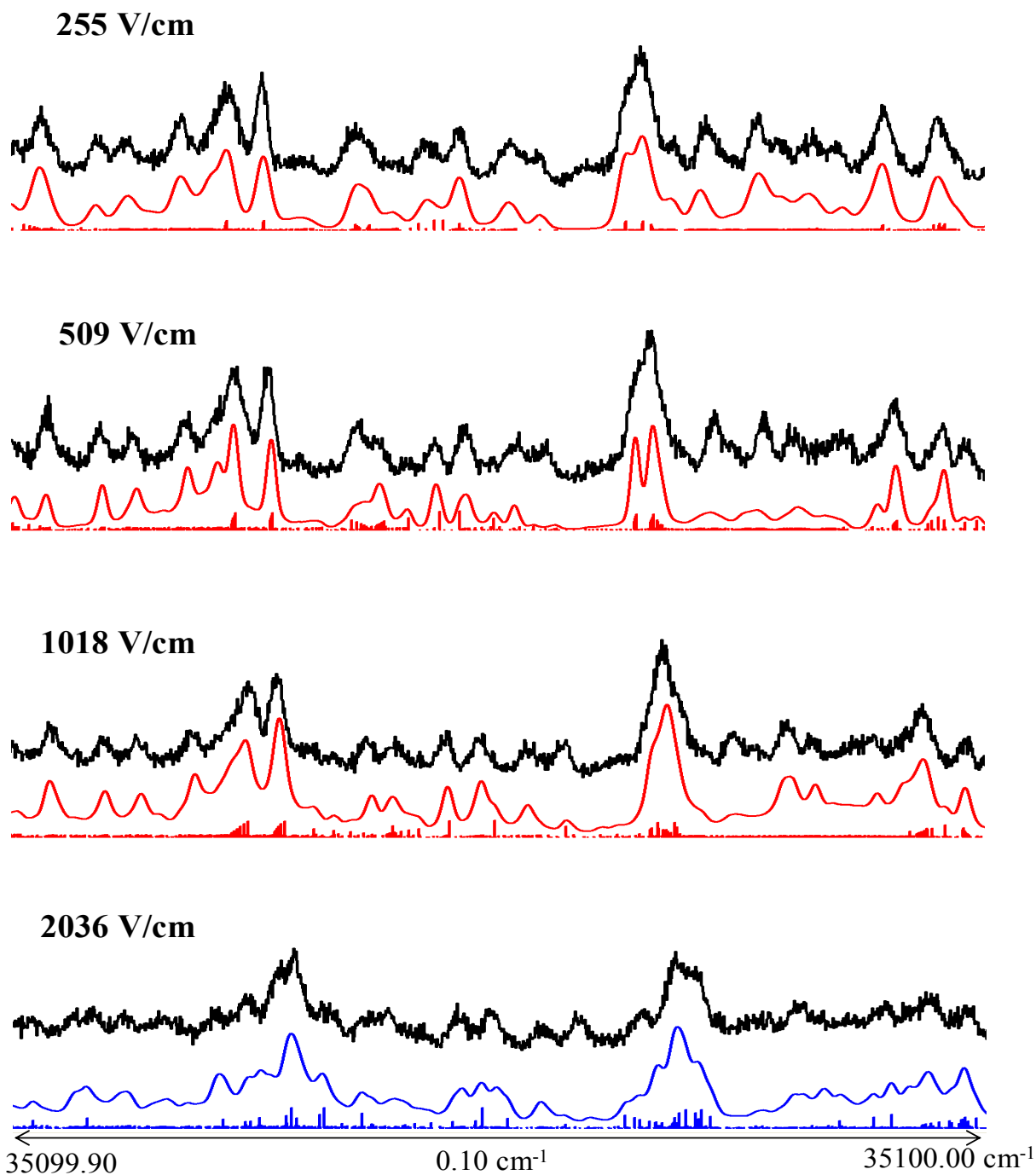


Figure 21. The Stark effect in indole-H₂O. Portion of the rotationally resolved spectrum of indole-H₂O extracted from near the origin (see Fig.18) of the B'←B'' subtorsional band showing the influence of the applied electric field.

Table 13. Experimental and theoretical rotational constants and electric dipole moments of indole-H₂O in its ground S₀ and excited S₁ electronic states.

Method	State	A(MHz)	B(MHz)	C(MHz)	R _{com} (Å) ^a	μ _a (D)	μ _b (D)	θ _D	μ (D)
Experiment	S ₀	2062.5(1)	945.1(1)	649.3(1)	4.666(1)	4.20(6)	1.2(3)	-16(4)	4.4(3)
Experiment	S ₁	1987.6(1)	963.5(1)	650.4(1)	4.602(1)	3.90(6)	0.9(3)	+13(4)	4.0(3)
MP2/6-31G**	S ₀	1901.2	1066.7	685.5		3.03	2.14	+35.2	3.71

^a Distance from the center of mass of indole to the water molecule

spectra examined yielded the same dipole moment values to within the standard deviation of the measurement.

Examination of these data shows that the electric dipole moments of indole-H₂O are substantially larger than those of either indole or water by themselves. This result strongly suggests that the two dipoles are aligned, as would be expected on simple energetic grounds, and further that the presence of one dipole significantly enhances the magnitude of the other. Additional, significant charge redistribution occurs on excitation by light; the S₁ dipole is ~ 10% smaller than that of the S₀ state, and its orientation changes by ~ 30°.

5.5. Discussion.

5.5.1. Indole.

While our technique is particularly useful for its ability to measure the dipole moments of electronically excited states, it also yields accurate values for the dipole moments of ground electronic states. The ground state dipole moment of indole has recently attracted attention for its role in the mechanism of ion transport in the gramicidin A channel [40]. Gramicidin A is a tryptophan-containing polypeptide which, in its head-to-head dimeric form, forms a transmembrane channel that is monovalent cation-selective. The transport of ions through membranes is controlled by the electrostatic interactions between the ion and the channel, particularly monopole-dipole interactions. It has been demonstrated that the dipole moment of the indolic side chain of tryptophan plays a key role in this interaction.

The ground state dipole moment of indole has been measured previously by Caminati and di Bernardo using microwave techniques [38]. They determined the dipole moment to be 2.09 ± 0.13 , with $\mu_a = 1.59 \pm 0.12$ and $\mu_b = 1.36 \pm 0.03$ D. Our measured value of 1.963 ± 0.013 , with

$\mu_a = 1.376 \pm 0.008$ and $\mu_b = 1.40 \pm 0.01$ D, is the same within experimental error but considerably more precise. Primarily, this is because microwave values are based upon transitions whose assignments may be influenced by ^{14}N quadrupole coupling hyperfine structure. It is common in microwave spectroscopy to operate in the weak-field limit, where the Stark interaction energy is much smaller than the quadrupole interaction energy. In this case, the Stark effect appears as a perturbation on the hyperfine splitting. However, we operate in the strong-field limit, where the hyperfine splitting appears as a perturbation on the Stark levels. The Stark effect can then be treated by ignoring the presence of the quadrupole interaction [36]. In fact, it is not necessary for us to account for quadrupole coupling in our spectra because its effects are masked by the experimental linewidth (23 MHz for indole). Essentially, what we measure are hyperfine-free line centers. Without the complications of hyperfine splitting, we are able to obtain more precise values for indole's dipole moment components.

We have also employed *ab initio* theory to explore the structure and electronic properties of indole [41]. Table 12 lists the relevant ground state parameters generated with MP2 theory and the 6-31G** basis set. The MP2 calculation yields rotational constants that are in excellent agreement with experiment. All reported values for the dipole components were transformed to the inertial frame of the molecule in order to be directly comparable to the experimental values. The dipole orientation is predicted very well by theory although the magnitude of the moment is overestimated by $\sim 10\%$.

Our measured value of 1.856 ± 0.013 ($\mu_a = 1.556 \pm 0.008$ and $\mu_b = 1.01 \pm 0.01$ D) for the first excited electronic state of indole provides precise, quantitative information about the changes in its charge distribution that are produced by the absorption of light. The value $\Delta\mu_a = +0.18 \pm 0.01$ D is very similar in magnitude to that found by Chang *et al.* [4] ($|\Delta\mu_a| = 0.14$ D)

but our significantly higher resolution allows us to measure its sign. We are also able to measure the previously unknown change in μ_b , $\Delta\mu_b = -0.39 \pm 0.02$ D. The simultaneous increase in μ_a and decrease in μ_b is significant because it reveals that the total dipole moment of indole actually decreases on excitation to its S_1 electronic state. This change is consistent with theoretical prediction that the S_1 state is the 1L_b state [23, 42].

Perhaps more important is the finding that the orientation of the electric dipole moment of indole changes significantly when the molecule absorbs light. Experiment gives only the absolute values of the dipole moment components and not their signs. Thus, we can determine only the magnitudes of the orientation angles, $\pm 45.5 \pm 0.4^\circ$ in the S_0 state and $\pm 33.0 \pm 0.6^\circ$ in the S_1 state. Theory suggests that the value $+46.8^\circ$ for the ground state. Thus, S_1 - S_0 excitation of indole produces a rotation of μ of either -12.5 or -78.5° with respect to the a axis.

Theory also aids in the resolution of this ambiguity. Figure 22 shows an electron density difference map calculated with MP2/CIS methods (6-31G** basis set) and described as

$$0.768 (|\Psi_{\text{LUMO}}|^2 - |\Psi_{\text{HOMO}-1}|^2) + 0.232 (|\Psi_{\text{LUMO}+1}|^2 - |\Psi_{\text{HOMO}}|^2)$$

Clearly evident from this map is a shift in electron density from the pyrrole ring to the benzene ring. In agreement with this prediction, we find an increase in μ_a and a decrease in μ_b . Thus, the angle that μ makes with the a axis in indole must be $+33.0^\circ$, and the S_1 - S_0 rotation angle must be -12.5° . This is shown explicitly in Figure 20.

5.5.2. Indole-water.

Previously, it was shown that both the position and the orientation of the attached water molecule in indole- H_2O change when the complex absorbs light [33], representing the first structurally resolved example of “solvent reorganization” on the molecular level. This is shown

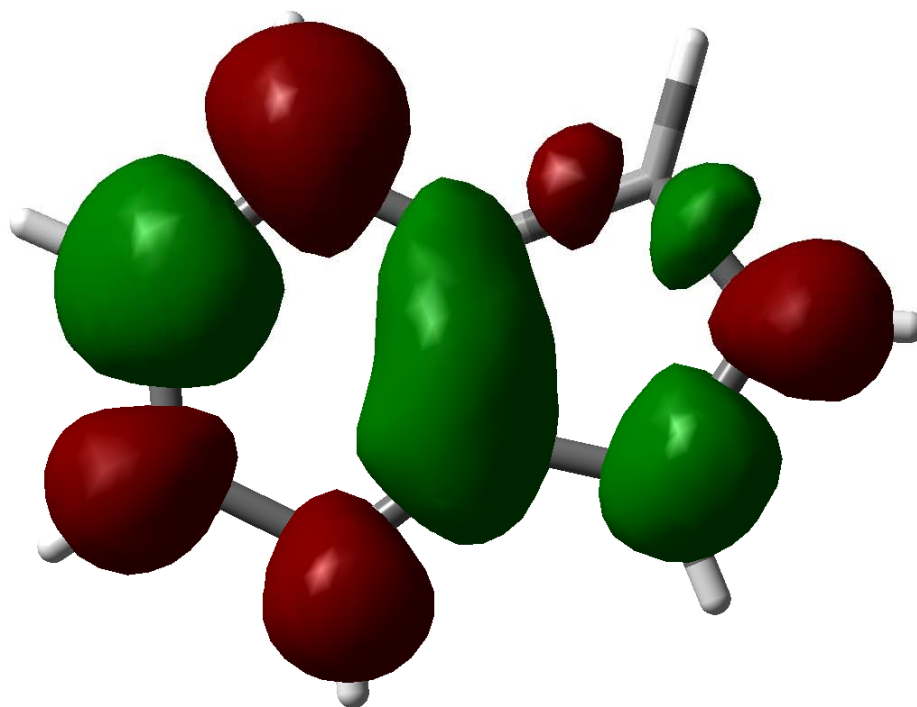


Figure 22. Electron density difference map for the $S_1 \leftarrow S_0$ transition of indole. Dark contours indicate regions of electron gain, and light contours indicate regions of electron loss.

explicitly in Figure 23. Thus, in the ground state, the N-H hydrogen is linked to one of the two sp^3 lone pairs of the water oxygen atom, resulting in an angle between the water plane and the hydrogen bond (HB) axis of $\sim 55^\circ$. In the excited state, the N-H hydrogen is linked to both lone pairs, resulting in a bifurcated structure with an angle between the water plane and the HB axis of $\sim 0^\circ$. (Additionally, neither structure is rigid; the water molecule undergoes a large amplitude inversion-hindered internal rotation about an axis lying in its bc plane (55° from b) in both states). Thus, the water dipole reorients when the photon is absorbed. Figure 23 clearly shows that this motion is a direct consequence of the light-induced change in the electronic distribution of the bare molecule. The dipoles of indole and water are essentially parallel to each other in both electronic states; it is the change in the orientation of the indole dipole that causes the water to move. This effect also explains why both the ordering and the energy separation of the 1L_b and 1L_a states of indole are extraordinarily sensitive to their local environment [26, 43-48].

The S_0 dipole moment of indole- H_2O was found to be 4.4 ± 0.3 , with $\mu_a = 4.20 \pm 0.06$ and $\mu_b = 1.2 \pm 0.3$ D. It decreases slightly upon electronic excitation to 4.0 ± 0.3 , with $\mu_a = 3.90 \pm 0.06$ and $\mu_b = 0.9 \pm 0.3$ D. No evidence for a μ_c component was found in either state. The slight change in μ suggests that the S_1 state of indole is a pure 1L_b state, as in the monomer. No evidence for $^1L_b/^1L_a$ state-mixing was found in our spectra [39].

Our final goal is to determine the value of μ_1^* , the induced dipole moment of an indole molecule that is polarized by the attached water molecule, in both electronic states. Water in its ground state has a dipole moment $\mu_w = 1.855(6)$ D[49]. Combining this value with the measured values for indole gives maximum values for indole- H_2O of 3.818 in S_0 and 3.711 D in S_1 , assuming the dipoles of the component parts are aligned. The measured values of 4.4 and 4.0 D

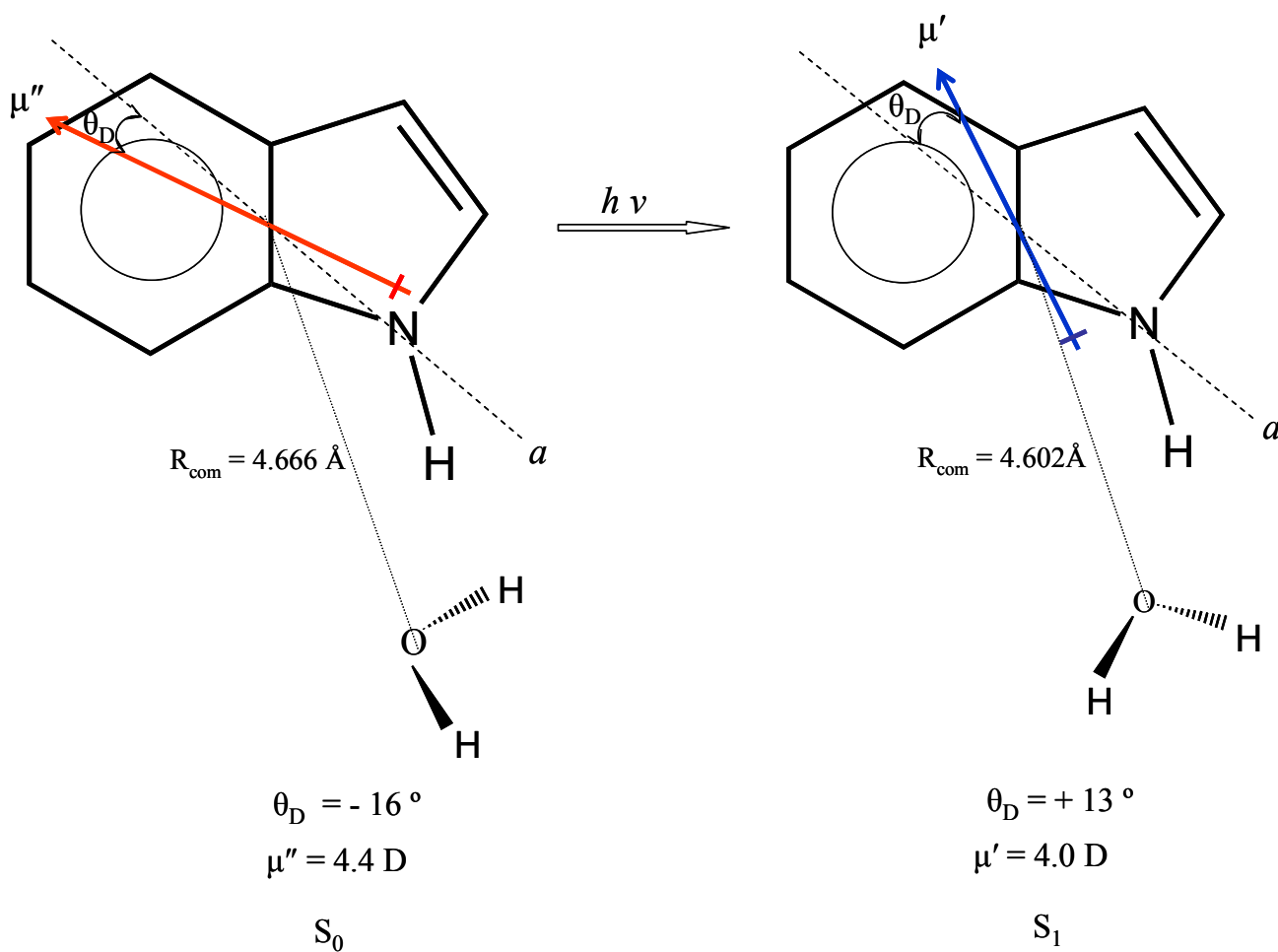


Figure 23. Illustration of indole-water showing its in-plane inertial axes and the orientations of its permanent electric dipole moments in the two electronic states.

are larger than these estimates by 13% in S_0 and 8% in S_1 . We attribute these differences to induced dipole moments produced by the attached water molecule.

Electrostatic models of the interactions between molecules have been successful in predicting the structure of the many van der Waals complexes. In a typical model, the complex dipole moment is represented as a sum of three terms,

$$\mu_{IW} = \mu_I + \mu_W + \mu_I^* \quad (4)$$

where μ_I and μ_W are the permanent dipole moments of the component parts, for which the experimental values are now known. μ_I^* is the induced dipole moment, arising primarily from polarization of the indole unit by the water dipole moment and quadrupole, as expressed in Eq. (5):

$$\mu_I^* = \alpha_I \cdot \{ [3\mathbf{R}(\boldsymbol{\mu} \cdot \mathbf{R})/R^5] - \boldsymbol{\mu}/R^3 + [5(\mathbf{R}^\dagger \cdot \boldsymbol{\Theta} \cdot \mathbf{R})/R^7] \mathbf{R} - (\boldsymbol{\Theta}^\dagger \cdot \mathbf{R} + \boldsymbol{\Theta} \cdot \mathbf{R})/R^5 \} \quad (5)$$

However, since induced dipoles were calculated with a and b inertial axis components separately, Eq. (5) can be simplified as Eq. (6)

$$\mu_{Ia,b}^* \approx \mu_{Wa,b} \cdot \frac{2 \cdot \alpha_{Ia,b}}{R_{COM}^3} + 3 \cdot \Theta_{Wa,b} \cdot \frac{\alpha_{Ia,b}}{R_{COM}^4} \quad (6)$$

Here, $\alpha_{Ia,b}$ is the polarizability volume of indole, $\Theta_{Wa,b}$ is the electric quadrupole moment of water, and θ is the angle between the a axis of the complex and the C_2 dipole axis of the water.

This axis was assumed to lie in the ab plane of the complex since the tunneling motion of the attached water molecule is fast compared to overall molecular rotation. R_{COM} is the COM distance between indole and water which also can be determined from experiment; the values (see Fig. 23) are $R_{\text{COM}} = 4.666$ and $R_{\text{COM}} = 4.602$ Å in the S_0 and S_1 states, respectively.

Table 14 lists the electrostatic properties of water and indole that are needed in this calculation. Polarizabilities and quadrupole moments were obtained by *ab initio* methods using a 6-31G** basis set. Predictably, these lead to large induced dipole moments whose magnitudes are strongly angularly dependent. For example, if we consider only the first (dipole) term in Eq.(5), we calculate a ground state induced moment of 0.567 D when the water dipole points along a and 0.346 D when the water dipole points along b . These values changes to 0.721 and 0.507 D, respectively, when indole is excited to its S_1 state. The larger induced dipole in the S_1 state may be traced to the larger polarizability and smaller R_{COM} in that state.

We now use Eq. (5) and the data in Table 3 to determine the induced dipole moments in indole-H₂O. Essentially quantitative agreement with experiment, especially when the quadrupole term in Eq. (5) is included, is obtained when the C_2 axis of water is oriented by -25° with respect to the a axis of the complex in the S_0 state and by $+35^\circ$ with respect to the a axis of the complex in the excited state. This is shown in Table 15. The induced dipole moments in these two orientations are $\mu^*_1 = 0.727$ ($\mu^*_{1a} = 0.592$ and $\mu^*_{1b} = 0.422$ D) in the S_0 state, and $\mu^*_1 = 0.540$ ($\mu^*_{1a} = 0.484$ and $\mu^*_{1b} = 0.238$ D) in the S_1 state. The S_1 induced dipole is smaller by 0.187 D. Primarily, this is because the dipoles of water and indole are nearly aligned (-25.7°) in the ground state, but less well aligned ($+48.3^\circ$) in the excited state. Also, the values of the water orientation angles required by the fit are in nearly perfect agreement with the values derived from our earlier analysis of the torsion-rotation perturbations in the high resolution spectrum [33]

Table 14. Electrostatic properties of water and indole in its S_0 and S_1 states.

	Water		Indole	
	S_0	S_0	S_0	S_1
μ_a (D)	1.855 ^a	1.376 (8) ^b	1.556 (8) ^b	
μ_b (D)		1.40 (1) ^b	1.01 (1) ^b	
Θ_a (D · Å)	2.47 ^c	6.067 ^c	5.282 ^d	
Θ_b (D · Å)	0.17 ^c	7.098 ^c	9.023 ^d	
α_a (Å ³)	0.76 ^c	17.63 ^c	22.74 ^d	
α_b (Å ³)	0.89 ^c	4.28 ^c	4.51 ^d	

^a Reference 49

^b This work

^c Calculated from MP2 / 6-31G**

^d Calculated from CIS / 6-31G**

Table 15. Observed and calculated dipole moments (in Debye) of indole and indole-H₂O in their S₀ and S₁ electronic states.

		Indole - water			
		Indole	Experimental	Calculated	
				w/o Θ	w/ Θ
S ₀	μ_a	1.376 (8)	4.20 (6)	4.11	4.24
	μ_b	1.40 (1)	1.2 (3)	1.15	1.18
	μ_{tot}	1.963 (13)	4.4 (3)	4.27	4.40
S ₁	μ_a	1.556 (8)	3.90 (8)	3.54	3.81
	μ_b	1.01 (1)	0.9 (3)	0.66	0.77
	μ_{tot}	1.856 (13)	4.0 (3)	3.60	3.89

The error limits reflect a less than 2° uncertainty in the vibrationally averaged orientation of the water molecule compared to the experimental data.

Figure 24 summarizes the results in graphical form. That the polarizing effect of the water molecule would increase the complex dipole moment was expected owing to the high polarizability of the indole molecule. What was unexpected is the magnitude of the effect; the induced moment in indole-H₂O is a substantial fraction (30-40 %) of the permanent dipole moment of indole. The distribution of electrons in the isolated molecule is significantly affected by the presence of a single solvent molecule in its vicinity. Also unexpected is the fact that the induced dipole is not parallel to the “inducing” one, especially in the ground state. Possibly this effect has its origin in the polarizability anisotropy, which is larger in the ground state. But most surprising of all is that a simple electrostatic model seems to capture the essence of the polarization phenomenon so well. If this result holds up under further scrutiny, then the prospects for success of recently derived polarizable force fields for other organic and biological molecules is high [50].

5.6. Summary.

We have observed and analyzed the Stark effect on the rotationally resolved S₁ ← S₀ fluorescence excitation spectra of indole and indole-H₂O. These analyses have yielded accurate values for the ground and first excited state permanent dipole moments of these systems. The S₀ dipole moment of indole was found to be 1.963 D and decreases slightly upon absorption of a UV photon to 1.856 D. The magnitude of this change is consistent with S₁ being the ¹L_b state. There is a significant change in the orientation of the dipole moment in S₁ which provides insight into the interaction between indole and surrounding solvent molecules. The indole-H₂O cluster is found to have a dipole moment of 4.4 and 4.0 D in its S₀ and S₁ states, respectively.

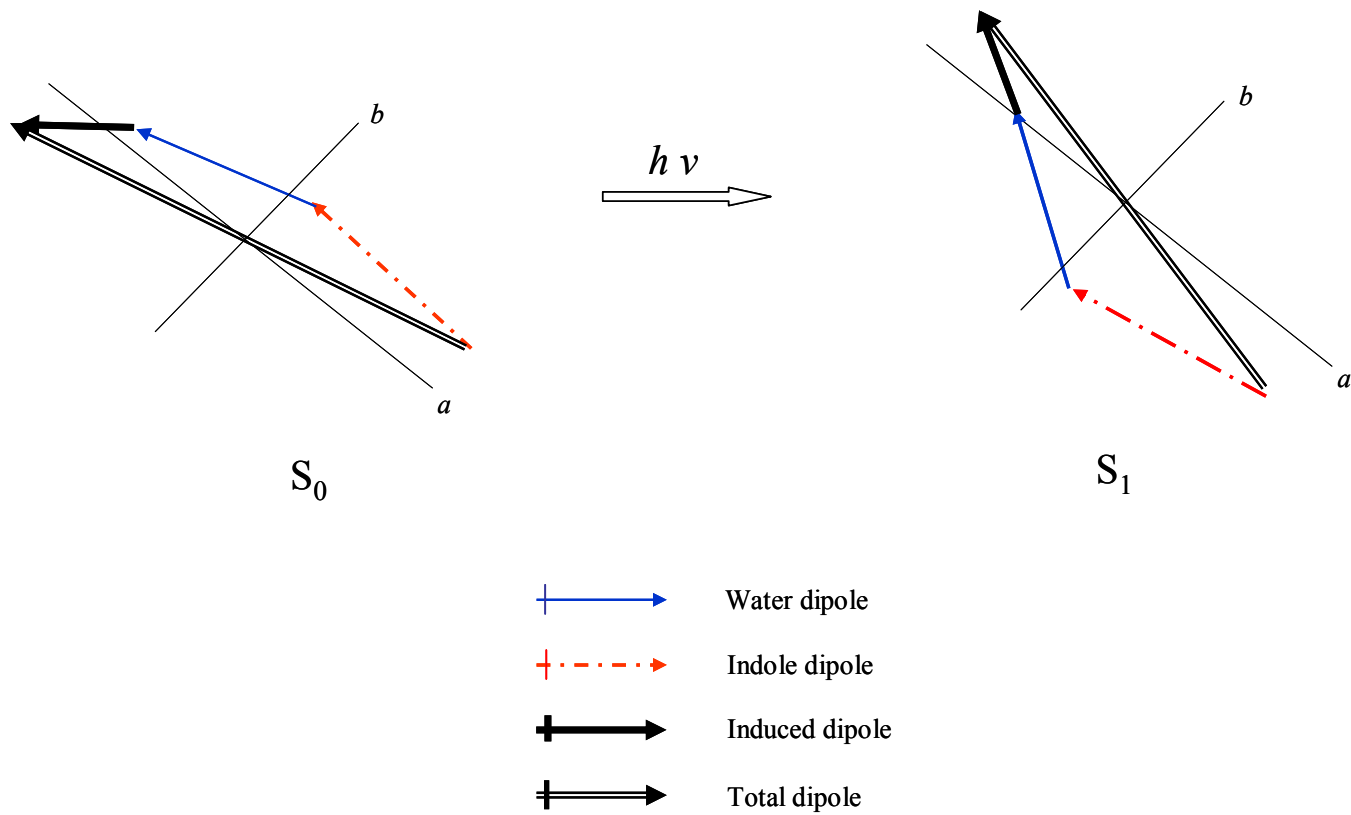


Figure 24. Vector diagram showing the total dipole moments of indole-water in both electronic states and their component parts.

A comparison of the dipole moments of the bare molecule and its single water complex makes possible the first experimental values of the induced dipole moment of an isolated molecule in different electronic states, $\mu_{\text{I}}^*(S_0) = 0.727$ and $\mu_{\text{I}}^*(S_1) = 0.540$ D. These values are quantitatively reproduced by a purely electrostatic calculation based on *ab initio* values of multipole moments.

5.7. Acknowledgements.

We thank Jon Hougen, Jeremy Hutson, Richard Suenram, and Tri Nguyen for helpful discussions. This work has been supported by NSF (CHE-0315584).

5.8. References.

- [1] W. Gordy and R. L. Cook, *Microwave Molecular Spectra*, 3rd ed., Wiley-Interscience: New York, 1984.
- [2] D. E. Freeman and W. Klemperer, *J. Chem. Phys.* **45**, 52 (1966)
- [3] J. R. Lombardi, *J. Chem. Phys.* **48**, 348 (1968)
- [4] C.-T. Chang, C.-Y. Wu, A. R. Muirhead and J. R. Lombardi, *Photochem. Photobiol.* **19**, 347 (1974)
- [5] W. A. Majewski and W. L. Meerts, *J. Mol. Spectrosc.* **104**, 271 (1984)
- [6] M. Okruss, B. Rosenow and A. Hese, *Chem. Phys. Lett.* **220**, 286 (1994)
- [7] M. Okruss, R. Müller and A. Hese, *J. Chem. Phys.* **110**, 10393 (1999)
- [8] T. M. Korter, D. R. Borst, C. J. Butler and D. W. Pratt, *J. Am. Chem. Soc.* **122**, 96 (2001)
- [9] D.R Borst, T. M. Korter and D. W. Pratt, *Chem.Phys.Lett.* **350**, 485 (2001)
- [10] J. A. Reese, T. V. Nguyen, T. M. Korter and D. W. Pratt, *J. Am. Chem. Soc.* **126**, 11387 (2004)
- [11] A.J. Stone, *Chem.Phys.Lett.* **83**, 233 (1981)
- [12] A.J. Stone, *Mol.Phys.* **56**,1065 (1985)
- [13] P.W. Fowler and A.J. Stone, *J.Phys.Chem.* **91**, 509 (1987)
- [14] C.R. Le Sueur and A.J. Stone, *J.Phys.Chem.* **95**, 3519 (1991)
- [15] K.C. Janda, L.S. Bernstein, J.M. Steed, S.E. Novick and W. Klemperer, *J.Am.Chem. Soc.* **100**, 8074 (1978)
- [16] R.S. Altman, M.D. Marshall, W. Klemperer and A. Krupnov, *J.Chem.Phys.* **79**, 52 (1983)
- [17] R.S. Altman, M.D. Marshall and W. Klemperer, *J.Chem.Phys.* **77**, 4344 (1982)

- [18] For a review, see P. R. Callis, in *Methods in Enzymology*, edited by L. Brand, M. L. Johnson, Academic: San Diego, 1997; Vol. 278, and references therein.
- [19] A. P. Demchenko, *Ultraviolet Spectroscopy of Proteins*, Springer-Verlag: Berlin, 1986.
- [20] R.F.Chen, in *Practical Fluorescence*, 2nd ed., edited by G.G.Guilbault (Marcel Dekker, New York, 1990), p. 575.
- [21] For a review, see: P. J. Suppan, *Photochem. Photobiol. A* **50**, 293 (1990)
- [22] a) P.R. Callis and B. K. Burgess, *J. Phys. Chem. B* **101**, 9429 (1997)
b) G. Weber, *J. Biochem.* **75**, 335 (1960)
- [23] L. Serrano-Andrés and B. O. Roos, *J. Am. Chem. Soc.* **118**, 185 (1996)
- [24] P.R. Callis, *J. Chem. Phys.* **95**, 4230 (1991)
- [25] L. S. Slater and P. R. Callis, *J. Phys. Chem.* **99**, 8572 (1995)
- [26] H. Lami and N. Glasser, *J. Chem. Phys.* **84**, 597 (1986)
- [27] J. R. Lombardi, *J. Phys. Chem. A* **102**, 2817 (1998)
- [28] W. A.Majewski, J. F. Pfanstiel, D. F. Plusquellic and D. W. Pratt, in *Laser Techniques in Chemistry*, edited by Myers, A. B.; Rizzo, T. R.; Wiley: New York, 1995; Vol. 23, p.101.
- [29] S. Gerstenkorn, and P. Luc, *Atlas du spectroscopie d'absorption de la molecule d'iode*, CNRS: Paris, 1978 and 1982.
- [30] D. G. Lister J. K. Tyler, J. H. Høg and N. W. Larsen, *J. Mol. Struct.* **23**, 253 (1974)
- [31] L. A. Philips and D. H. Levy, *J. Chem. Phys.* **85**, 1327 (1986)
- [32] G. Berden, W. L Meerts and E. Jalviste, *J. Chem. Phys.* **103**, 9596 (1995)
- [33] T. M. Korter, D. W. Pratt and J. Küpper, *J. Phys. Chem.* **102**, 7211 (1998)
- [34] D. R. Borst and D. W. Pratt, unpublished.

- [35] J. K. G. Watson, in *Vibrational Spectra and Structure*, edited by Durig, J. R.; Elsevier: Amsterdam, 1977; Vol.6, p.1.
- [36] W. Gordy, R. L. Cook, *Microwave Molecular Spectra*, 3rd ed., Wiley-Interscience: New York, 1984.
- [37] A. Held, B. B. Champagne and D. W. Pratt, *J. Chem. Phys.* **95**, 8732 (1991)
- [38] W. Caminati and S. di Bernardo, *J. Mol. Struct.* **240**, 253 (1990)
- [39] J. R. Lombardi, *J. Phys. Chem. A* **103**, 6335 (1999)
- [40] M. Cotton, C. Tian, D. D. Busath, R. B. Shirts and T. A. Cross, *Biochemistry* **38**, , 9185 (1999) ; W. Hu and T. A. Cross, *Biochemistry* **34**, 14147 (1995)
- [41] M. J. Frisch, G. W. Trucks, H. B. Schlegel, G. E. Scuseria, M. A. Robb, J. R. Cheeseman, V. G. Zakrzewski, J. A. Montgomery, R. E. Stratmann, J. C. Burant, S. Dapprich, J. M. Millam, A. D. Daniels, K. N. Kudin, M. C. Strain, O. Farkas, J. Tomasi, V. Barone, M. Cossi, R. Cammi, B. Mennucci, C. Pomelli, C. Adamo, S. Clifford, J. Ochterski, G. A. Petersson, P. Y. Ayala, Q. Cui, K. Morokuma, D. K. Malick, A. D. Rabuck, K. Raghavachari, J. B. Foresman, J. Cioslowski, J. V. Ortiz, B. B. Stefanov, G. Liu, A. Liashenko, P. Piskorz, I. Komaromi, R. Gomperts, R. L. Martin, D. J. Fox, T. Keith, M. A. Al-Laham, C. Y. Peng, A. Nanayakkara, C. Gonzalez, M. Challacombe, P. M. W. Gill, B. G. Johnson, W. Chen, M. W. Wong, J. L. Andres, M. Head-Gordon, E. S. Replogle and J. A. Pople, *Gaussian 98*, Revision A9; Gaussian, Inc.: Pittsburgh, PA, 1998.
- [42] A. L. Sobolewski and W. Domcke, *Chem. Phys. Lett.* **315**, 293 (1999)
- [43] E. H. Strickland, J. Horwitz and C. Billups, *Biochemistry* **9**, 4914 (1970)
- [44] M. Martinaud and A. Kadiri, *Chem. Phys.* **28**, 473 (1978)

- [45] A. A. Rehms and P. R. Callis, *Chem. Phys. Lett.* **140**, 83 (1987)
- [46] P. Illich, C. Haydock and F. G. Prendergast, *Chem. Phys. Lett.* **158**, 129 (1989)
- [47] D. R. Demmer, G. W. Leach, E. A. Outhouse, J. W. Hager and S. C. Wallace, *J. Phys. Chem.* **94**, 582 (1990)
- [48] M. J. Tubergen and D. H. Levy, *J. Phys. Chem.* **95**, 2175 (1991)
- [49] S. A. Clough, Y. Beers, G. P. Klein and L. S. Rothman, *J. Chem. Phys.* **59**, 2254 (1973)
- [50] C.S. Ewig, M.Waldman and J.R. Maple, *J. Phys. Chem. A* **106**, 326 (2002); J.W. Ponder, *et al.*, in press

APPENDIX A

Structures, charge distribution, and dynamical properties of weakly bound complexes of aromatic molecules in their ground and electronically excited states.

Cheolhwa Kang and David W. Pratt

Department of Chemistry

University of Pittsburgh

Pittsburgh, PA 15260 USA

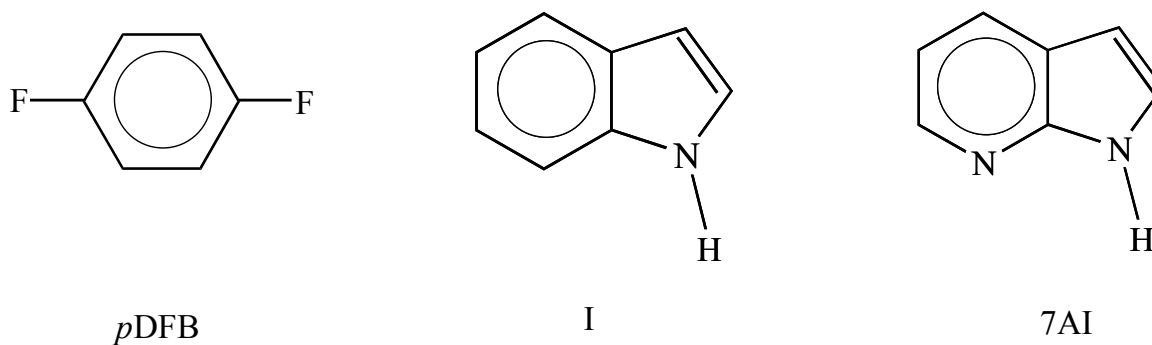
Accepted for publication in the *International Reviews in Physical Chemistry*

Introduction

Advances in science are often driven by advances in instrumentation. Our developing understanding of the forces between molecules is no exception. The pioneering work in their field was done by Levy and co-workers [1], who demonstrated that the use of supersonic jets to simplify the electronic spectra of large molecules led to the “adventitious” formation of a wide variety of complexes held together by weak van der Waals and somewhat stronger hydrogen bonds. Performing these experiments with vibrational and rotational resolution, and at other frequencies (*e.g.*, IR and microwave) gave exciting new information about the equilibrium geometries and dynamical properties of many new molecules whose existence in nature had not previously been demonstrated. Water aggregates like $(\text{H}_2\text{O})_2$, $(\text{H}_2\text{O})_3$, \dots $(\text{H}_2\text{O})_n$ come to mind but there are many other beautiful examples [2-5]. This information, in turn, has fueled the development of powerful new theoretical tools for calculating intermolecular potentials [6]. Predictions based on these calculation are likely to stimulate many further experiments, thereby “completing” the scientific cycle of experiment, theory, and hypothesis in this new field.

Understanding the factors that contribute to the potential energy of interaction between two or more species is an important research objective. All encounters between atoms and molecules, whether reactive or nonreactive, are (at least in the beginning) generated by such potentials. Of particular interest are the changes in the potentials that occur where two species approach each other, and how these changes depend upon angular coordinates. The “induced fit” that characterizes the behavior of many enzyme-substrate complexes is a particular example. Beyond such molecular assemblies, properties of collection of molecules in liquids, solutions, and solids also depend on their interaction at long range, and how the interaction between two species are affected by the presence of others.

Described here are the results of recent high resolution electronic spectroscopy experiments on several weakly bound complexes of organic molecules. The substrates include *p*-difluorobenzene (*p*DFB), indole (I), and 7-azaindole(7AI), see below.



The complexing “agents” include argon (Ar), nitrogen (N₂), and water (H₂O). We thus explore the properties of atomic, diatomic, and triatomic complexes of increasingly complex host molecules. Our experiments are rotationally resolved. Hence, we determine the equilibrium geometries of each complex in its electronic ground state. A particular focus is how these geometries change when the substrate to which the atom or molecule is attached became more asymmetric. Similar information is obtained about the electronically excited state. In many cases, the geometries of the excited state are different from the ground state, owing to changes in the electron distribution of the substrate when it absorbs light. van der Waals “bonding” is entirely the result of electron correlation; such correlation, in turn, is significantly enhanced in excited states, compared to ground state.

A second focus of this paper is on the permanent electric dipole moments of these complexes in their ground and electronically excited state. There have been measured for the first time using a newly developed Stark cell in our high resolution apparatus, by means of which

homogeneous electric fields may be applied to the sample. Two such studies will be described here, on 7AI-Ar and I-H₂O (IW). These studies give quantitative information about the changes in the charge distribution that are produced when a molecule absorbs light, thereby according for differences in the structures of the different complexes in their ground and electronically excited state. In the case of IW, the dipole measurements also give information about induced dipole moments, that is, the changes in the charge distributions of a substrate molecule that are produced when the complex is formed, precursor to induced fits.

A third and final focus of this paper is in the dynamical properties of weakly bound complex in their ground and electronically excited state. The relatively weak interaction between closed shell molecules that is the hallmark of such species gives rise to intermolecular bonds that are not rigid. As a result, Ar, N₂, and H₂O all undergo large amplitude motions when they are attached to *p*DFB, I, or 7AI. Additionally, in the case of N₂ or H₂O, the attached molecule undergoes other internal motions such as hindered rotation and inversion. Surprisingly, the observed high resolution spectra are extraordinary sensitive to these dynamics. Thus, properly interpreted, one can derive intermolecular potentials in both ground and electronically excited state from such data.

A.2 Experimental

Rotationally resolved electronic spectra were obtained using the CW molecular beam laser spectrometer (see Fig. 1) described in detail elsewhere [7]. The clusters were generated by molecular beam of a gaseous mixture of solute/solvent diluted with Ar (or He) carrier gas. Each of clusters has different optimal conditions to form the complexes. The present conditions were as follows. The molecular beam was formed by expansion of substrate molecules with (1) Ar

complexes; flowing Ar carrier gas (~ 0.7 bar for 7AI, ~ 1.3 bar for indole) (2) N₂ complex; seeded in a mixture of 10-15% N₂ in He carrier gas (~ 0.7 bar for *p*DFB) (3) H₂O complexes; He carrier gas (~ 2.7 bar) was enriched with water vapor passing through a container holding water at room temperature. The substrate molecules were kept in the sample housing whose temperature was controlled to obtain enough vapor pressure. This molecular beam was expanded into a differentially pumped vacuum system. The expansion was skimmed 2 cm downstream with a 1 mm skimmer and crossed 13 cm farther downstream by a continuous wave ring dye laser operating with selected dye and intracavity frequency doubled in BBO, yielding 100–200 μ W of ultraviolet radiation. Fluorescence was collected using spatially selective optics, detected by a photomultiplier tube and photon counting system, and processed by a computerized data acquisition system. Relative frequency calibrations of the spectra were performed using a near-confocal interferometer having a mode-matched FSR of 299.7520 ± 0.0005 MHz at the fundamental frequency of the dye laser. Absolute frequencies in the spectra were determined by comparison to transition frequencies in the electronic absorption spectrum of I₂ [8].

The apparatus has been modified to generate a homogeneous, static electric field in the laser/molecule interaction region for the Stark-effect measurements. Briefly, the experiment was as follows. Two spherical mirrors are positioned one above and one below the intersection of the laser and molecular beams to collect the fluorescence. The top mirror has a focus at the intersection and the bottom mirror is focused at a hole (2 mm) drilled in the center of the top mirror. Inside the spherical collecting mirrors, two stainless steel wire grids were placed one above and one below the laser/molecular beam plane, separated by ~ 1 cm with ceramic spacers. Two power supplies were used to hold one grid at some positive voltage and the other at some negative voltage relative to a common ground. This experimental setup yields an electric field

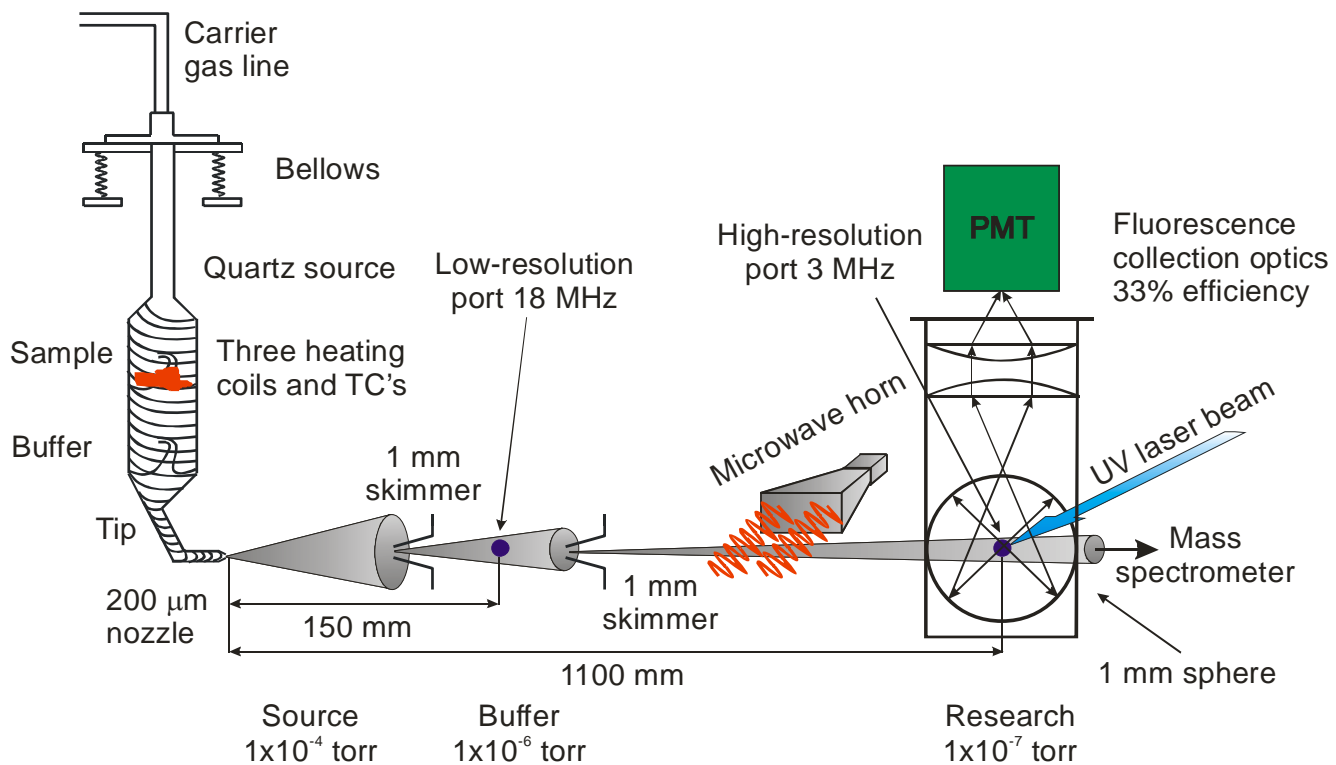


Figure 1. Overall layout of the high resolution CW laser/molecular beam spectrometer.

perpendicular to the polarization of the laser radiation and thus forces a selection rule of $\Delta M = \pm 1$. Electric field strengths were calibrated using the known value of μ_a in the ground state of aniline [9] and the combination-difference method of spectral assignment. The aniline calibration yielded an effective electrode separation of 0.982 ± 0.004 cm.

A.3 Argon atom complexes

Our first example of the application of these techniques is taken from the literature. Figure 2 shows the rotationally resolved fluorescence excitation spectrum of the 0_0^0 band in the S_1 - S_0 transition of *p*DFB-Ar obtained by Neusser and co-workers [10]. The same group also obtained the analogous spectrum of the bare molecule [10]. Now, the rotational motions of such large molecules are “slow” on the time scale of their vibrational motions (even the intermolecular ones!). Therefore, the high resolution electronic spectroscopy experiment explores the *equilibrium* geometries of the two electronic states, averaged over their zero-point motions along all coordinates. This is the principal strength of eigenstate spectroscopy in the gas phase.

Information about these geometries is obtained in the first instance by fitting the experimental spectra with rigid rotor Hamiltonians for both states,

$$\hat{H} = AP_a^2 + BP_b^2 + CP_c^2 \quad (1)$$

Here, A, B, and C are the usual rotational constants, inversely related to the moments of inertia around each of the three principal axes (*e.g.*, $A = h / 8\pi^2 c I_a$, etc).

(later, centrifugal distortion constants can be included [11]). Details of our fitting procedures are described elsewhere [12]. Suffice it to say here that a typical least-squares fit is performed on hundreds of lines, yielding rotational constants for both electronic states that are usually

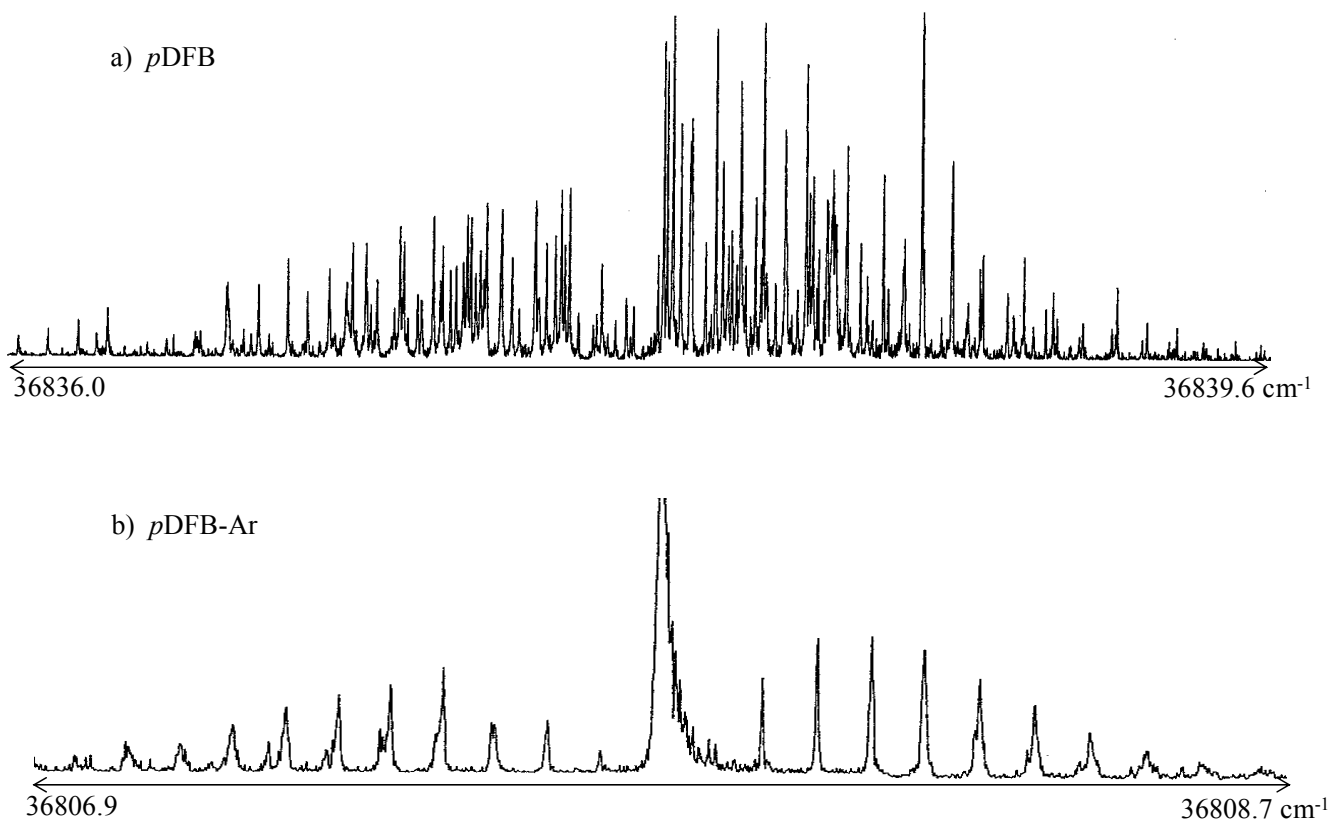


Figure 2. Rotationally resolved fluorescence excitation spectra of the origin bands in the S_1 - S_0 transitions of (a) bare *p*DFB at 36837.8 cm^{-1} and (b) the *p*DFB-argon van der Waals complex at 39807.8 cm^{-1} (Ref. [10]).

determined to precisions are order of a few tenths of a MHz, substantially less than the single rovibronic linewidth of a few MHz. Additional parameters derived from these fits include the band origin frequency, the polarization of the band (*i.e.*, the electronic TM orientation), and other terms that describe the strengths of couplings between other degrees of freedom and rotational motion (*vide infra*).

Listed in Table 1 are the values of the rotational constants of *p*DFB and *p*DFB-Ar in their S_0 and S_1 electronic states that were determined from fits of their high resolution spectra [10]. Note, first, that the ground and excited state rotational constants of *p*DFB itself are significantly different. A decreases by 357.1 MHz, or 6.3 %. As discussed elsewhere, this decrease signals a large change in geometry when *p*DFB absorbs light, which in turn, demonstrates that its S_1 state has a significantly different electronic distribution from the S_0 state. Next we note that the rotational constants of *p*DFB-Ar are very different from those of *p*DFB, reflecting the complex's larger mass. We also see that the A rotational constant of the complex is very nearly the same as the C rotational constant of the bare molecule. This indicates that the identities of the a and c inertial axes have been switched on complex formation, and that the Ar atom lies above or below the aromatic plane in the equilibrium geometry of *p*DFB-Ar (confirmed by TM orientation). And finally, we note that the S_0 and S_1 rotational constants of the complex also are different. A and B decreases, but C increases when the photon is absorbed, evidencing another differences in the geometries of the two electronic states of *p*DFB-Ar.

Quantitative information about the equilibrium geometries of *p*DFB-Ar in its two states can be obtained using Kraitchman's equations [13]. As shown in Figure 3, attaching a mass m to a substrate molecule M with principal moments of inertia I_a , I_b , I_c changes its moments in a way that depends on the added mass m and its position in the inertial frame. Therefore,

Table 1. Inertial parameters of *p*DFB and its Ar complex in its ground and excited electronic states.

State	Parameter	<i>p</i> DFB	<i>p</i> DFB - Ar
S_0	A, MHz	5639.1	1139.5
	B, MHz	1428.2	1029.7
	C, MHz	1139.5	695.5
	$\Delta I, u \text{ \AA}^2$	0.0	-207.7
S_1	A, MHz	5282 (3)	1129 (3)
	B, MHz	1435.1 (6)	1106 (3)
	C, MHz	1128.6 (6)	706.0 (9)
	$\Delta I, u \text{ \AA}^2$	-0.02	-188.7

$$\begin{array}{ccc}
 \left| \begin{array}{c} I_a \\ \\ I_c \end{array} \right| & \xrightarrow[\text{at the point (x,y,z)}]{\text{Adding mass}} & \left| \begin{array}{ccc} I_a + \mu(y^2+z^2) & -\mu xy & -\mu xz \\ -\mu xy & I_b + \mu(x^2+z^2) & -\mu yz \\ -\mu zx & -\mu yz & I_c + \mu(y^2+x^2) \end{array} \right| = \left| \begin{array}{c} I_{a'} \\ \\ I_{c'} \end{array} \right| \\
 \text{Bare molecule inertia tensor} & & \text{Complex inertia tensor}
 \end{array}$$

Figure 3. Kraitchman's equations.

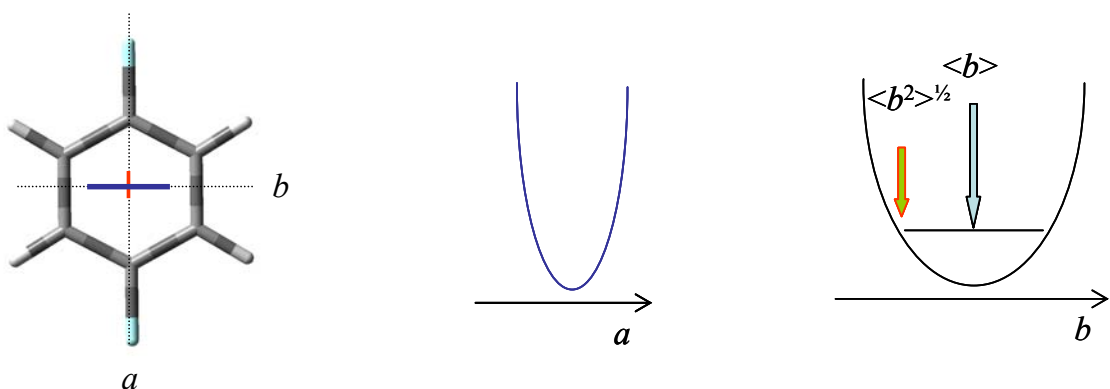
knowing its mass, one can determine the a , b , and c coordinates of Ar atom in the complex by comparing its rotational constants with those of the bare molecule. This is the Kraitchman procedure [13]. To be valid, it is only necessary that the geometry of the host molecule be unaffected by complex formation. Clearly, such an assumption must break down occasionally (for example, in the case of “induced fits”), but this is not likely in weakly bound van der waals complexes.

Table 2 lists the COM coordinates of the Ar atom in p DFB-Ar that were determined in this way. First, we focus on the values of $|c|$, the out-of-plane displacement coordinate. The Ar is located at a distance of 3.55 Å above (or below) the aromatic plane in the S_0 state. The intermolecular potential energy surface is likely to be quite “stiff” in this direction; hence, the value $|c| = 3.55$ Å is likely to be close to the equilibrium value. The value of $|c|$ decreases to 3.48 Å in the S_1 state, evidencing stronger binding in that state, a fact that is also evidenced by the red shift of the origin band of the complex relative to that of the bare molecule. A blue shifted origin band would indicate a less tightly formed Ar atom in the excited state. Thus, we conclude further that the S_1 wavefunction of p DFB is significantly more diffuse, leading to enhanced electron correlation (and tighter binding) in that state.

p DFB is a D_{2h} molecule; hence, we might expect the two in-plane coordinates, a and b to be zero, in both states. This is not the case. The reason that these two coordinates are not zero is that the Ar atom undergoes large vibrational displacements along these coordinates, in both coordinates. Rotational constants are a measure of r.m.s. displacements along these coordinates, not their average values (see below) [14].

Table 2. Center-of-mass (COM) coordinates of the Ar atom in the principal axis frame of *p*DFB in *p*DFB-Ar, as determined from Kraitchman's equations.

Å	S ₀	S ₁
$\langle \mathbf{a}^2 \rangle^{1/2}$	0.0095(27)	0.0350(4)
$\langle \mathbf{b}^2 \rangle^{1/2}$	0.07(2)	0.346(4)
$\langle \mathbf{c}^2 \rangle^{1/2}$	3.5505(5)	3.4827(4)



Thus, they are extremely sensitive to the detailed shape of the intermolecular potential along a and b . In this case, the large increase in $|b|$ in the S_1 state of $pDFB-Ar$ is particularly striking; it is an order of magnitude large than $|a|$.

Figure 4 illustrate what we believe to be the equilibrium for this remarkable effect. Shown there is a difference density plot, showing the region of the molecule in which the π -electron density changes when $pDFB$ absorbs light. These were calculated using the Gaussian 98 suite of programs [15]. A 6-31G* basis set was employed, the MP2 method was used for the S_0 state, and the CIS method was used for the S_1 state. These calculations qualitatively reproduce the changes in the rotational constants that occur when the molecule absorbs light. These changes are a consequence of a quinoidal distortion of the ring. Thus, as Fig. 4 shown, there is a shift in π -electron density from regions parallel to the C-F bands to regions perpendicular to these bonds. As a result, this distribution is much more anisotropic in the S_1 state.

One measure of this anisotropy is the quadrupole moment of the charge distribution. Theoretical values of these are shown in Table 3. Q_a and Q_b , though having different signs, are similar in magnitude in the S_0 state. Thus the motion of the attached Ar should more or less equal

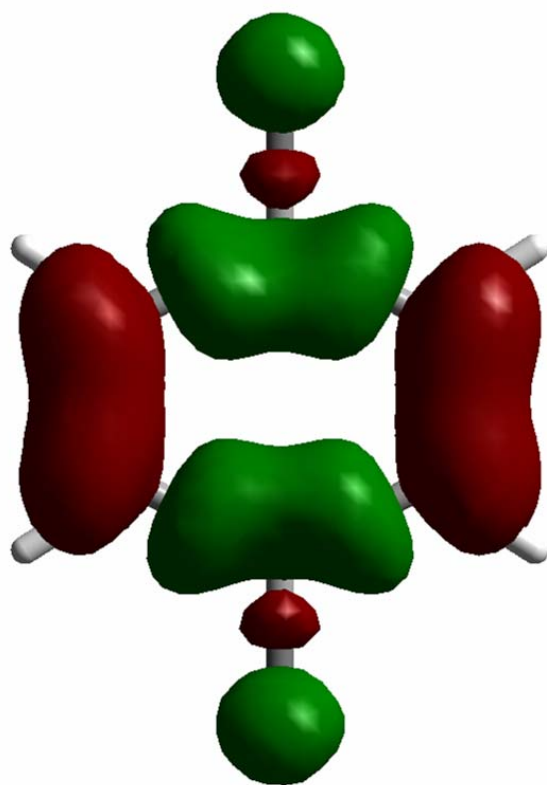


Figure 4. Electron density difference map for the S₁-S₀ transition of *p*DFB. Red contours indicate regions of electron gain, and green contours indicate regions of electron loss

Table 3. Quadrupole moments of *p*-difluorobenzene in its S₀ and S₁ electronic states, according to theory (MP2/CIS 6-31G**).

Parameter ^a	S₀	S₁
Q_a	-19.27	-9.64
Q_b	+19.18	+12.62
Q_c	+0.10	-2.97

amplitudes in both direction. However, when the molecule is excited to its S_1 state, this distribution changes; $|Q_b|$ is much larger than $|Q_a|$. This leads to larger amplitude motions in direction perpendicular to a , and to larger vibrationally averaged values of $|b|$, compared to $|a|$. Thus illustrated, perhaps for the first time, is a significant dependence of the vibrational motion the weakly bound Ar to the electronic distribution of the substrate to which it is attached.

*p*DFB has fairly high symmetry. Therefore, it was of interest to learn how the properties of van der Waals complexes might be modified by making the substrate less symmetric. This was the purpose of our experiments on indole-Ar (I-Ar) and 7-azaindole-Ar (7AI-Ar). Figure 5 compares the high resolution spectrum of I-Ar with that of indole itself [16]. The complex-induced change in the orientations of the inertial axes is immediately apparent. The hybrid band character of the origin band (61.6% a and 38.4 % b) is changed to 12% a , 47% b , and 41% c in I-Ar. Beyond this, a rigorous fit of the spectrum (see Fig. 6) requires an additional assumption that inertial axis tilting occurs when the photon is absorbed.

“ Axis tilting” refers to the intentional situation that can develop when the principal axes of the moment of inertial tensor in two different electronic states of a molecule do not coincide. The phenomenon was first detected in the electronic spectra of acetylene and other small molecules, and explained in a landmark paper by Hougen and Watson [17]. More recently, axis tilting has been detected in several large molecules [18]. Fundamentally, since the intensities in an electronic spectrum depend upon the projection of the TM on the inertial axes, and since these projection change when axis tilting occurs, this can lead to anomalous intensities in a fully resolved spectrum. A full discussion of such “ quantum interference” effects and how they might be exploited is given elsewhere [19].

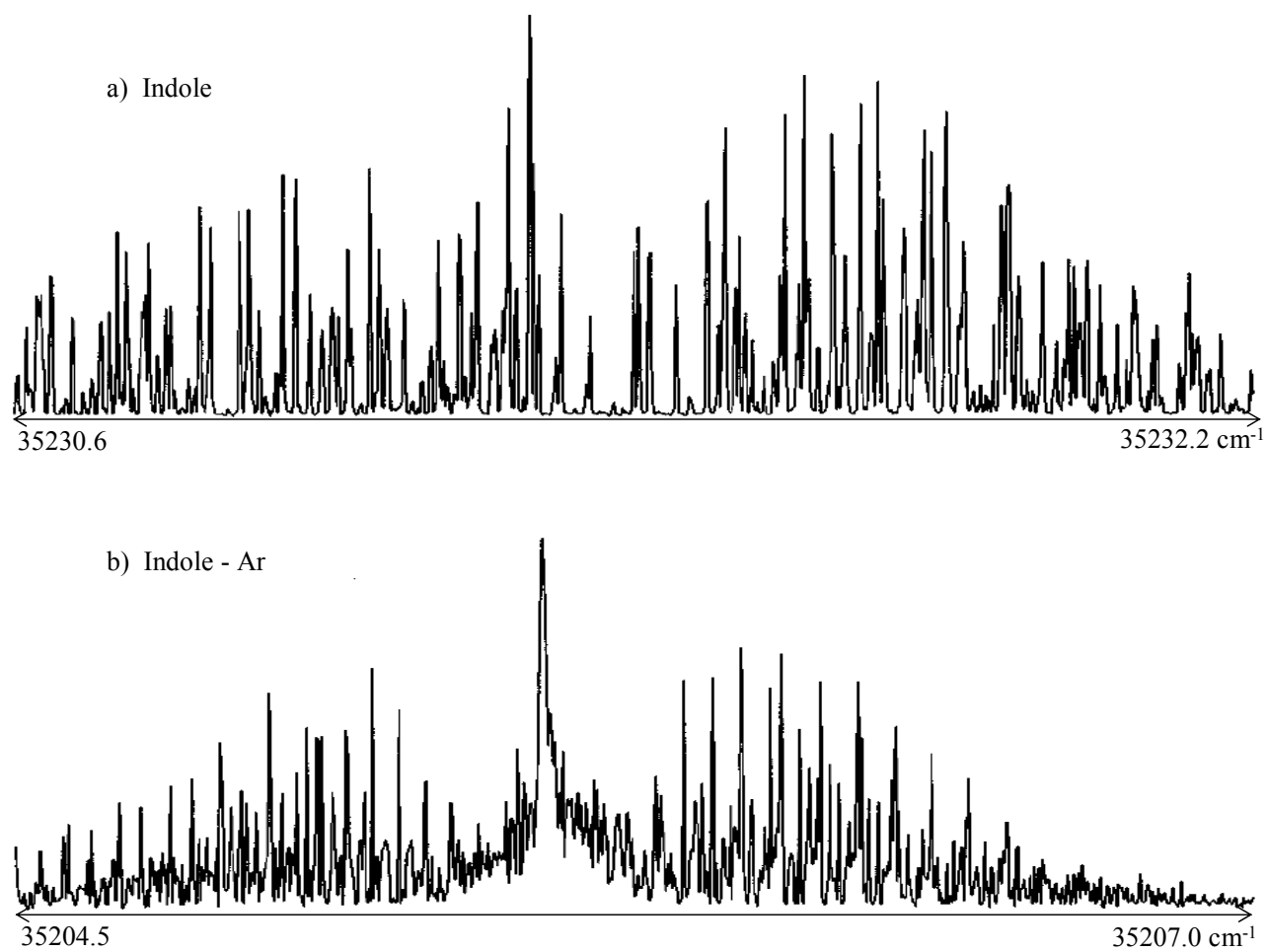


Figure 5. Rotationally resolved fluorescence excitation spectra near 284 nm of the origin Bands in the S_1 - S_0 transitions of (a) bare indole at 35231 cm^{-1} and (b) the indole-argon van der Waals complex at 35205 cm^{-1} (Ref. [17]).

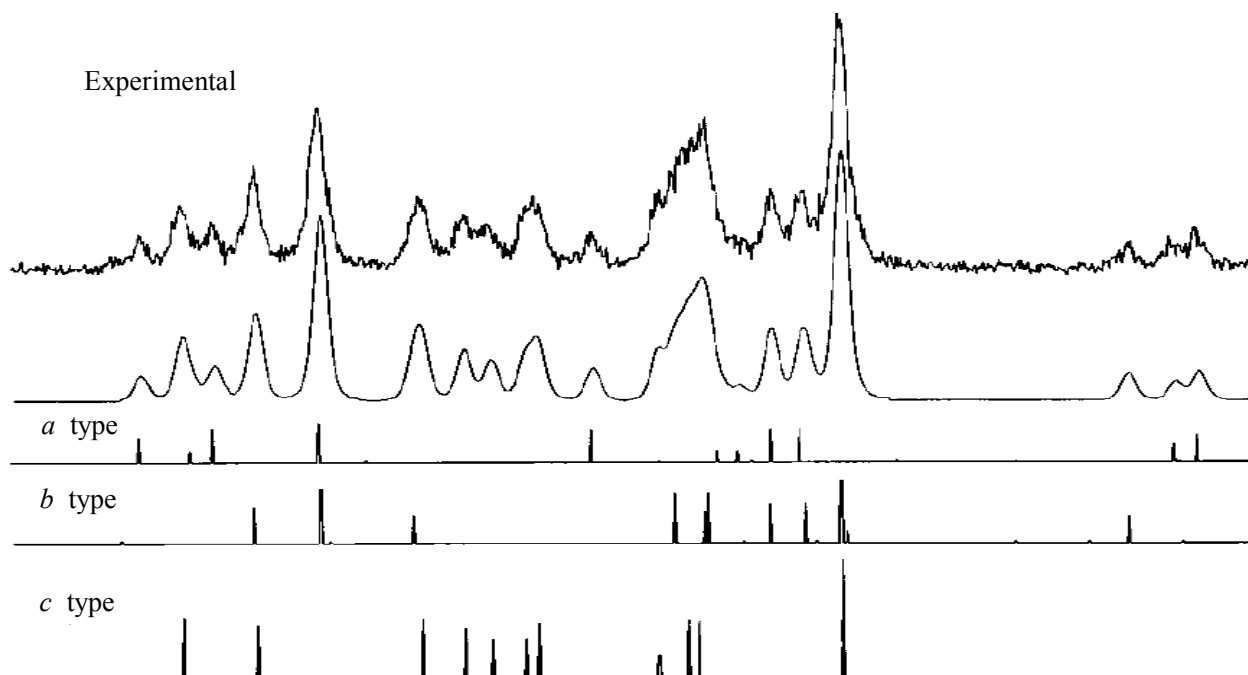


Figure 6. A portion of the high resolution spectrum of indole-argon at full experimental resolution, extracted from the R branch. The top trace is the experimental spectrum. The second trace is the sum of the *a*-, *b*-, and *c*-type calculated spectra in the lower three traces, each of which has been convoluted with a 22 MHz FWHM Voigt lineshape profile (16 MHz Gaussian component and 8 MHz Lorentzian component) (Ref. [17]).

The axis tilting that occurs in I-Ar is clearly a consequence of changes in electronic distribution that take place when the molecule absorbs light. Since the substrate itself is asymmetric, a change in their distribution results in a change in the equilibrium position of the Ar atom, not just in its vibrationally averaged coordinates. We therefore expected a similar result when we undertook a study of the similar molecule, 7AI-Ar. Figure 7 shows its high resolution spectrum which shows no evidence of axis tilting at all ! Apparently, either the equilibrium geometry of 7AI-Ar, or the change in their geometry which occurs when it absorbs light, is significantly different from that in I-Ar [20].

As discussed elsewhere [18], quantum interference effects are most pronounced in a fully resolved spectra when the band is a hybrid band. The 0_0^0 band of 7AI-Ar is a mainly b-type band, so large interference effects are not expected, in any event.

Table 4 lists the COM coordinates of the Ar atom in the principal axis frame of indole (in the I-Ar complex) and 7AI (in the 7AI-Ar complex) that were determined from Kraitchman analyses of their corresponding spectra.

In this case, fits of the spectra of both I-Ar and 7AI-Ar evidence significant centrifugal distortion effects [11]. Correction for these effects has been applied to the data in Table 4. Examining the results, we see that the Ar atom lies above (or below) the I (7AI) plane at a distance of 3.43 (3.41 Å), slightly less than the corresponding distance on pDFB. The van der Waals “bond” appears to be slightly decreases by ~ 0.4 Å on absorption of light, again in accord with the red shift of the Ar complex bands (-26 cm^{-1} in both I and 7AI). But the most interesting data in this table are the in-plane coordinates, a and b . Both $|a|$ and $|b|$ are large in I-Ar, and roughly equal in both electronic states. Their magnitudes decrease on S_1 excitation. But in 7AI-Ar, $|b|$ is significantly larger than $|a|$ in both states, and $|a|$ increases in the S_1 state, whereas

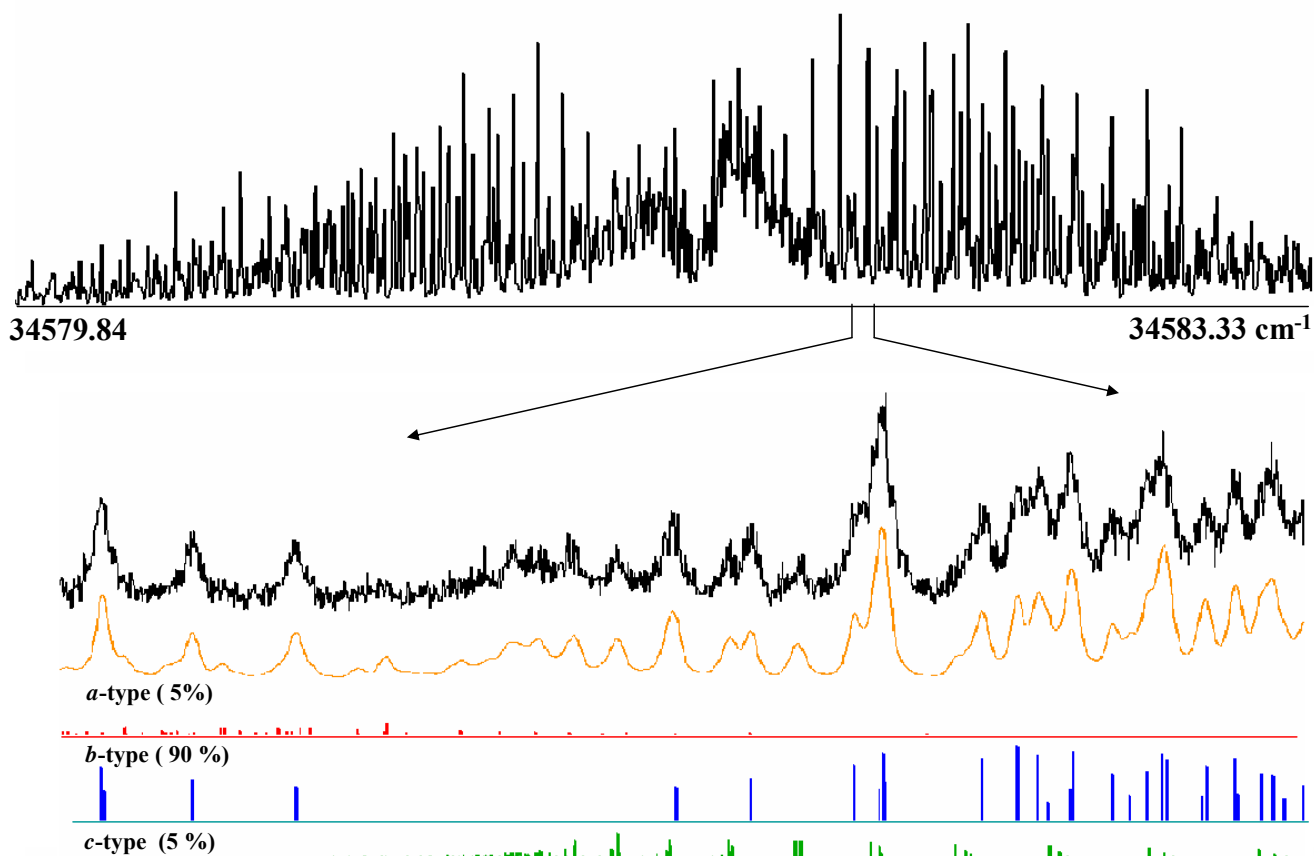


Figure 7. Rotationally resolved fluorescence excitation spectrum of the 7-azaindole-Ar complex. The top trace shows the overall experimental spectrum. The bottom traces show a $\sim 0.1 \text{ cm}^{-1}$ portion of the experimental spectrum and two simulations, with and without a superimposed lineshape function. The individual *a*-, *b*-, and *c*-type contributions are also shown (Ref.[21]).

Table 4. Comparison of center-of-mass (COM) coordinates of the Ar atom in the principal axis frame of 7-azaindole in 7-azaindole-Ar, and of indole in the indole-Ar complex, as determined from a Kraitchman analysis.

State	Coordinate	Indole frame (Å)	7-Azaindole frame (Å)
S_0	$ a $	0.411(1)	0.088(4)
	$ b $	0.4482(1)	0.477(4)
	$ c $	3.434(4)	3.4076(6)
	$ r $	3.4881(3)	3.4420 (3)
S_1	$ a $	0.3707(5)	0.115(3)
	$ b $	0.3727(5)	0.411(4)
	$ c $	3.400(4)	3.380(4)
	$ r $	3.4410(3)	3.4069(3)

$|b|$ decreases. The substantial differences in the coordinates of the Ar atom in the two complexes provide compelling evidence that their intermolecular PES's are different, as well.

Before discussing these differences, we first address the sign ambiguities in the two coordinates, $|a|$ and $|b|$. Each coordinate could be either positive or negative, since the moments of inertia (upon which the Kraitchman analysis is based) depend on the squares of the displacements of the different atoms from the three inertial axes. In the case of I-Ar, this means that there are four possible binding sites, shown in Figure 8. Two of the sites (I & II) are displaced toward the six-membered ring, and two of the sites (III & IV) are displaced toward the five-membered ring; site IV is almost to the ring nitrogen atom. Fortunately, the four sites can be distinguished by deuterating the N-H hydrogen, recording and analyzing the high resolution spectrum of N-deuterated I-Ar, using Kraitchman's equations [13] to determine the COM coordinates of the N-H hydrogen atom, in I-Ar, and comparing these coordinates to theoretical ones. Their comparison led to a clear choice of site IV as the preferred binding site [16]. The Ar atom is localized above the five-membered ring, displaced toward the N atom.

We can understand this result as being a consequence of an additional attractive interaction between the Ar atom and the nitrogen lone pair electrons, which occupy an out-of-plane π -type orbital perpendicular to the ring. Calculations suggest that the S_1 - S_0 electronic transition of indole results in significant change displacement for the five-membered ring to the six-membered ring, which accords with recent measurements of the dipole moments in its S_0 and S_1 electronic states (*vide infra*). This explains, then, why the magnitudes of $|a|$ and $|b|$ in I-Ar decrease when the photon is absorbed, a "motion" that is responsible for the observed axis tilting in its spectrum.

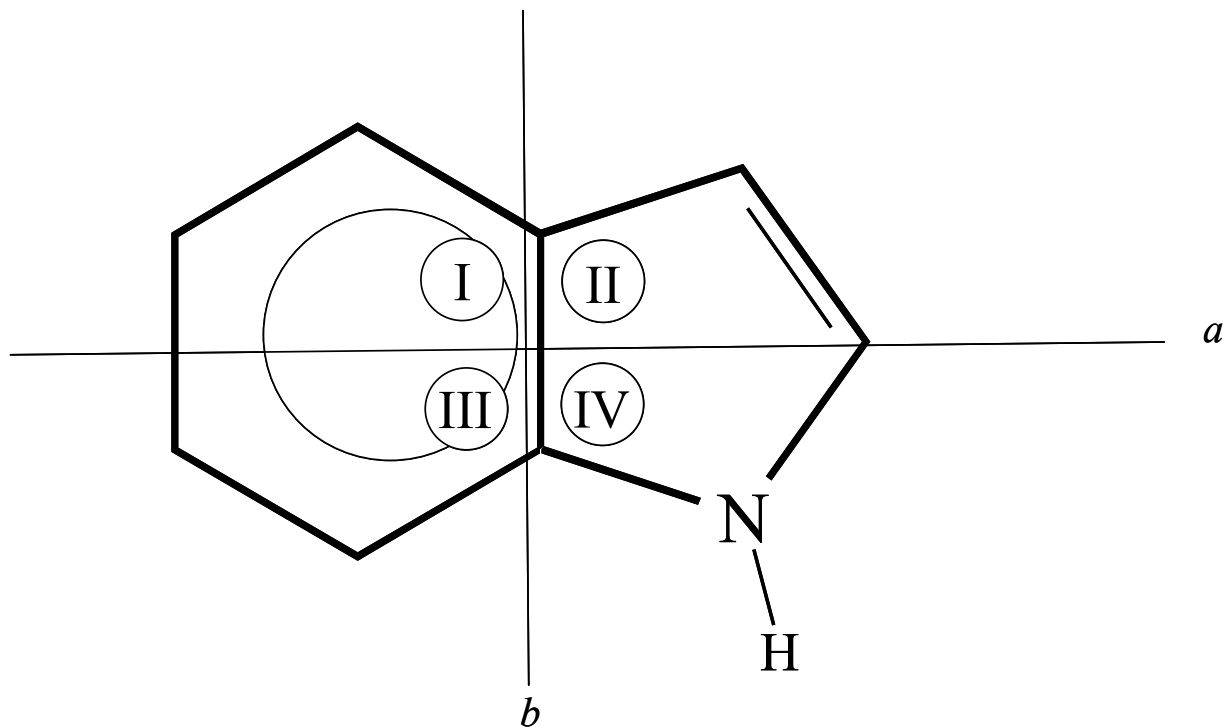


Figure 8. Two-dimensional projections of the geometry of the indole-argon van der Waals complex, as determined from a Kraitchman analysis. The four possible positions of the Ar atom listed in Table 4 are shown as circles. Only site IV is consistent with the results on *N*-deuterated-indole-Ar.

$|a|$ and $|b|$ are different in 7AI-Ar because the intermolecular forces are different. Figure 9 and 10 show minimum energy paths along the a axis of the PES's of I-Ar and 7AI-Ar calculated using MP2/6-31G** methods [15]. Both surfaces have two non-equivalent minima, at $\{-0.30, -0.45\text{\AA}\}$ and $\{0.85, -0.45\text{\AA}\}$ in I, and at $\{-0.30, -0.45\text{\AA}\}$ and $\{0.45, -0.45\text{\AA}\}$ in 7AI. But the differences in energy between these two minima are very different in the two complexes. In I-Ar, the minimum with positive a is $\sim 50\text{ cm}^{-1}$ lower energy than the minimum with negative a , giving a preferred binding site for the Ar atom that is shifted away from the center of the ring and towards the nitrogen atom. In contrast, the energy difference between one side of the ring and the other in 7AI is very small. The barrier separating the two minima is very low, of order 1 cm^{-1} , and is barely seen on the scale of the figure, meaning that Ar atom is not localized on either ring. The vibrationally averaged probability density is spread out along the a axis with a maximum $\langle a^2 \rangle^{1/2}$ value near zero, in excellent agreement with the Kraitchman analysis result.

The main source of attraction that is responsible for the minima in these surfaces is likely to be a dipole-induced dipole interaction between the bare molecule and the Ar atom. I and 7AI are apparently very different in their respect. While the two host molecules have comparable dipole moments in their ground states, 1.903 D in I [21] and 1.45 D in 7AI [22], the orientations of these two dipole are quite different. The dipole moment in I is oriented along the N-C axis towards the benzene ring ($\theta_d = 45.5^\circ$) whereas the dipole moment in 7AI has a large component pointing towards the pyridine ring ($\theta_d = -24.1^\circ$). The nitrogen lone pair in 7AI makes a large contribution to this dipole. Thus, while there is only one attractive nitrogen atom in I-Ar, there are two attractive nitrogen atoms in 7AI, which leads to a delocalization of the Ar atom. The Ar atom spends most of its time in between the two local minima. Recent Stark-effect measurements have shown that electronic excitation of 7AI leads to large changes in both the

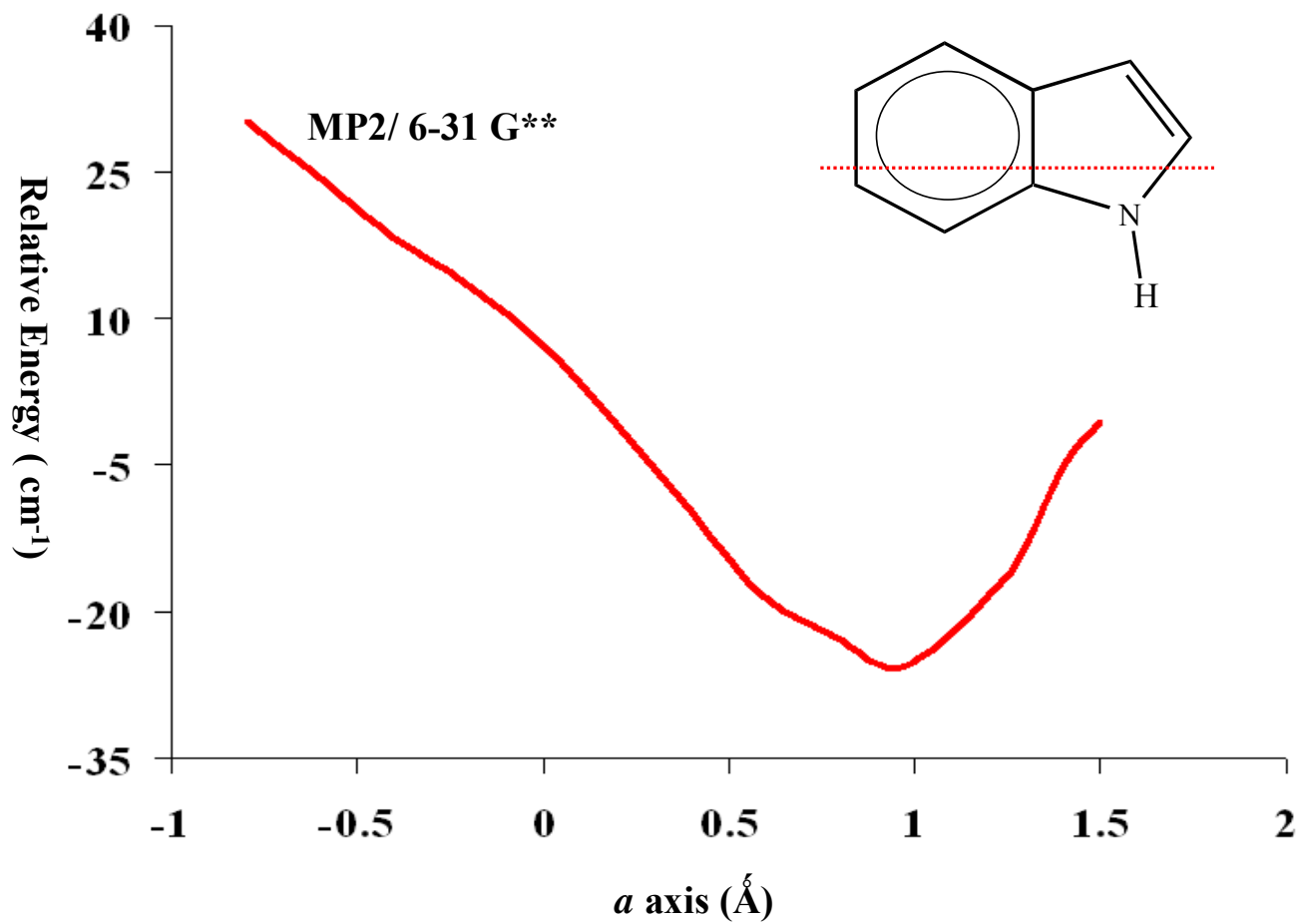


Figure 9. Potential profile of the intermolecular PES in the S_0 state of indole-Ar along the minimum energy path.

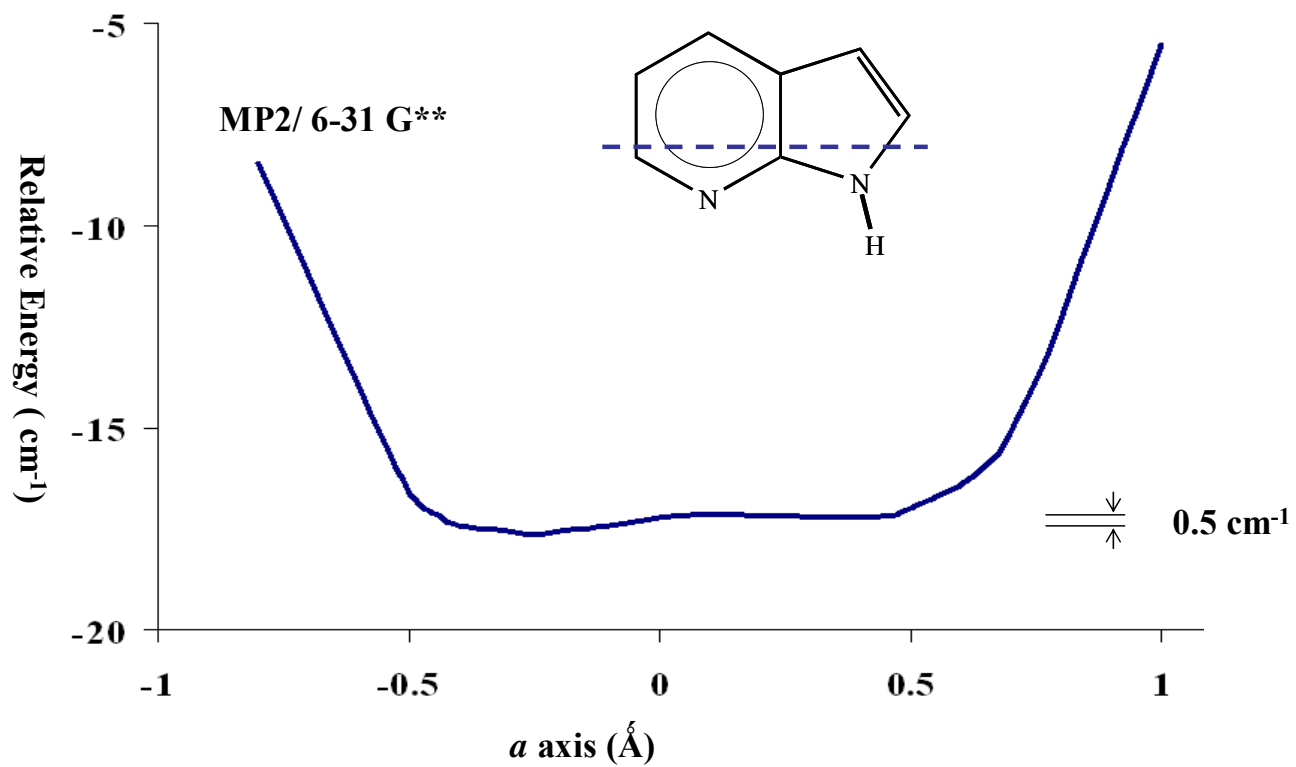


Figure 10. Potential profile of the intermolecular PES in the S_0 state of azaindole-Ar along the minimum energy path.

magnitude and orientation of its dipole moment; μ_a increases by 53 % and μ_b decreases by 15 % in the S_1 state, compared to the ground state. The 0.03 Å (31 %) increase in $|a|$ and 0.07 Å (14 %) decrease in $|b|$ in the Ar complex of 7AI are likely consequences of this light-induced change in electronic distribution.

A wide variety of other rare gas complexes of organic molecules have been studied using high resolution techniques. These include fluorene-Ar [23], *trans* stilbene-Ar [24], , triphenylamine-Ar [25], 1- and 2-fluoronaphthalene-Ar [26], aniline-Ar [27, 28], 4-fluorostyrene-Ar [29], pyrazine-Ar [30], 1- and 3-methylindole-Ar [31], and tetracene-Ar [32]. In aniline-Ar (An-Ar) [27], it was found that the Ar atom resides at a distance of ~ 3.5 Å above the aromatic plane, and that distance decreases slightly on excitation to the S_1 state. Additionally, the Ar atom exhibits significant large amplitude motion in both states. Despite this fact, it remains localized on one side of ring; the anti structure is more stable. Thus, the symmetric double well along the inversion coordinate of the bare molecule is converted into an asymmetric double well. At higher energies, An-Ar (and other weakly bound complexes) undergo vibrational predissociation (VP); these spectra have been shown to exhibit line broadenings and spectral perturbation from which the timescales and the important role of IVR in promoting the VP process has been elucidated.

A.4 N₂ complexes

Figure 11 shows the rotationally resolved S_1 - S_0 fluorescence excitation spectrum of the N₂ van der Waals complex of *p*DFB. This spectrum differs from that of the bare molecule in three ways. First, the origin band is shifted by ~ 27 cm⁻¹ with respect to that of *p*DFB itself. Second, the band type of the two spectra differs. Whereas the bare molecule exhibits a pure *b*-

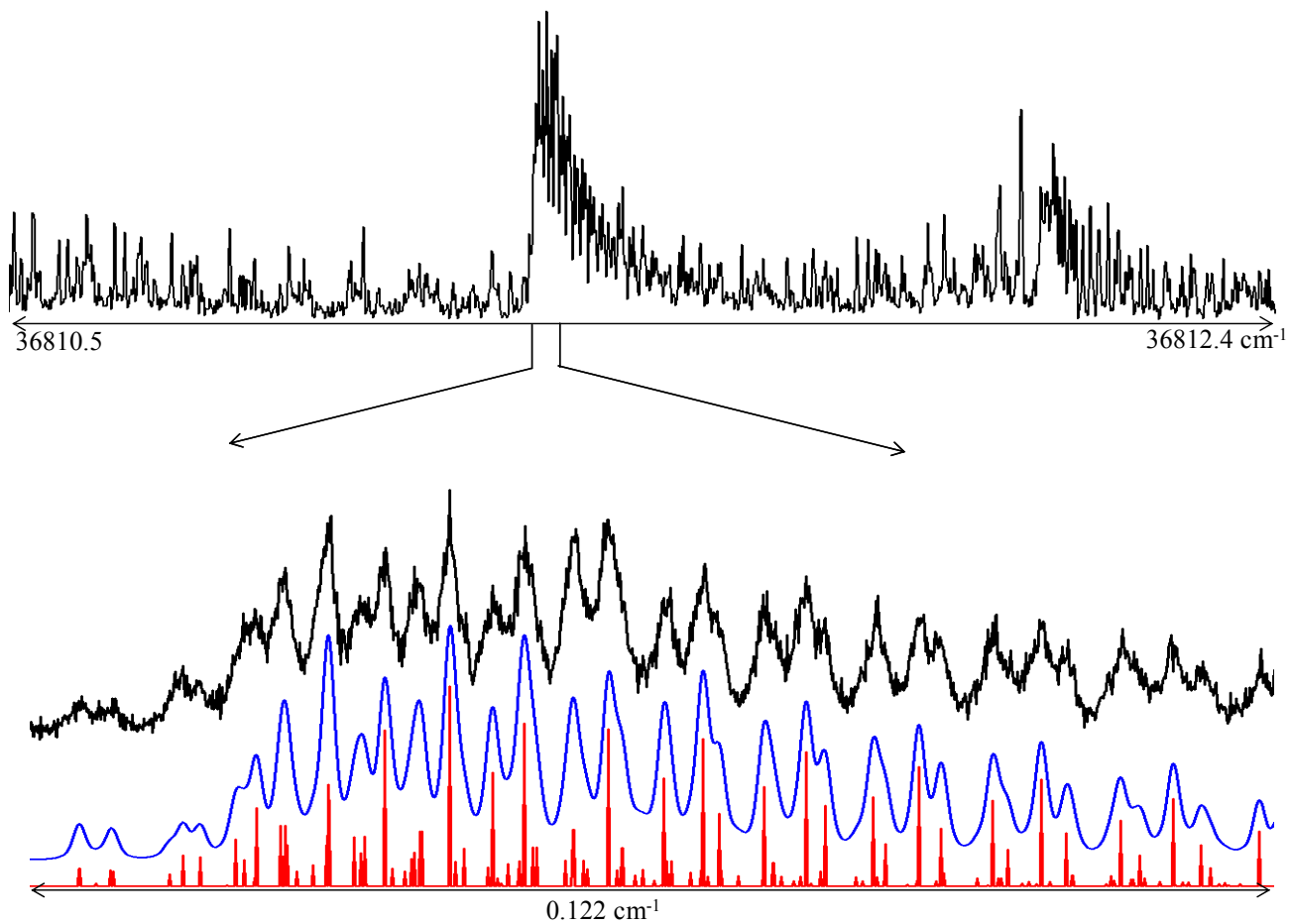


Figure 11. Rotationally resolved fluorescence excitation spectrum of the *p*-difluorobenzene-dinitrogen complex. The top trace shows the overall experimental spectrum. The bottom traces show a $\sim 0.1 \text{ cm}^{-1}$ portion of the experimental spectrum and two simulations, with and without a superimposed lineshape function (Ref. [35]).

type spectrum, showing no central Q branch, the spectrum of *p*DFB-N₂ exhibits an obvious Q branch and follows *c*-type selection rules. Both of these effects were observed in *p*DFB-Ar. But *p*DFB-N₂ exhibits a new feature not encountered before; its S₁-S₀ origin band is split into two subbands, with a relative intensity of 2:1. The electronic origin of the bare molecule (and its Ar complex) consists of only a single band.

Fitting spectra like this has provided many new challenges in high resolution electronic spectroscopy. The effective Hamiltonian is significantly more complicated than a rigid rotor one. On the other hand, the larger numbers of parameters that are needed to describe such spectra provide more information about the molecule, its complex, and the forces that hold it together. In the particular case of *p*DFB, the “new” motion that is revealed is a hindered internal rotation of the attached N₂. Thus, if such spectra can be fit, we learn a great deal about the anisotropy of the intermolecular potential. That is what makes small molecules like N₂, H₂O, NH₃, and CH₄ interesting binding partners in the van der Waals (and hydrogen bonded) complexes of organic molecules.

The Hamiltonian that governs the internal motion of the attached N₂ is

$$\hat{H}_{\text{eff}}^t = F p^2 + (V_2/2) (1 - \cos 2\tau) \quad (2)$$

Here, *F* is the reduced rotational constant for the motion described by the angle τ , *p* is the angular momentum of the N₂ motion, and *V*₂ is an effective hindering potential. (The same Hamiltonian would be used to describe the motion of a two-fold rotor like an OH group covalently bound to an aromatic molecule.) A single rotor of this type has two torsional levels for each torsional quantum number *v*, a single A torsional level and a single B torsional level. Degenerate in the infinite barrier limit, the two levels are split by tunneling through a finite barrier. A similar situation exists in both electronic states. However, since the barriers are likely

to be different, the tunneling splitting will be different, and the allowed electronic transitions (A-A and B-B) also will be split, by the difference in the tunneling splitting in the two electronic states. This is why the spectrum of *p*DFB-N₂ is split into two subbands. Each subband, in turn, is described by different rotational constants, since the A and B torsional levels are different regions of the potential.

Fortunately, there is one other interaction that influences the spectra of such species, and that is torsion-rotation interaction. As is apparent, torsions possess (a partially quenched) angular momentum, and this couples to the corresponding angular momentum associated with overall rotational motion. A detailed discussion of this coupling, first analyzed in detail by Herschbach [33], may be found in the monograph of Gordy and Cook [34].

Suffice it to state here that one can determine the axis about which the motion is occurring, its orientation in the molecular frame, and the barrier to internal rotation in both electronic states by carefully measuring such couplings in a high resolution spectrum. We have written elsewhere about several application of this method.

Unfortunately, it has so far proved impossible to fit the weaker of the two subbands in Fig. 11. However, more than 200 lines in the stronger subband have been fit to high precision (OMC = 4.4 MHz), when centrifugal distortion terms are included [11].

Information about the geometry of the complex was obtained from its planar moments of inertia (P). There are related to the ordinary moments of inertia (I) by $P_a = (I_a + I_b - I_c) / 2$, etc. Values of these for both *p*DFB and *p*DFB-N₂ are listed in Table 5.

In the bare molecule, the c inertial axis is perpendicular to the ring plane and a inertial axis lies in the plane, passing through the fluorine atoms. Examining the data in Table 5, we see that $P_a(p\text{DFB-N}_2) (= P_a) \approx P_a(p\text{DFB}) (= P_a^m)$. This means that the orientation of the *a* axis in

Table 5. Moments of inertia I and planar moments of inertia P of *para*-difluorobenzene (*p*DFB) and its nitrogen complex, and differences between the moments of inertia of the complex and the monomer.^a

	Parameter	<i>p</i> DFB		<i>p</i> DFB-N ₂	
		I^m	P^m	I	P
Ground State	a	89.64(1)	353.91(2)	370.3(1)	353.1(10)
	b	353.91 (2)	89.64(2)	447.9(2)	275.5(10)
	c	443.55(4)	0.00(2)	628.7(20)	94.8(10)
	$a - a^m$			280.8(1)	-0.8(7)
	$b - c^m$			4.5(2)	275.5(11)
	$c - b^m$			274.7(20)	5.1(10)
Excited State	a	95.66(1)	352.28(2)	363.1(1)	351.7(10)
	b	352.38(2)	95.56(2)	448.8(1)	266.0(10)
	c	447.83(4)	0.10(2)	617.8(19)	97.1(10)
	$a - a^m$			267.5(1)	-0.6(10)
	$b - c^m$			1.0(1)	265.9(11)
	$c - b^m$			265.4(19)	1.5(10)

^a All values in uÅ². Uncertainties in the last digits are given in parentheses.

p DFB is unchanged on complexation. We also see that $P_c \approx P_b^m$. This means that the orientation of the b and c axes are exchanged when the N_2 is attached, thus explaining why the 0_0^0 band of p DFB- N_2 is c axis polarized. The S_1 - S_0 TM of the complex still lies in the plane of p DFB, approximately perpendicular to a .

Table 5 also lists values of the differences in the relevant planar moments of p DFB- N_2 , from which more structured information can be obtained. Thus, among the differences, $P_b - P_c^m$ is by far the largest. A large $P_b - P_c^m$ ($P_c^m \approx 0$) requires that the N_2 molecule lies on the top (or the bottom) of the benzene ring, in both electronic states. A complex configuration with the N_2 molecule lying in or near the plane of p DFB would require $P_b \approx 0$ and a- and/or b-type selection rules. Of further interest are the values of $P_a - P_a^m$ and $P_c - P_b^m$. Though small, neither of these planar moment of differences is zero. This means that the N_2 molecule cannot be attached to p DFB “end-on”, perpendicular to the complex ac plane. Instead, the N_2 molecule must lie more or less in a plane parallel to the ac plane. This is a surprising result, since N_2 is roughly spherical. Its in-plane and out-of-plane polarizabilities must be substantially different.

The value of the moment of inertia of the N_2 molecule is $8.5 \text{ amu } \text{\AA}^2$ [35]. Neither planar moment difference in p DFB- N_2 is as large as this, but $P_c - P_b^m = 5.1 \text{ amu } \text{\AA}^2$ and $P_a - P_a^m = -0.8 \text{ amu } \text{\AA}^2$ in the S_0 state. The fact that these values are substantially different suggests that the N_2 molecule has a preferred orientation; the $N \equiv N$ axis is roughly parallel to the complex c axis in this state, perpendicular to the line joining the two fluorine atoms. $P_c - P_b^m$ is significantly smaller in the S_1 state, being approximately equal (in magnitude) to $P_a - P_a^m$. this suggests that the preferred orientation of the $N \equiv N$ axis changes when the photon is absorbed.

A more rigorous treatment of this problem requires that the effects of large amplitude motion be taken into account. Two types of motion would seem to be important, “radial”

motions and “angular” ones. Radial motions result in displacements of the N₂ molecule’s COM from its equilibrium position. Angular motions result in tilts of the N₂ molecule’s N≡N bond axis with respect to its equilibrium position. Both types of motion should be fast on the time scale of overall molecular rotation. Thus, the measured rotational constants are vibrationally averaged values over both kinds of coordinates.

Previous studies of the dynamical properties of similar complexes in the gas phase suggest that the intermolecular potential energy surface is relatively steep along the radial coordinate, and relatively flat along the angular ones. The same would be expected to be true for *p*DFB-N₂ [36]. Therefore, radial motions are ignored in what follows. Angular motions are taken into account by defining the coordinates ρ and τ shown in Fig. 12. ρ is a “tilt” angle that describes the orientation of the N≡N axis in the *ab* plane ($\rho = 90^\circ$ in the parallel configuration), and τ is a “torsional” angle that describes the orientation of the N≡N axis in the *ac* plane ($\tau = 0^\circ$ when the N≡N axis is parallel to the *a* axis). Using these coordinates, a set of equations can be written that describe the relations between the moments and products of inertia of the complex $I_{\alpha\alpha'}$ ($\alpha, \alpha' = a, b, c$) and those of the bare molecule I_a^m . These are [34]

$$I_a = I_a^m + (\sin^2 \tau \sin^2 \rho + \cos^2 \rho) I_{N_2} + \mu(b^2 + c^2) \quad (3)$$

$$I_b = I_c^m + \sin^2 \rho I_{N_2} + \mu(a^2 + c^2) \quad (4)$$

$$I_c = I_b^m + (\cos^2 \tau \sin^2 \rho + \cos^2 \rho) I_{N_2} + \mu(a^2 + b^2) \quad (5)$$

$$I_{ab} = -\cos \tau \sin \rho \cos \rho I_{N_2} - \mu ab \quad (6)$$

$$I_{ac} = -\sin \tau \cos \tau \sin^2 \rho I_{N_2} - \mu ac \quad (7)$$

$$I_{bc} = -\sin \tau \sin \rho \cos \rho I_{N_2} - \mu bc \quad (8)$$

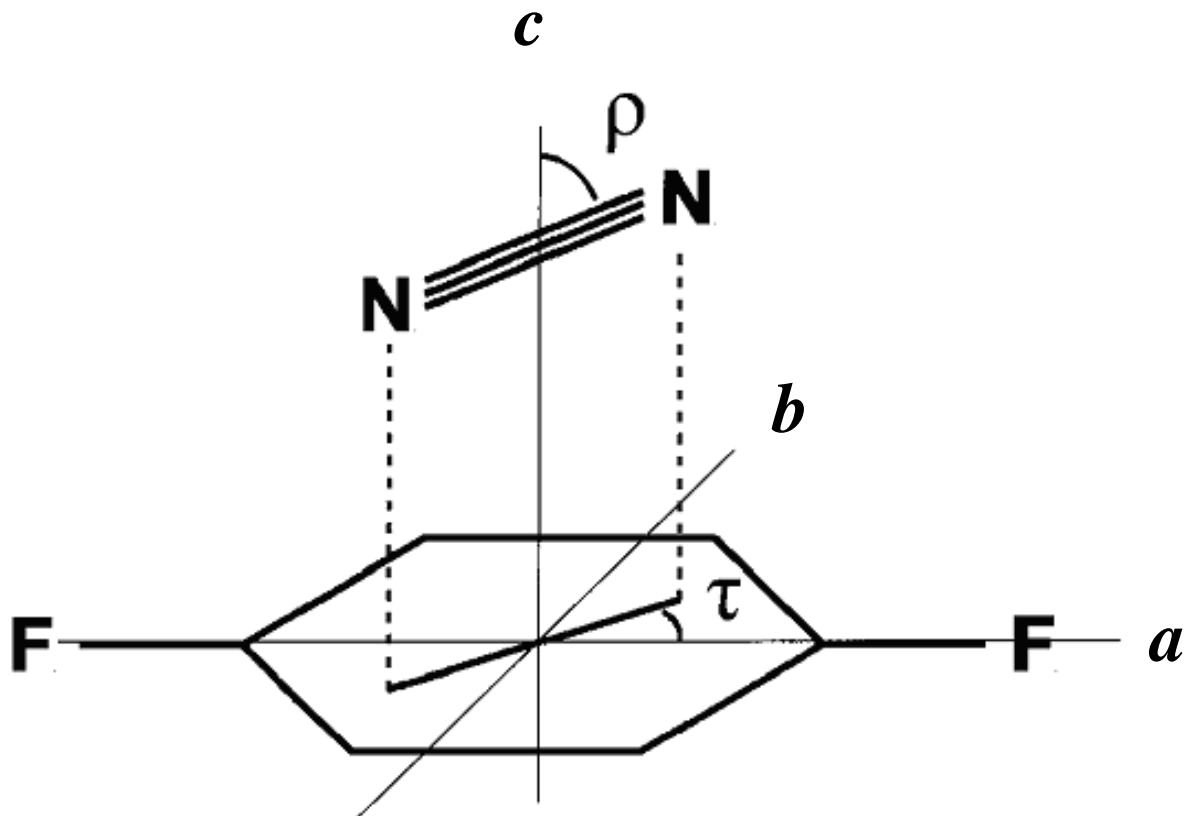


Figure 12. Geometry of the *p*DFB-N₂ complex. The position of the center of mass of N₂ is defined in the principal axis system (*a*,*b*,*c*) of the bare molecule; the orientation of N₂ is defined by ρ (angle between the molecular axis of N₂ and the *c* axis), and τ (angle of rotation of N₂ around the *c* axis.) The figure assumes that this axis is perpendicular to the plane.

Here, $\mu = m_{\text{N}_2} m_{\text{DFB}} / (m_{\text{N}_2} + m_{\text{DFB}}) = 22.4839 \text{ u}$ is the reduced mass of the complex, and a , b , and c are the COM coordinates of the attached N_2 molecule in the principal axis system of the bare molecule (cf. Figure 12). The potential $V(\tau)$ should be 2-fold symmetric, given the likely electronic distribution of $p\text{DFB}$ in both states. (Only a motion that interchanges the nitrogen nuclei can explain the observed 2:1 intensity ratio between the two sub-bands in the UV spectrum). Hence, averaging over τ should result in zero values for $\langle a \rangle$ and $\langle c \rangle$; the COM of the attached N_2 should lie on b . Similarly, the average values of $\langle \sin \tau \rangle$ and $\langle \cos \tau \rangle$ also should be zero. Thus, since I_{ab} , I_{ac} , and I_{bc} (Eqs. 6 - 8) are zero, I is diagonal.

We now use Eqs. 3 – 5 to obtain estimates of $\langle a^2 \rangle$, $\langle b^2 \rangle$, $\langle c^2 \rangle$, ρ , and τ in both electronic states. Unfortunately, there is not enough information to determine all of these parameters independently. So, we first treat the attached N_2 as a point particle with mass μ and ignore its moment of inertia I_{N_2} . Equations 3 - 5 then reduce to the familiar equations of Kraitchman [13]. Comparisons of the experimental moments I_a , etc. of the complex with the corresponding moments I_a^{m} , etc. of the bare molecule then yield estimates of the mean square displacements $\langle a^2 \rangle$, $\langle b^2 \rangle$, and $\langle c^2 \rangle$ of the COM of the attached N_2 in both electronic states. These are listed in Table 6. Examining these data, we see that $\langle c^2 \rangle^{1/2} = 3.53 \text{ \AA}$ in the S_0 state and $\langle c^2 \rangle^{1/2} = 3.45 \text{ \AA}$ in the S_1 state. The decrease in $\langle b^2 \rangle^{1/2}$ in the S_1 state is consistent with the red shift of the S_1 - S_0 origin band of $p\text{DFB-N}_2$ relative to the bare molecule; N_2 is more strongly bound in the S_1 state. The values of $\langle a^2 \rangle^{1/2}$ are relatively small and the values of $\langle b^2 \rangle^{1/2}$ are relatively large, in both electronic states. Previous studies of rare gas complexes of aromatic molecules have yielded vibrationally averaged in-plane coordinates that are more nearly equal, as in 1-fluoronaphthalene-Ar and 2-fluoronaphthalene-Ar [35]. In contrast, $p\text{DFB-N}_2$ exhibits very different values of the two, $\langle a^2 \rangle^{1/2} = 0.09 \text{ \AA}$ and $\langle b^2 \rangle^{1/2} = 0.69 \text{ \AA}$ in the S_0 state. These data

Table 6. Mean square displacements of the nitrogen molecule in the COM coordinate system of *p*DFB-N₂, in its S₀ and S₁ electronic states.^a

Parameter	Ground (S ₀) State	Excited (S ₁) State
$\langle a^2 \rangle^{1/2}/\text{\AA}$	0.09(2)	0.08(2)
$\langle b^2 \rangle^{1/2}/\text{\AA}$	3.53(1)	3.45(1)
$\langle c^2 \rangle^{1/2}/\text{\AA}$	0.69(2)	0.35(2)

^a Uncertainties in parentheses.

suggest that the N₂ molecule moves with significantly larger amplitude (or has significantly greater spatial extent) along *b* than along *a*, which again supports the idea that it is preferentially oriented along *b*, rather than *a*. The value of $\langle b^2 \rangle^{1/2}$ is much smaller in the S₁ state. All of these values are subject to some uncertainty, given the poorly defined potentials along the intermolecular coordinates. But they have at least some quantitative significance.

Next, we re-express Eqs. 3 - 5 in terms of the planar moment differences $P_a - P_a^m$, $P_b - P_c^m$, and $P_c - P_b^m$, obtaining

$$P_a - P_a^m = \frac{1}{2}(1 + \langle \cos 2\tau \rangle) \sin^2 \rho I_{N_2} + \mu \langle a^2 \rangle \quad (9)$$

$$P_b - P_c^m = \cos^2 \rho I_{N_2} + \mu \langle b^2 \rangle \quad (10)$$

$$P_c - P_b^m = \frac{1}{2}(1 - \langle \cos 2\tau \rangle) \sin^2 \rho I_{N_2} + \mu \langle c^2 \rangle \quad (11)$$

Finally, we compare the experimental values of $P_a - P_a^m$, $\langle a^2 \rangle$, etc. (Tables 5 and 6) with Eqs. 9-11, thereby obtaining estimates of $\langle \rho \rangle$ and $\langle \tau \rangle$. Equation 10 yields $\langle \rho \rangle = 45 \pm 10^\circ$ in the S₀ state and $\langle \rho \rangle = 65 \pm 15^\circ$ in the S₁ state. Apparently, the N₂ molecule spends a significant amount of time in near-perpendicular orientations, especially in the ground state. Equations 9 and 11 yield $\langle \tau \rangle = 70 \pm 10^\circ$ in the S₀ state. The corresponding value in the S₁ state is not well determined. Equation 9 gives a similar value, but eq 11 gives a value much less than this, $\langle \tau \rangle = 15 \pm 10^\circ$. We conclude, then, that the N₂ molecule lies mainly in the plane, parallel to the *c* axis in the S₀ state, but rotates more freely in the S₁ state.

The above analysis is deficient in two respects. First, it neglects possible contributions to *B* from the torsional motion itself. Second, it neglects possible contributions to $\langle a^2 \rangle$, $\langle b^2 \rangle$, and $\langle c^2 \rangle$ from the moment of inertia of the attached N₂. A more rigorous treatment of these problems has been given by Schaefer [37].

Estimates of the barriers to internal motion in p DFB-N₂ may be obtained in the following way. First, we assume that the N₂ molecule is rigidly attached to p DFB with its N≡N axis lying in a plane parallel to the ac plane. We further assume the N₂ exhibits a hindered rotation about the c axis which is governed by a 2-fold potential, $V_2(\tau)$. In that event, $\rho = 90^\circ$, $\langle a^2 \rangle = \langle b^2 \rangle = 0$, and $B_{\text{rigid}} = \hbar^2 / (2h[I_c^m + I_{N_2}])$, from eq 2. The difference between this “rigid-body” value of B and the observed B_{eff} can then be used to estimate V_2 via the relation [38]

$$B_{\text{eff}} - B_{\text{rigid}} = FW_A^{(2)} \left(\frac{I_{N_2}}{I_c^m + I_{N_2}} \right)^2 \quad (11)$$

where F is the internal rotor constant

$$F = \frac{\hbar^2}{2hI_{N_2}} \left(\frac{I_c^m + I_{N_2}}{I_c^m} \right) = 60.78 \text{ GHz} \quad (12)$$

and W_A^2 is a second-order perturbation coefficient. In the high barrier approximation, this coefficient can be related to the energy difference between the two lowest torsional states, ΔE [38]

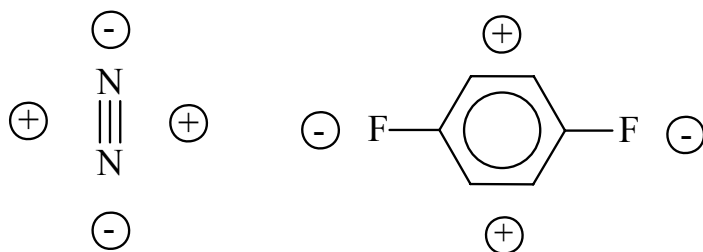
$$W_A^2 = -\frac{1}{2}\pi^2 w_1 \approx \frac{1}{4}\pi^2 (b_2 - b_1) = \frac{1}{4}\pi^2 \frac{\Delta E}{F} \quad (13)$$

from which the reduced barrier height,

$$s = 4V_N / (N^2 F) \quad (14)$$

can be derived. This simple model yields $s = 6.10$ and $V_2 = 12.4 \text{ cm}^{-1}$ for the S₀ state, and $s = 3.77$ and $V_2 = 7.6 \text{ cm}^{-1}$ for the S₁ state. More refined models [37] give the estimates $\sim 10 \text{ cm}^{-1}$ and $\sim 2 \text{ cm}^{-1}$. These estimates reproduce the observed separation of the two subbands in the spectrum, $\sim 21.3 \text{ GHz}$, showing that they are at least approximately correct.

That the $\text{N}\equiv\text{N}$ bond axis is more or less uniquely oriented along the short in-plane axis in the ground state is easily rationalized. *p*DFB and N_2 are both quadrupolar molecules; owing to their high symmetry, their first nonvanishing multipole moments are the quadrupole moments, as shown below. Clearly, the stable configuration of the S_0



state of *p*DFB- N_2 should be the one in which the N_2 is attached to the top (or the bottom) of the aromatic plane, perpendicular to the two C-F bonds. This is exactly what is observed. Further, as we have seen in an analysis of the data for *p*DFB-Ar (*vide supra*, p), the quadrupole tensor of *p*DFB is less anisotropic in the S_1 state of *p*DFB (*cf.* Table 3 and Figure 4). Thus, when *p*DFB is excited by light, the π -electron distribution in the ring becomes more isotropic, V_2 decreases, and there is no longer a preferred orientation of N_2 in the plane. Thereby manifest is a comparison of the results for *p*DFB-Ar and *p*DFB- N_2 are changes in the intermolecular potential that occur when the weakly bound species became less symmetric.

The situation in *p*DFB- N_2 stands in sharp contrast to fact in aniline- N_2 [39]. Here, a large increase in barrier height is observed on S_1 - S_0 excitation, from $\sim 25\text{cm}^{-1}$ in the S_0 state to $\sim 65\text{cm}^{-1}$ in the S_1 state. But N_2 is bound by a dipole-induced dipole interaction in aniline- N_2 , leading to an equilibrium geometry in both states in which the $\text{N}\equiv\text{N}$ bond axis is parallel to the

long axis of the ring. Excitation of aniline to its S_1 state increases its dipole moment [40], thus explaining the large increase in V_2 .

A.5 Water Complexes.

Due to the important role of water as a solvent and its ability to form hydrogen bonds with other molecules, either as a proton donor or acceptor, water-containing complexes have attracted a lot of attention in recent years, especially water complexes of aromatic molecules [41, 42]. If the aromatic molecule contains a functional group with oxygen or nitrogen, it normally forms a water complex with a σ hydrogen bond. In phenol- H_2O [43 - 45], the water binds as proton acceptor to the hydroxy group, whereas it binds as proton donor to the oxygen of the methoxy group in anisole- H_2O [46 - 48]. In aniline- H_2O , the water acts as proton donor to the amino group with a hydrogen bond almost perpendicular to the ring plane [49], whereas in the nitrogen-containing heterocycles pyrrole- H_2O [50] and indole- H_2O [51, 52], the water forms a $N-H \cdots O \cdots H_2O$ hydrogen bond as proton acceptor.

Other water binding motifs exist in aromatic molecules. In the water complex of the nonpolar, hydrophobic benzene molecule, water binds with its hydrogens pointing towards the π electron system, although large-amplitude motions make the elucidation of the exact structure difficult [53 - 57]. In complexes with more than one water molecule, the water molecules form a cluster, which is hydrogen bonded to the π electron system of benzene [46,53,58,59]. And in the benzene-water cation, the oxygen atom of water approaches the $C_6H_6^+$ cation in the aromatic plane, an arrangement that is about 160 cm^{-1} lower in energy than the “a-top” geometry [60].

We focus on two water-containing systems here, *p*DFBW [61] and IW [51]. Figure 13 shows the high resolution electronic spectrum of the *p*DFBW complex. This band is blue shifted

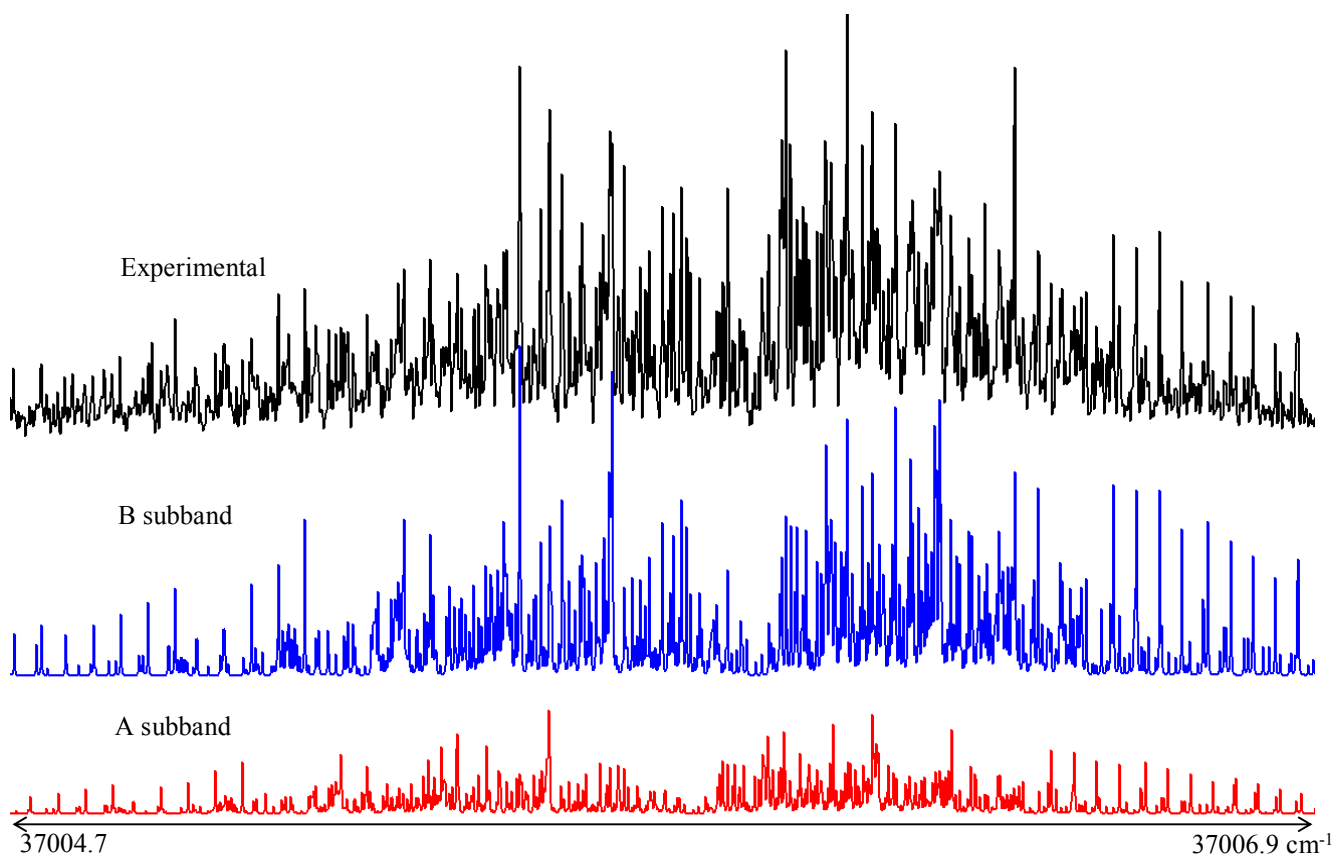


Figure 13. Rotationally resolved fluorescence excitation spectrum of the origin band of the $S_1 \leftarrow S_0$ transition of $p\text{DFB-H}_2\text{O}$, shifted 168.1 cm^{-1} to the blue of the S_1 - S_0 origin band of $p\text{DFB}$. The origin band of the complex is a superposition of two subbands which are separated by 0.121 cm^{-1} . The top trace is the experimental spectrum. The second and third traces are the calculated B and A subbands, respectively (Ref. [66])

by 168.1 cm^{-1} relative to the origin band of the bare molecule. It also contains an underlying subband structure; there are two overlapping bands in the spectrum that are separated by 3.63 GHz (0.121 cm^{-1}), as determined by an autocorrelation method. They also have different relative intensities (1:3), with the weaker subband being shifted to lower frequency. The different intensities have their origin in the nuclear spin statistical weights of the rotational levels in the complex. The two hydrogens of the attached water molecule are being exchanged by a motion that renders them equivalent, on a time scale that is fast compared to overall rotation. The fact that the weaker subband lies to lower frequency reveals that the barrier to their motion in the excited state is less than that in the ground state. We shall return to this important point later.

We initially worked to fit the stronger of the these two subbands. The fitting procedure began with the simulation of a spectrum using assumed geometries of the complex. We assumed that the water lies in the plane of *p*DFB and that the one O-H bond of the water is involved in the formation of a six-membered ring system with the F-C-C-H fragment of *p*DFB, as shown in Fig. 14. The simulated spectrum was compared with the experimental spectrum and several transitions were assigned. An effective way to fit the spectrum is using “selected quantum number” feature of *jb95* [12]. Each of the resolved lines was first assigned with $K_a=0$ and subsequently followed by $K_a = 1,2,3,\dots$, because the intensity significantly decreases as K_a increases. A least-squares fit of assigned quantum numbers to the spectrum with the procedure outlined above was used to modify the assumed rotational constants. This procedure was repeated iteratively until all stronger lines were accounted for. To fit the weaker band, a second spectrum was generated using the rotational constants of the stronger subband and moved along the frequency axis based on the autocorrelation results. A selected K_a quantum number assignment was carried out in the manner described above and optimized by a least-squares fit.

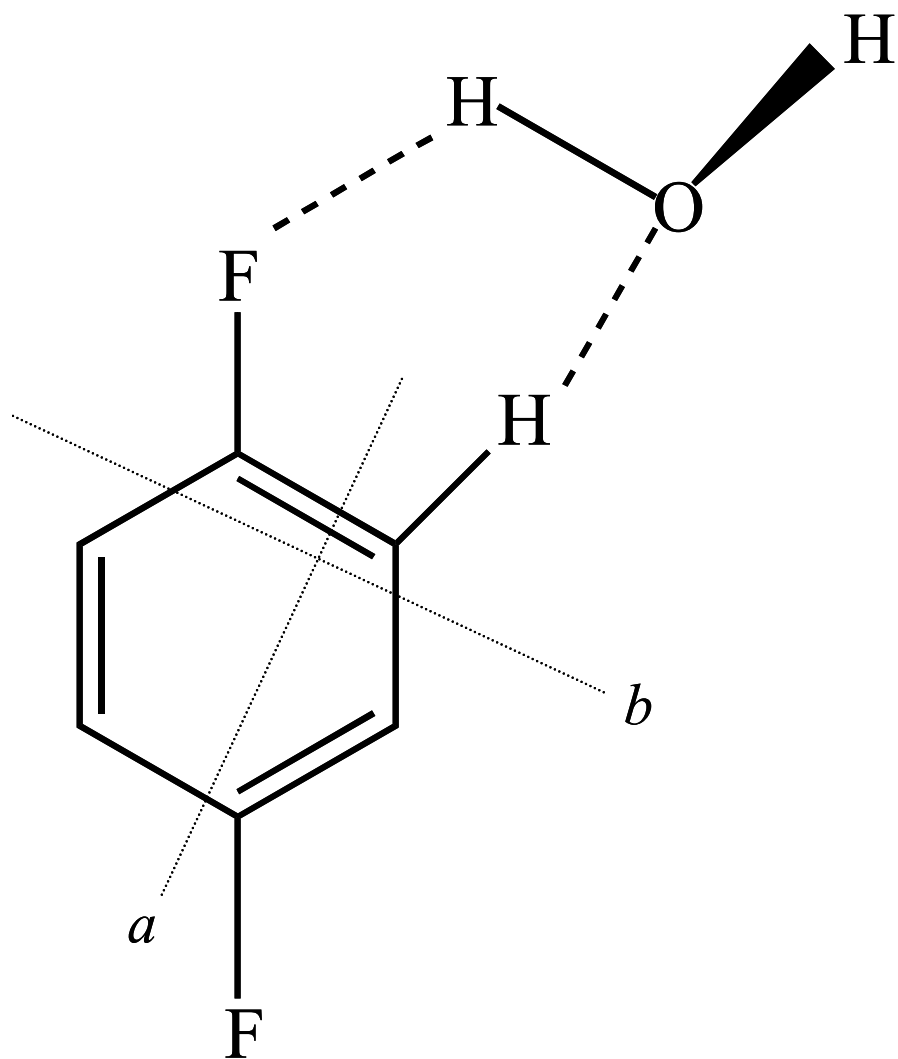


Figure 14. Approximate structure of the doubly hydrogen-bonded complex of *p*-difluorobenzene with a single water molecule. *a* and *b* denote its in-plane inertial axes.

This fit is shown in Fig. 15. Table 7 lists the inertial parameters that were determined from this fit.

Inertial defects (ΔI) often are used as measure of a molecule's planarity. For a rigid planar structure, ΔI is zero whereas for a rigid nonplanar structure, ΔI is negative. Concerning the *p*DFBW, the magnitude of its inertial defects are relatively small ($\Delta I'' = -0.68 \text{ amu } \text{\AA}^2$ in the ground state and $\Delta I' = -0.74 \text{ amu } \text{\AA}^2$ in the excited state), but significantly different from those of bare molecule ($\Delta I'' = 0.00(5) \text{ amu } \text{\AA}^2$, $\Delta I' = -0.020(5) \text{ amu } \text{\AA}^2$) [10,37]. But the values for *p*DFBW are lower than that expected for two out-of-plane hydroxy hydrogen atoms. For comparison, the IW complex [51] exhibits an inertial defect of $\Delta I'' = -1.41 \text{ amu } \text{\AA}^2$ in the ground state. This is about twice *p*DFBW's value. The differences are mainly explained by out-of-plane vibrational motions of the two hydrogens in water. Indole itself is essentially planar in both electronic states, and both water hydrogens are out-of-plane in the complex. While it is difficult to reach structural conclusions based on the results for a single isotopomer, the data for *p*DFBW suggests that, on average, the oxygen atom and one hydrogen atom of the water molecule lie in the plane, and that the second hydrogen atom lies out-of-plane. Both hydrogens undergo large amplitude motion along out-of-plane coordinates.

More information about the structure of the complex and the possible motion of the water molecule can be deduced from the Kraitchman analysis [13] shown in Table 8. This analysis gives the position of the COM of the attached molecule from a comparison of the moments of inertia of the bare molecule and the complex. The relatively small, non-zero $|c|$ values in both electronic states are due to the out-of-plane motions of the two hydroxy hydrogen atoms. The in-plane displacements $|a| = 3.605$ and $|b| = 2.85 \text{ \AA}$ in the ground state increase on electronic excitation by 0.05 - 0.10 \AA . An increase in these distances is consistent with

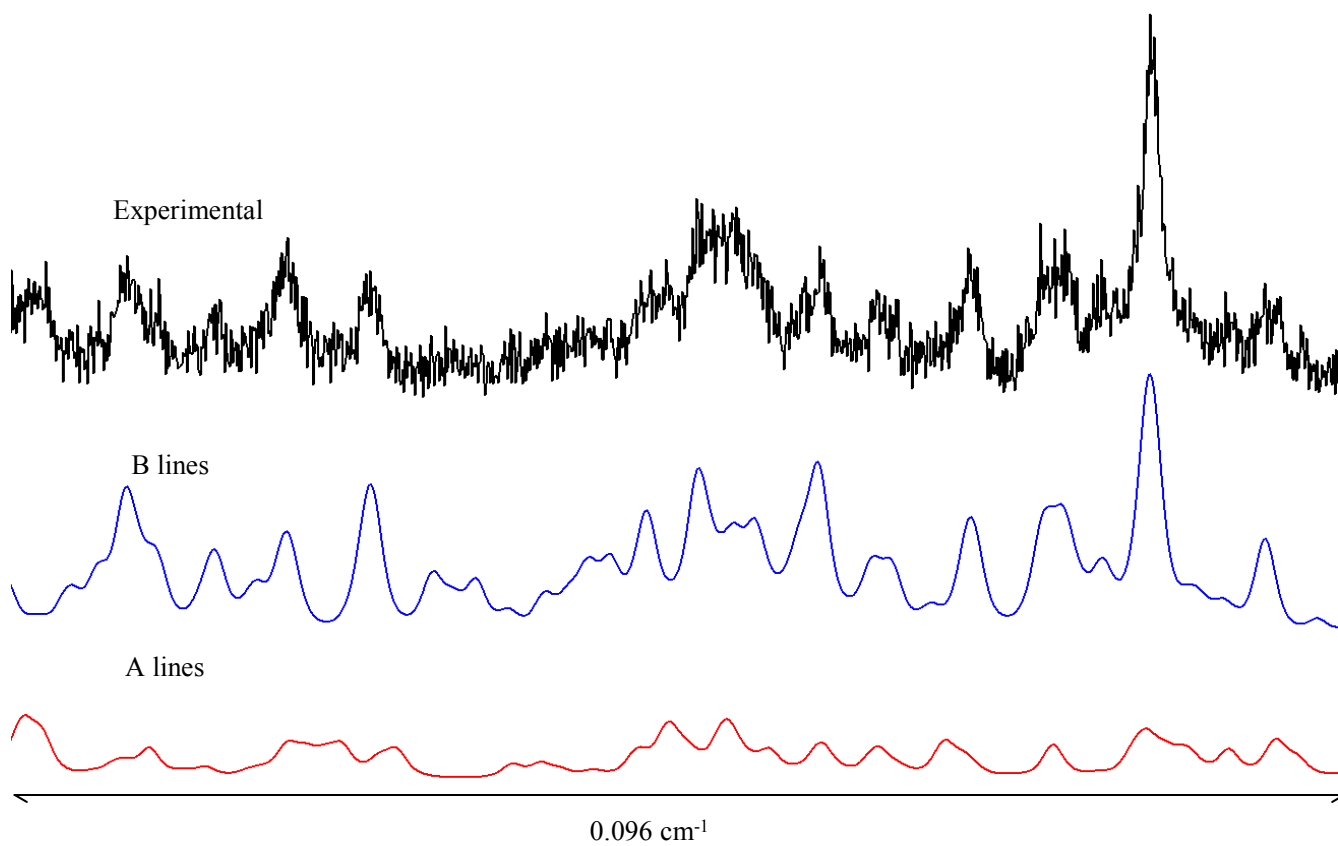


Figure 15. Portion of the high resolution spectrum of *p*DFB-H₂O at full experimental resolution, extracted from the R branch of the stronger subband. The top trace is the experimental spectrum. The second and third traces show the separate calculated contributions of the two subbands in this region (Ref. [66]).

Table 7. Inertial parameters of *p*DFB and its water in the zero-point vibrational levels of their S_0 and S_1 electronic states.

		<i>p</i> DFB-H ₂ O	
		A subband	B subband
S_0	A, MHz	3310.0 (2)	3309.6 (2)
	B, MHz	806.1 (1)	806.1 (1)
	C, MHz	648.7 (1)	648.8 (1)
	ΔI , amu Å	-0.68	-0.68
S_1	A, MHz	3185.1 (2)	3184.6 (2)
	B, MHz	795.4 (1)	795.5 (1)
	C, MHz	637.1 (1)	637.1 (1)
	ΔI , amu Å	-0.80	-0.74

TABLE 8. Center of mass (COM) coordinates of the water molecule in the principal axis frames of the bare *p*DFB molecule and of the *p*DFB-H₂O complex.

State	coordinate	<i>p</i> DFB frame (Å)	complex frame (Å)
S ₀	<i>a</i>	3.605(5)	3.848(7)
	<i>b</i>	2.858(4)	1.132(3)
	<i>c</i>	0.23(3)	0.067(9)
	<i>r</i>	4.6545 (5)	4.012(6)
S ₁	<i>a</i>	3.703(5)	3.916(8)
	<i>b</i>	2.905(3)	1.107(2)
	<i>c</i>	0.24(3)	0.065(10)
	<i>r</i>	4.713(5)	4.070(6)

decreasing the strength of both hydrogen bonding interactions, which responsible for the blue shift of the origin band of the water complex relative to that of the bare molecule.

It is interesting to compare the results for *p*DFBW to those for the analogous benzonitrile-water (BNW) complex [62-65]. In both complexes, the oxygen is bound to an *ortho* hydrogen and one hydroxy hydrogen is bound to the fluorine or the cyano group. In the electronic ground state S_0 , the structures of these complexes are very similar. The water COM in BNW is slightly further away from the aromatic ring (coordinates with respect to the ring center: 3.59/3.14/0.00 Å). However, *p*DFBW and BNW differ in their behavior upon excitation into S_1 . Whereas there is no significant change in the *a* and *b* center-of-mass coordinates in BNW (they decrease by less than 0.01 Å), the coordinates increase by 0.05- 0.10 Å in *p*DFBW. The larger structural change in *p*DFBW also is reflected in the larger blue shift of the origin of the complex with respect to that of the monomer; 168.1 cm^{-1} in *p*DFB. In contrast, BNW exhibits a red shift of $\sim 69.8 \text{ cm}^{-1}$ with respect to that of BN itself [65]

More specific information about the motion of the water molecule in *p*DFBW comes from an analysis of the observed tunneling splitting of 3.63 GHz. Also, each of the subbands has slightly different rotational constants due to the coupling between torsional motion of water and overall rotation. The differences between the rotational constants of two subbands are calculated from $\Delta A'' = A_{v_0''} - A_{v_1''}$, $\Delta A' = A_{v_0'} - A_{v_1'}$ and so forth [66]. According to Table 7, the rotational constants of the two subbands of the water complex are the same to within the error limits except for the A values; $\Delta A'' = 0.4 \text{ MHz}$ in the ground state and $\Delta A' = 0.5 \text{ MHz}$ in the excited state. This shows that the axis about which the motion of the water molecule is primarily occurring in the two states is approximately the same, and is approximately parallel to the *a* principal inertial axis of the complex.

As discussed in the analysis of the tunneling splitting in BNW [65], there exist several possible models for the motion of the attached water molecule. All require the breaking and remaking of at least one of the hydrogen bonds (F---H-O or H---O-H). One of the simplest models is an internal rotation of the H₂O about its C₂-(*b*-)axis within a planar equilibrium structure. The spectrum was analyzed with a semirigid internal rotor model consisting of a rigid frame with C_s symmetry and one rigid internal rotor of C_{2v} symmetry [67,68]. For each electronic state, the molecule-fixed axis system (*x*, *y*, *z*) was rigidly attached to the frame with its origin at the COM of the whole molecule. The *z* axis was chosen to be parallel to the internal rotation axis, and the *y* axis was chosen to be parallel to the complex *c* principal axis, perpendicular to the symmetry plane of the frame. In a least-squares fit, the moments of inertia of the complex I_{xx}, I_{yy}, I_{zz}, and the potential term V₂ of the potential for both states were determined. The planar moment of the H₂O internal rotor P_x was fixed to the value obtained from ground state rotational constant B₀ = 435 GHz [69]. This procedure yields upper limits for the V₂ potential barriers for V''₂ = 450 cm⁻¹ and V'₂ = 290 cm⁻¹. The angle θ between the internal rotation axis and the *a* principal axis of the complex was estimated to be around 70° in S₁ whereas no preferred orientation was found for S₀. This result leads to a predicted subband splitting of 3.6 GHz, in good agreement with the experimental value of 3.63 GHz. However, it is clear that the axis about which the water molecule is moving in the ground state cannot be its *b* axis because such a motion would require a breaking of the hydrogen bond, a much higher energy process than 450 cm⁻¹. With the value θ=70° in the excited state, since the internal rotation axis also has a component along the *b* axis, the rotational B constant of the complex also should be perturbed. But, no observed differences in the B values of the two subbands was observed.

In a second model, the water molecule was assumed to rotate about an axis in its bc plane, 55° off its b axis ($F = 339$ GHz [69]), which corresponds to a rotation about one of the lone pairs of the oxygen atom. This motion [70] leads to a barrier estimate of $V_2'' = 330 \pm 20$ cm^{-1} in the ground state and $V_2' = 230 \pm 30$ cm^{-1} in the excited state, with a predicted subband splitting of 3.33 ± 0.9 GHz, in good agreement with the experimental value of 3.63 GHz. However, this simple motion does not provide for the equivalent exchange of the two hydrogens, which is needed to reproduce the observed 3:1 intensity ratio.

In the third, and preferred model, the observed tunneling splitting and differences in rotational constants are attributed the combined effects of inversion and restricted internal rotation, as shown in Figure 16. This process breaks down into two steps, switching of the lone pairs and restricted internal rotation of the water molecule. While the actual pathway includes two separate steps, the net effect is a C_2 rotation of the water about its b symmetry axis. The two motions taken together are equivalent to the “acceptor switching” motion in the H_2O dimer [2]. Importantly, the combined motion renders the two hydroxyl hydrogens equivalent, explaining the observed 3:1 intensity ratio.

In this model, the determined values of V_2 ($V_2'' = 330$ and $V_2' = 230$ cm^{-1}) are the effective barrier heights for the combined inversion-torsional motion. But we imagine that the two steps make different contributions to V_2 . The barrier to water inversion in ground state $p\text{DFBW}$ is likely to be relatively low, probably much less than the 130 cm^{-1} barrier in the water dimer [2]. In contrast, the barrier to the torsional motion of the attached H_2O in $p\text{DFBW}$ is likely to be higher, owing to the stronger C-F---H-O interaction. The strength of this interaction is significantly decreased in the S_1 state; a principal reason for this decrease is the electron density redistribution in $p\text{DFB}$. As we have discussed earlier, the fluorine lone pair electron density in

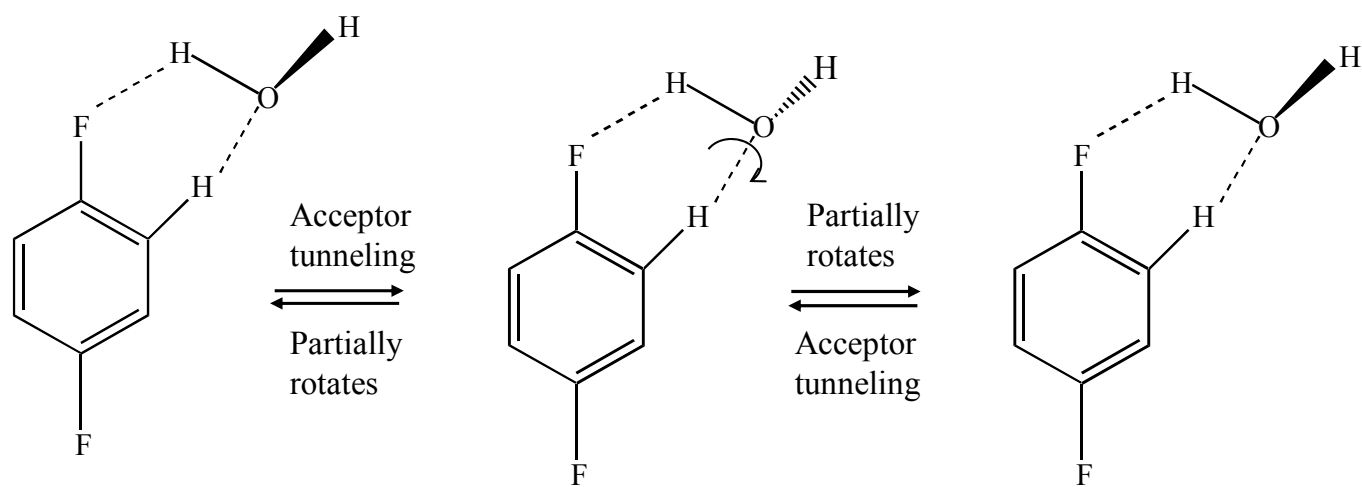


Figure 16. Combined inversion and restricted internal rotation of the water molecule in *p*DFB-H₂O.

the S_1 state of *p*DFBW is significantly reduced, compared to the ground state, leading to a significantly reduced value of V_2 in the excited state. MP2/6-31G** calculations confirm that, in the ground state, the C-F---H-O binding energy is about 300 cm^{-1} , whereas the C-H--O-H binding energy is much weaker, 30 cm^{-1} or so.

The geometry of the C-F---H-O intermolecular interaction is considerably different from those of O-H---O and O-H---N hydrogen bonds. Whereas the normal hydrogen bonding angle is almost linear, the angle C-F---H is significantly decreased to around 110° [71], making for weaker interactions. In comparison with $\text{CH}_2\text{F}_2\text{-H}_2\text{O}$ ($\sim 700\text{ cm}^{-1}$) [72], our O-H---F intermolecular interaction ($\sim 300\text{ cm}^{-1}$, including the water inversion motion) appears to be significantly weaker. Arguably, the acceptor ability of $\text{C}(\text{sp}^2)\text{-F}$ is not as good as that of $\text{C}(\text{sp}^3)\text{-F}$. Still, the strength of any hydrogen bond depends more on donor acidity than on acceptor basicity, an effect that is nicely confirmed by comparisons of the properties of *p*DFB and BN water complexes. The V_2 barriers in the BN-water are nearly the same in both states [65]. There are obviously only very small changes in the electronic structure of BN upon excitation, which is also indicated by a small increase of its dipole moment (+0.09 D) [73].

Because the water molecule in *p*DFBW is linked to the substrate *p*DFB *via* two points of attachment (*cf.* Fig. 14 & 15), its motion (and the change in their motion when the photon is absorbed) is rather restricted. IW is different in this respect. The water molecule in IW is linked to the substrate I molecule by only one point of attachment, an acceptor H-O --- H-N hydrogen bond. Other motion then become feasible, including possible changes in both the position and the orientation of the attached water molecules. Such a “solvent reorganization” is an important concept in the condensed phase. In what follows, we briefly review what has been learned about this phenomenon from high resolution electronic spectroscopy experiments in the gas phase.

Figure 17 shows the rotationally resolved fluorescence excitation spectrum of the origin band of the S_1 - S_0 transition of IW, shifted 132 cm^{-1} to the red of the corresponding band of indole itself. Again we find two subbands in the spectrum, a consequence of a tunneling motion of the attached water molecule. The two subbands again have an intensity ratio of 1:3, with the weaker subband being shifted to the red; the subband separating in 0.444 cm^{-1} (13.3 GHz) in this case. Fits of these two subbands also showed that there are small but significant differences in the inertial parameters of the two subbands, as in the case of *p*DFBW. These data are shown in Table 8.

A Kraitchman analysis of these data [13] shows that the water molecule is attached to the indole frame *via* a *quasi*-linear N-H ---OH₂ hydrogen bond with the water plane more or less perpendicular to the indole plane. The COM distance of the water molecule from the indole frame also decreases by $\sim 0.1\text{ \AA}$ when the photon is absorbed, reflecting an increase in the strength of the hydrogen bond in the S_1 state, compared to the ground state. (this is consistent with the observed red shift of 132 cm^{-1}). But the most interesting light-induced motion of the attached water molecule is a change in its orientation in the S_1 state, compared to the ground state.

Examining the data in Table 9, we see that only the A'' values of the two ground -state subtorsional levels are different ($\Delta A'' = 1.69 \pm 0.25\text{ MHz}$), whereas both the A' levels and the B' values of the two excited-state subtorsional are different ($\Delta A' = 1.27 \pm 0.27$, $\Delta B' = 0.59 \pm 0.31\text{ MHz}$). This shows that the axes about which the motion of the water molecule is occurring in the two states cannot be the same.

Two limiting models have been developed to deal with this problem, summarized in Table 10. In the first, the motion of the water molecule is assumed to be a simple rotation about

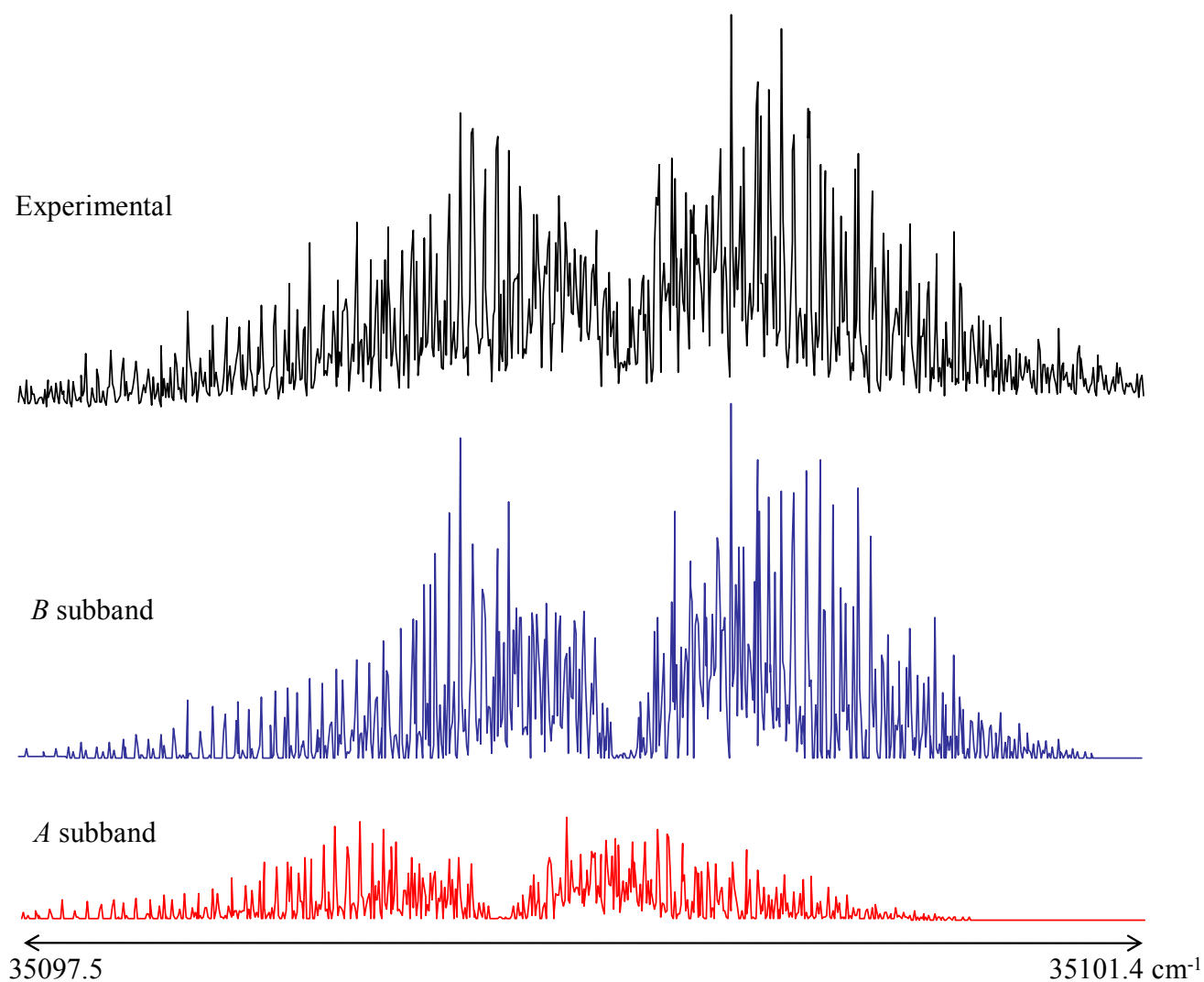


Figure 17. Rotationally resolved fluorescence excitation spectrum of the origin band of the S_1-S_0 transition of indole- H_2O , shifted 132 cm^{-1} to the red of the S_1-S_0 origin band of indole. The origin band of the complex is a superposition of two subbands which are separated by 0.4441 cm^{-1} . The top trace is the experimental spectrum. The second and third traces are the calculated B and A subbands, respectively (Ref. [56]).

Table 9. Inertial parameters of indole and its water in the zero-point vibrational levels of their S_0 and S_1 electronic states.

		Indole – H ₂ O	
		A subband	B subband
S_0	A, MHz	2064.2 (2)	2062.5 (1)
	B, MHz	945.0 (3)	945.1 (1)
	C, MHz	649.2 (2)	649.3 (1)
	ΔI , amu Å	-1.142	-1.412
S_1	A, MHz	1989.0 (2)	1987.6 (1)
	B, MHz	964.1 (3)	963.5 (1)
	C, MHz	650.4 (2)	650.4 (1)
	ΔI , amu Å	- 1.249	-1.745

Table 10. Inertial rotation calculations on Indole-H₂O

State	Parameter	rotation about water's <i>b</i> axis	rotation about an axis in the <i>bc</i> plane, 55° off the <i>b</i> axis
S_0	rotor constant (GHz)	435.352	339.277
	θ (deg)	0 ± 15	0 ± 15
	V_2 (cm ⁻¹)	198.2 ± 14.0	168.5 ± 12.0
	subtorsional splitting (GHz)	15.273 ± 3.021	9.276 ± 2.000
S_1	rotor constant (GHz)	435.352	339.277
	θ (deg)	55 ± 15	55 ± 15
	V_2 (cm ⁻¹)	140.1 ± 25.0	121.7 ± 20.0
	subtorsional splitting (GHz)	36.592 ± 13.550	22.223 ± 8.231

its b axis, with an internal rotor constant of 435 GHz in both electronic states of the complex [69]. Then, using the principal axis method in the high-barrier approximation [66], we estimate from the observed differences in the rotational constants of the two subtorsional levels a rotor axis angle (with respect to the a axis of the complex) of $\theta = 0^\circ$ and a barrier height of $V_2 = 198 \text{ cm}^{-1}$ in the ground state and $\theta = 55^\circ$ and $V_2 = 140 \text{ cm}^{-1}$ in the excited state. This leads to a predicted subband splitting of 21.319 GHz, in poor agreement with the experimental value of 13.314 GHz. In the second model, the water molecule is assumed to rotate about an axis in its bc plane, 55° off the b axis, with an internal rotor constant of 339 GHz [69]. This model yields rotor angles of $\theta (S_0) = 0^\circ$ and $\theta (S_1) = 55^\circ$ as before but significantly lower values of the barriers, $V_2(S_0) = 169 \text{ cm}^{-1}$ and $V_2(S_1) = 122 \text{ cm}^{-1}$. This leads to a predicted subband splitting of 12.947 GHz, in good agreement with the experimental value. We cannot explain our data by assuming that the water internal rotation axis itself changes when the photon is absorbed (*cf.* Table 10). Therefore, we conclude that the axis about which the water molecule is moving lies in its bc plane, 55° off the b axis, in *both* electronic states of the complex and that the orientation of this axis relative to the a axis of IW changes by 55° on S_1 excitation.

Shown in Figure 18 are sketches of the local solvent structures in IW in the two electronic states that are consistent with these results. Both structures have linear (or nearly linear) HB's; however, the orientation of the water plane relative to the HB axis in the two states is different. In the ground state, the N-H hydrogen is linked to one of the two sp^3 lone pairs of the oxygen atom, resulting in an angle between the water plane and the HB axis of $\sim 55^\circ$. In the excited state, the N-H hydrogen is linked to both lone pairs, resulting in a bifurcated structure with an angle between the water plane and the HB axis of $\sim 0^\circ$. Apparently, the observed solvent reorganization is a consequence of “radial-angular coupling”; i.e., decreasing the heavy-atom

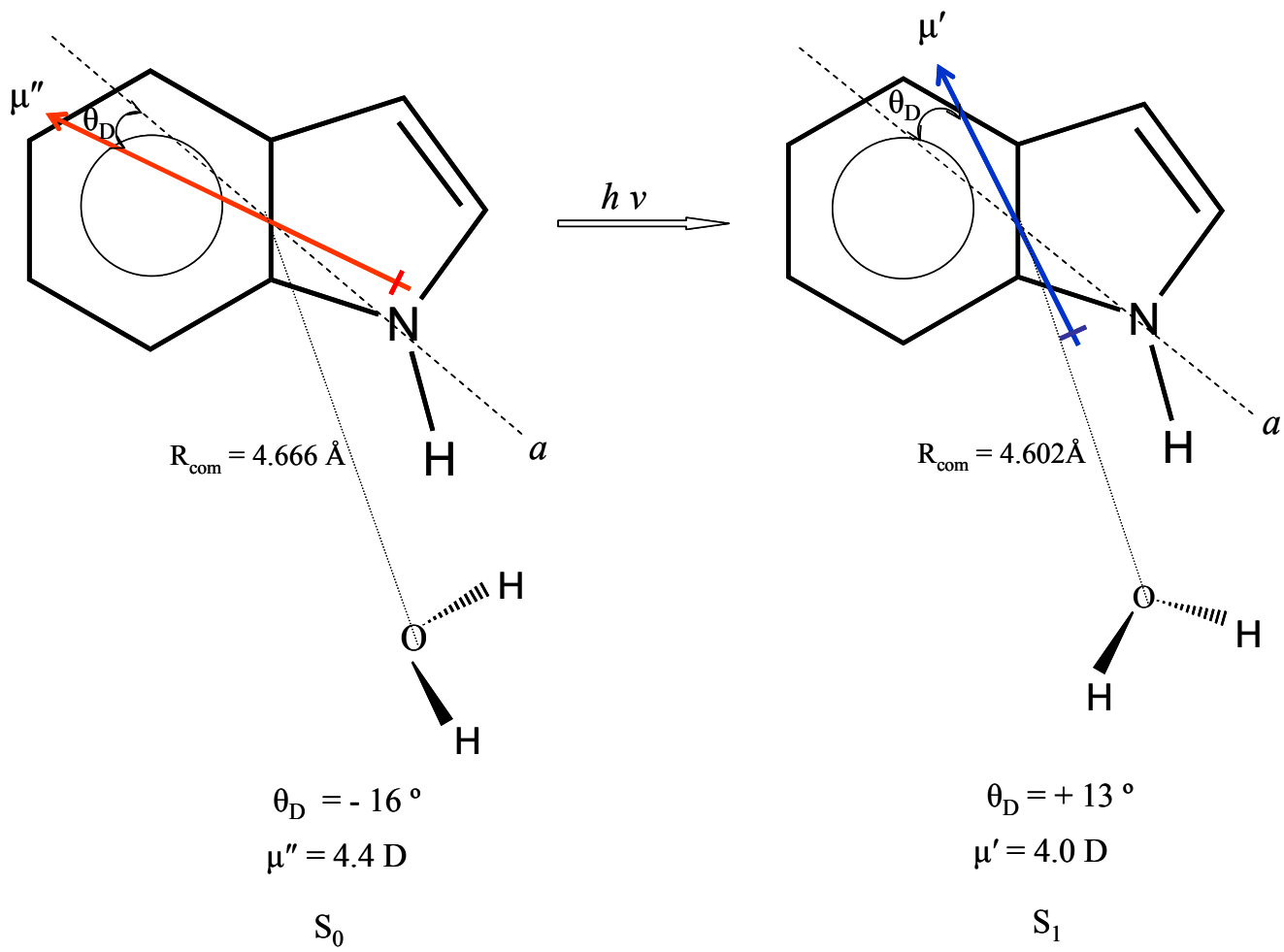


Figure 18. Indole-water showing its inertial axes and the orientation of its permanent electric dipole moments in the two electronic states.

separation R by electronic excitation produces in a change in the preferred orientation of the solvent plane with respect to the HB axis [74].

In retrospect, it is clear that the axis about which the water molecule is moving in the ground state cannot be its b axis because such a motion would require a breaking of the HB, a much higher energy process than $100 - 200 \text{ cm}^{-1}$. It is also clear that the motion of the water molecule cannot be a simple torsional motion about an axis 55° off its b axis, since such a motion would not render the two water hydrogens equivalent. Therefore, the observed tunneling splitting (and differences in rotational constants) must, in fact, be due to the combined effects of internal rotation and inversion, or “wag”, similar to the motion of the water molecule in p DFBW. Such a motion accounts, at least in a qualitative way, for the observed out-of-plane motion of the water molecule. The derived values of V_2 are thus effective barrier heights for the torsion-inversion motion.

According to the time-honored concept of solvent reorganization, solvent molecules move in response to a change in the local electronic environment, produced by the absorption of light. Molecules in electronically excited states are presumed to have dipole moments whose magnitudes and orientations are different from those in the ground state. Recently, we have tested this idea by performing Stark-effect experiments on served molecules. In the case of indole [21], we find that $\mu = 1.963 \text{ D}$ in the S_0 state, and $\mu = 1.856 \text{ D}$ in the S_1 state. These two values are not very different. But we also find that the orientation of the electronic dipole moment changes significantly when the molecule absorbs light, by $\sim 13^\circ$, reflecting a shift in electron density from the pyrrole ring to the benzene ring. Thus, it is indeed true that the water molecule reorients when the indole absorbs light because such a reorientation leads to a more favorable relative orientation of their respective dipoles (*cf.* Fig. 18). To the best of our

knowledge, this is the first “rotationally-resolved” and fully documented demonstration of this effect in the literature.

Being able to perform Stark-effect experiments on isolated molecules in the gas phase puts us in a unique position to determine the induced dipole moment that is produced when a solvent molecule like water is attached to a polarizable molecule like indole. Shown in Fig. 19 is a portion of the rotationally resolved electronic spectrum of IW and its response to an applied electric field. Clearly evident are Stark-induced splittings and shifts in both the positions and intensities of the observed lines. Fitting these data, it was found that the dipole moment of IW is 4.4 ± 0.3 D in the ground state and 4.0 ± 0.3 D in the excited S_1 state. Now, water in its ground state has a dipole moment $\mu_w = 1.855(6)$ D [75]. Combining this value with the measured values for indole gives maximum values for IW of 3.818 in S_0 and 3.711 D in S_1 , assuming the dipoles of the component parts are aligned. The measured values of 4.4 and 4.0 D are larger than these estimates by 13% in S_0 and 8% in S_1 . We attribute these differences to induced dipole moments produced by the attached water molecule.

Electrostatic models of the interactions between molecules have been successful in predicting the structure of many van der Waals complexes [76-78]. In a typical model, the complex dipole moment is represented as a sum of three terms,

$$\mu_{IW} = \mu_I + \mu_w + \mu_I^* \quad (15)$$

where μ_I and μ_w are the permanent dipole moments of the component parts, for which the experimental values are now known. μ_I^* is the induced dipole moment, arising primarily from

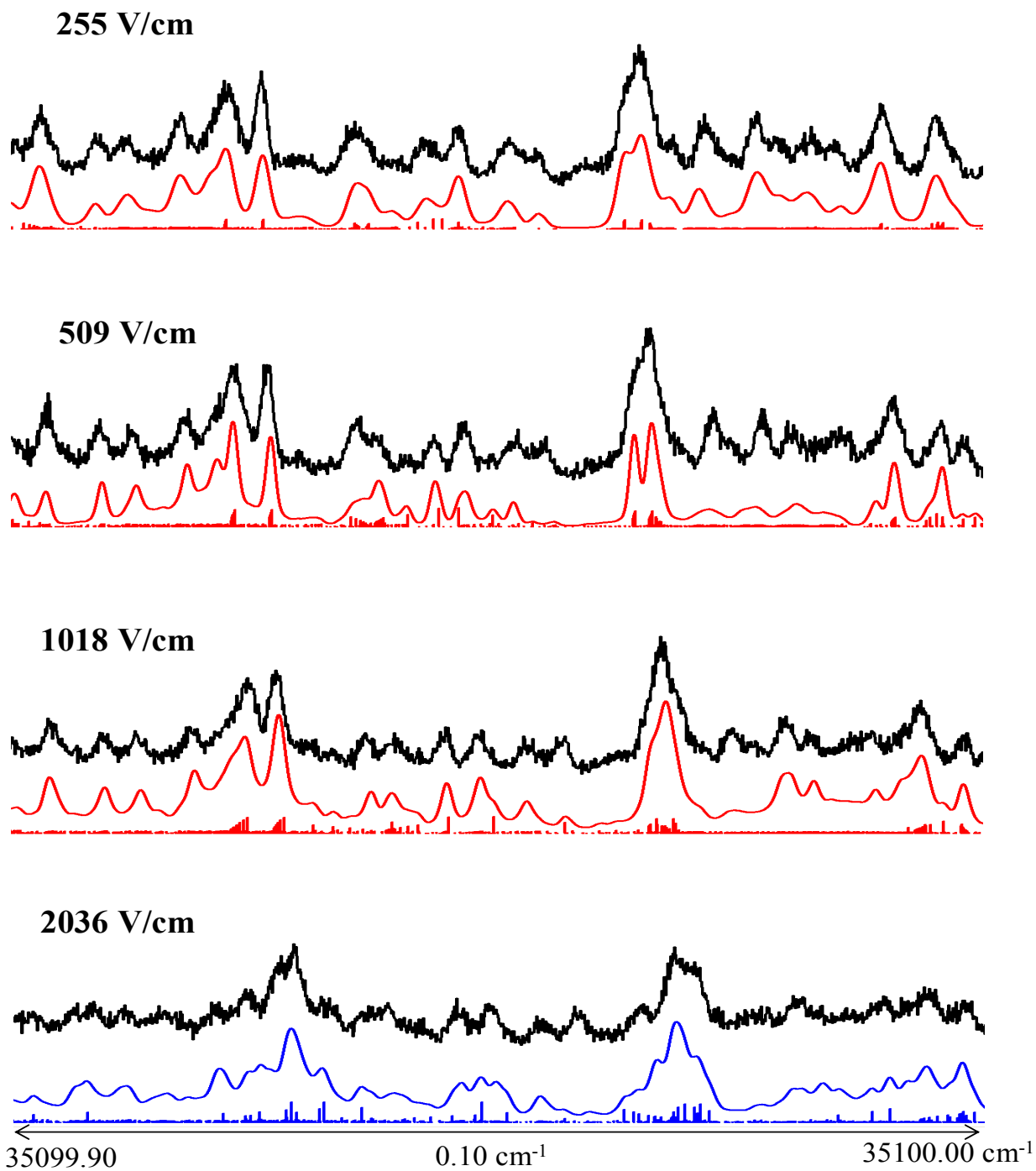


Figure 19. Portion of the rotationally resolved spectrum of indole-H₂O extracted from near the origin of the B'←B'' subtorsional band showing the influence of the applied field (Ref. [24]).

polarization of the indole unit by the water dipole moment and quadrupole, as shown in Eq. (15):

$$\mu_{I}^{*} = \alpha_{I} \cdot \{ [3\mathbf{R}(\boldsymbol{\mu} \cdot \mathbf{R})/R^5] - \boldsymbol{\mu}/R^3 + [5(\mathbf{R}^{\dagger} \cdot \boldsymbol{\Theta} \cdot \mathbf{R})/R^7] \mathbf{R} - (\boldsymbol{\Theta}^{\dagger} \cdot \mathbf{R} + \boldsymbol{\Theta} \cdot \mathbf{R})/R^5 \} \quad (16)$$

Expressed in the inertial coordinate system of indole, Eq. (16) can be simplified to

$$\mu_{I a,b}^{*} \approx \mu_{W a,b} \cdot \frac{2 \cdot \alpha_{I a,b}}{3 R_{COM}} + 3 \cdot \Theta_{W a,b} \cdot \frac{\alpha_{I a,b}}{4 R_{COM}} \quad (17)$$

Here, $\alpha_{I a,b}$ is the polarizability volume of indole, $\Theta_{W a,b}$ is the electric quadrupole moment of water, both referred to either the *a* or *b* inertial axis of indole. The water molecule may be assumed to lie in the *ab* plane of the complex since its tunneling motion is fast compared to overall molecular rotation. R_{COM} is the COM distance between indole and water which also can be determined from experiment; the values (see Fig. 18) are $R_{COM} = 4.666$ and $R_{COM} = 4.602$ Å in the S_0 and S_1 states, respectively.

Polarizabilities and quadrupole moments that are needed in these calculations were obtained by *ab initio* methods using a 6-31G** basis set. Predictably, these lead to large induced dipole moments whose magnitudes are strongly angularly dependent. For example, if we consider only the first (dipole) term in Eq.(17), we calculate a ground state induced moment of 0.567 D when the water dipole points along *a* and 0.346 D when the water dipole points along *b*. These values changes to 0.721 and 0.507 D, respectively, when indole is excited to its S_1 state. The larger induced dipole in the S_1 state may be traced to the larger polarizability and smaller R_{COM} in that state.

We now use Eq. (17) to determine the induced dipole moments in IW. Essentially quantitative agreement with experiment is obtained when the C_2 axis of water is oriented by -25° with respect to the a axis of the complex in the S_0 state and by $+35^\circ$ with respect to the a axis of the complex in the excited state. This is shown in Table 11. The induced dipole moments in these two orientations are $\mu^*_1 = 0.727$ ($\mu^*_{1a} = 0.592$ and $\mu^*_{1b} = 0.422$ D) in the S_0 state, and $\mu^*_1 = 0.540$ ($\mu^*_{1a} = 0.484$ and $\mu^*_{1b} = 0.238$ D) in the S_1 state. The S_1 induced dipole is smaller by 0.187 D. Primarily, this is because the dipoles of water and indole are nearly aligned (-25.7°) in the ground state, but less well aligned ($+48.3^\circ$) in the excited state. The values of the water orientation angles required by the fit are in nearly perfect agreement with the values derived from our earlier analysis of the torsion-rotation perturbations in the high resolution spectrum [51]. The error limits reflect a less than 2° uncertainty in the vibrationally averaged orientation of the water molecule compared to the experimental data.

Figure 20 summarizes the results in graphical form. That the polarizing effect of the water molecule would increase the complex dipole moment was expected owing to the high polarizability of the indole molecule. What was unexpected is the magnitude of the effect; the induced moment in IW is a substantial fraction (30-40 %) of the permanent dipole moment of indole. The distribution of electrons in the isolated molecule is significantly affected by the presence of a single solvent molecule in its vicinity. Also unexpected is the fact that the induced dipole is not parallel to the “inducing” one, especially in the ground state. Possibly this effect has its origin in the polarizability anisotropy, which is larger in the ground state. But most surprising of all is that a simple electrostatic model seems to capture the essence of the polarization phenomenon so well. If this result holds up under further scrutiny, then the

Table 11. Observed and calculated dipole moments of indole and indole-H₂O in their S₀ and S₁ electronic states.

		Indole - water			
		Indole	Experimental	Calculated	
				w/o Θ	w/ Θ
S ₀	μ_a	1.376 (8)	4.20 (6)	4.11	4.24
	μ_b	1.40 (1)	1.2 (3)	1.15	1.18
	μ_{tot}	1.963 (13)	4.4 (3)	4.27	4.40
S ₁	μ_a	1.556 (8)	3.90 (8)	3.54	3.81
	μ_b	1.01 (1)	0.9 (3)	0.66	0.77
	μ_{tot}	1.856 (13)	4.0 (3)	3.60	3.89

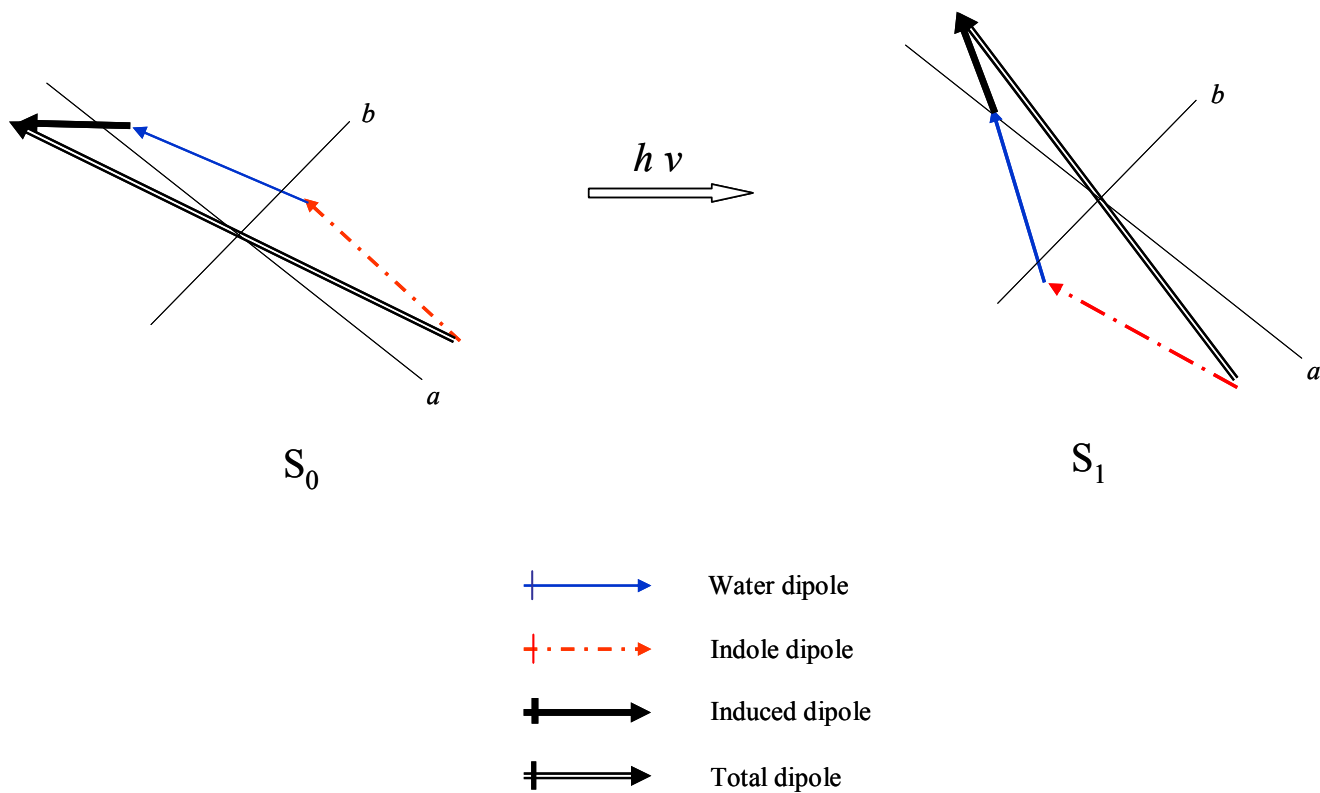


Figure 20. Illustration of indole-H₂O showing the directions of its dipole moments in both of its electronic states

prospects for success of recently derived polarizable force fields for other organic and biological molecules is high [79].

A.6 Summary

An immense amount of information can be derived from the fully resolved electronic Ar, N₂, and H₂O complexes of organic spectrum of an isolated large molecule and its weakly bound complexes in the gas phase. This information includes their geometries in the two electronic states “connected” by the photon. That is, the experiment gives information about the position (and orientation) of the attached atom or molecule, and how this changes when the molecule absorbs light. Motions of the attached species along different intermolecular coordinates are revealed by perturbations in the spectrum. And, finally, the application of an externally applied field to the sample produces Stark splittings and shifts of the lines in the spectrum from which one can derive both the permanent and induced dipole moments of weakly bound complexes in both electronic states. Light-induced changes in the charge distributions of such species are often intimately linked to their changes in structure.

The particular species discussed include a molecules like *p*-difluorobenzene, indole, and 7-azaindole. The interactions explored include dipole-dipole, dipole-induced dipole, and quadrupole-quadrupole interactions. Different species exhibit different structures and dynamics depending on the nature of the interactions of the component parts. Thus, symmetry (or lack of symmetry) is important. The methods of analysis described here will find many applications in increasingly complex systems, including those in biology.

A.7 Acknowledgment

David Borst, Tim Korter, Martin Schafer, Wayne Sinclair, and John Yi have each made major contributions to this work. We thank them all. We also are grateful to Tom Shattuck and his colleagues at Colby College for their hospitality as this paper was being written, and to the National Science Foundation for its support of our research (CHE-0315584).

BIBLIOGRAPHY

Chapter 1.

- [1] D. H. Levy, NATO Advanced Study Institutes Series, Series B: Physics B57 (Quantum Dyn. Mol.), 115-42 (1980).
- [2] C.-J. Tsai and K. D. Jordan, *Chem. Phys. Lett.* **213**, 181 (1993).
- [3] J. G. Gregory and D. C. Clary, *J. Chem. Phys.* **105**, 6626 (1996).
- [4] J. B. Paul, R. A. Provencal, C. Chapo, A. Petterson, and R. J. Saykally, *J. Chem. Phys.* **109**, 10201 (1998).
- [5] R. S. Fellers, L. B. Braly, R. J. Saykally, and C. Leforestier, *J. Chem. Phys.* **110**, 6306 (1999).
- [6] J. M. Hutson, A. Ernesti, M. M. Law, C. F. Roche, and R. J. Wheatley, *J. Chem. Phys.* **105**, 9130 (1996).

Chapter 2.

- [1] Q. Ju and C. S. Parmenter, Abstract MH07, 53rd International Symposium on Molecular Spectroscopy, Columbus, OH, 1998. See also Q. Ju, Ph.D. Thesis, Indiana University, December 1998.
- [2] P. W. Joireman, R. T. Kroemer, D. W. Pratt, and J. P. Simons, *J. Chem. Phys.* **105**, 6075 (1996).
- [3] Th. Weber, A. M. Smith, E. Riedle, H. J. Neusser, and E. W. Schlag, *Chem. Phys. Lett.* **175**, 79 (1990).
- [4] Y. Ohshima, H. Kohguchi, and Y. Endo, *Chem. Phys. Lett.* **184**, 21 (1991).
- [5] H. J. Neusser, R. Sussman, A. M. Smith, E. Riedle, and Th. Weber, *Ber. Bunsenges. Phys. Chem.* **96**, 1252 (1992).

- [6] B. D. Gilbert, C. S. Parmenter, M.-C. Su, H.-K. Oh, and Z.-Q. Zhao, *Appl. Phys.* **B59**, 397 (1994).
- [7] B. D. Gilbert, C. S. Parmenter, and H.-K. Oh, *J. Phys. Chem.* **99**, 2444 (1995).
- [8] Y. Hu, W. Lu, and S. Yang, *J. Photochem. Photobiol.* **A106**, 91 (1997).
- [9] Y. Hu, W. Lu, and S. Yang, *J. Chem. Phys.* **105**, 5305 (1996).
- [10] M. S. Ford, S. R. Haines, I. Pugliesi, C. E. H. Dessent, and K. Müller-Dethlefs, *J. Electron Spectrosc.* **112**, 231 (2000).
- [11] K. Yamanouchi, S. Isogai, and S. Tsuchiya, *J. Mol. Struct.* **146**, 349 (1986).
- [12] M. Schäfer and D. W. Pratt, *J. Chem. Phys.* **115**, 11147 (2001).
- [13] R. Disselkamp and E. R. Bernstein, *J. Chem. Phys.* **98**, 4339 (1993).
- [14] S. Sun and E. R. Bernstein, *J. Chem. Phys.* **103**, 4447 (1995).
- [15] W. A. Majewski, J. F. Pfanstiel, D. F. Plusquellic, and D. W. Pratt, in *Laser Techniques in Chemistry*, ed. A. B. Myers and T. R. Rizzo (Wiley, New York, 1995), pp. 101-148.
- [16] S. Gerstenkorn and P. Luc, *Atlas du spectre d'absorption de la molécule d'iode* (CNRS, Paris, 1978).
- [17] R. Sussman, R. Neuhauser, and H. J. Neusser, *Can. J. Phys.* **72**, 1179 (1994).
- [18] J. K. G. Watson in *Vibrational Spectra and Structure*, ed. by J. R. Durig (Elsevier, Amsterdam, 1977), Vol. 6, p.1, and references therein.
- [19] A. Lofthus and P. H. Krupenie, *J. Phys. Chem. Ref. Data* **6**, 113 (1977).
- [20] See, for example, B. B. Champagne, J. F. Pfanstiel, D. W. Pratt, and R. C. Ulsh, *J. Chem. Phys.* **102**, 6432 (1995).
- [21] W. Gordy and R. L. Cook, *Microwave Molecular Spectra*, 3rd Ed. (Wiley Interscience, New York, 1984).

- [22] D. R. Herschbach, *J. Chem. Phys.* **31**, 91 (1959).
- [23] J. Makarewicz, *J. Mol. Spectrosc.* **176**, 169 (1996).
- [24] M. Schäfer, *J. Chem. Phys.* **115**, 11139 (2001).
- [25] M. J. Frisch, G. W. Trucks, H. B. Schlegel, G. E. Scuseria, M. A. Robb, J. R. Cheeseman, V. G. Zakrzewski, J. A. Montgomery, R. E. Stratmann, J. C. Burant, S. Dapprich, J. M. Millam, A. D. Daniels, K. N. Kudin, M. C. Strain, O. Farkas, J. Tomasi, V. Barone, M. Cossi, R. Cammi, B. Mennucci, C. Pomelli, C. Adamo, S. Clifford, J. Ochterski, G. A. Petersson, P. Y. Ayala, Q. Cui, K. Morokuma, D. K. Malick, A. D. Rabuck, K. Raghavachari, J. B. Foresman, J. Cioslowski, J. V. Ortiz, A. G. Baboul, B. B. Stefanov, G. Liu, A. Liashenko, P. Piskorz, I. Komaromi, R. Gomperts, R. L. Martin, D. J. Fox, T. Keith, M. A. Al-Laham, C. Y. Peng, A. Nanayakkara, M. Challacombe, P. M. W. Gill, B. G. Johnson, W. Chen, M. W. Wong, J. L. Andres, C. Gonzalez, M. Head-Gordon, E. S. Replogle and J. A. Pople, *Gaussian 98 (Revision A.9)*, Gaussian, Inc., Pittsburgh, PA, 1998.
- [26] T. M. Korter, D. R. Borst, C. J. Butler, and D. W. Pratt, *J. Am. Chem. Soc.* **123**, 96 (2001).

Chapter 3.

- [1] B. Brutschy, *Chem. Rev.* **100**, 3891 (2000)
- [2] K.S. Kim, P. Tarakeshwar, and Lee, J.Y., *Chem. Rev.* **100**, 4145 (2000)
- [3] M. Gerhards, M. Schmitt, K. Kleinermanns, and W. Stahl, *J. Chem. Phys.* **104**, 967 (1996)
- [4] G. Berden, W.L. Meerts, M. Schmitt, and K. Kleinermanns, *J. Chem. Phys.* **104**, 972 (1996)
- [5] S. Melandri, A. Maris, P.G. Favero, and W. Caminati, *Chem. Phys.* **283**, 185 (2002)
- [6] H.-D. Barth, K. Buchhold, S. Djafari, B. Reimann, U. Lommatzsch, and B. Brutschy, *Chem. Phys.* **239**, 49 (1998)

- [7] M. Becucci, G. Pietraperzia, M. Pasquini, G. Piani, A. Zoppi, R. Chelli, E. Castellucci, and W. Demtröder, *J. Chem. Phys.* **120**, 5601 (2004)
- [8] J.W. Ribblett, W. E. Sinclair, D. R. Borst, J.T. Yi, and D.W. Pratt, in press.
- [9] U. Spoerel, and W. Stahl, *J. Mol. Spectrosc.* **190**, 278 (1998)
- [10] M.J. Tubergen, A.M. Andrews, and R. L. Kuczkowski, *J. Phys. Chem.* **97**, 7451 (1993)
- [11] J.R. Carney, F.C. Hagemeister, and T.S. Zwier, *J. Chem. Phys.* **108**, 3379 (1998)
- [12] T.M. Korter, D.W. Pratt, and J. Küpper, *J. Phys. Chem. A.* **102**, 7211 (1998)
- [13] A.J. Gotch, and T.S. Zwier, *J. Chem. Phys.* **96**, 3388 (1992)
- [14] S. Suzuki, P.G. Green, R.E. Bumgarner, S. Dasgupta, W.A. Goddard, III, and G.A. Blake, *Science* **257**, 942 (1992)
- [15] H.S. Gutowsky, T. Emilsson, and E. Arunan, *J. Chem. Phys.* **99**, 4883 (1993)
- [16] R.N. Pribble, A.W. Garrett, K. Haber, and T.S. Zwier, *J. Chem. Phys.* **103**, 531 (1995)
- [17] T. Emilsson, H.S. Gutowsky, G. de Oliveira, and C.E. Dykstra, *J. Chem. Phys.* **112**, 1287 (2000)
- [18] A.W. Garrett, and T.S. Zwier, *J. Chem. Phys.* **96**, 3402 (1992)
- [19] R.N. Pribble, and T.S. Zwier, *Faraday Discuss. Chem. Soc.* **97**, 229 (1994)
- [20] N. Solcà, and O. Dopfer, *Chem. Phys. Lett.* **347**, 59 (2001)
- [21] V. Brenner, S. Martrenchard-Barra, P. Millie, C. Dedonder-Lardeux, C. Jouvet, and D. Solgadi, *J. Phys. Chem.* **99**, 5848 (1995)
- [22] P. Tarakeshwar, K.S. Kim, and B. Brutschy, *J. Chem. Phys.* **110**, 8501 (1999)
- [23] W. Caminati, S. Melandri, I. Rossi, and P.G. Favero, *J. Am. Chem. Soc.* **121**, 10098 (1999)
- [24] B.J. Smith, D.J. Swanton, J.A. Pople, H.F. Schaefer III, and L. Radom, *J. Chem. Phys.* **92**, 1240 (1990)

- [25] V.R. Thalladi, H.C. Weiss, D. Blaser, R. Boese, A. Nangia, and G.R. Desiraju, *J. Am. Chem. Soc.* **120**, 8702 (1998)
- [26] W.A. Majewski, J.F. Pfanstiel, D.F. Plusquellic, and D.W. Pratt, in *Laser Techniques in Chemistry*, edited by Myers A.B.; Rizzo, T., (Wiley, New York, **1995**), pp. 101-148.
- [27] S. Gerstenkorn, and P. Luc, Atlas du spectre d'absorption de la molecule d'iode (CNRS, Paris, **1978**).
- [28] R. Sussman, R. Neuhauser, and H.J. Neusser, *Can. J. Phys.* **72**, 1179 (1994) See also M. Schäfer, C.-H. Kang, and D. W. Pratt, *J. Phys. Chem. A* **107**, 10753 (2003)
- [29] Described in D.F. Plusquellic, R.D. Suenram, B. Maté, J.O. Jensen, and A.C. Samuels, *J. Chem. Phys.* **115**, 3057 (2001)
- [30] J. Kraitchman, *Am. J. Phys.* **21**, 17 (1953)
- [31] R.M. Helm, H. Vogel, H.J. Neusser, V. Storm, D. Consalvo, and H. Dreizler, *Z. Naturforsch. Teil A* **52**, 655 (1997)
- [32] V. Storm, H. Dreizler, and D. Consalvo, *Chem. Phys.* **239**, 109 (1998)
- [33] S. Melandri, D. Consalvo, W. Caminati, and P.G. Favero, *J. Chem. Phys.* **111**, 3874 (1999)
- [34] M. Schäfer, D.R. Borst, D.W. Pratt, and K. Brendel, *Mol. Phys.* **100**, 3553 (2002)
- [35] P.R. Bunker, *Molecular Symmetry and Spectroscopy* (Academic Press, New York/San Francisco/London, **1979**).
- [36] X.Q. Tan, W.A. Majewski, D.F. Plusquellic, and D.W. Pratt, *J. Chem. Phys.* **94**, 7721 (1991)
- [37] A. Bauder, E. Mathier, R. Meyer, M. Ribeaud, and H.H. Günthard, *Mol. Phys.* **15**, 597 (1968)
- [38] M. Schäfer, *J. Chem. Phys.* **115**, 11139 (2001)

[39] F.C. DeLucia, P. Helminger, R.L. Cook, and W. Gordy, *Phys. Rev.* **A5**, 487 (1972)

[40] Actually, because of electron repulsion between the lone pairs of the fluorine and oxygen atoms, the water molecule does not freely rotate about the axis of the H---O-H hydrogen bond. The two hydroxyl hydrogens experience a simultaneous inversion in the course of its internal rotation motion.

[41] R.S. Fellers, L.B. Braly, R.J. Saykally, and C. Leforestier, *J. Chem. Phys.* **110**, 6306 (1999) and references therein.

[42] D.R. Borst, T.M. Korter, and D.W. Pratt, *Chem. Phys. Lett.* **350**, 485 (2001)

Chapter 4.

[1] C. A. Taylor, M. A. El-Bayoumi, and M. Kasha, *Proc. Natl. Acad. Sci. USA.* **63**, 253 (1969).

[2] K. C. Ingham, and M. A. El-Bayoumi, *J. Am. Chem. Soc.* **96**, 167 (1974).

[3] A. Douhal, S. K. Kim, and A. H. Zewail, *Nature.* **378**, 260 (1995).

[4] K. Sakota, A. Hara, and H. Sekiya, *Phys. Chem. Chem. Phys.*, **6** 32 (2004)

[5] S. K. Kim, E. R. Bernstein, *J. Phys. Chem.* **94** 3531 (1990)

[6] Y. Huang, S. Arnold, M. Sulkes, *J. Phys. Chem.* **100**, 4734 (1996)

[7] J. Caltalan, P. Perez, *J. Theor. Biol.* **81**, 213 (1979)

[8] P. Ilich, *J. Mol. Struct.*, **354**, 37 (1995)

[9] A. Nakajima, M. Hirano, R. Hasumi, K. Kaya, H. Watanabe, C. C. Carter, J. M. Williamson, T. A. Miller, , *J. Phys. Chem A*, **101**, 392 (1997)

[10] A. C. Borin, L. Serrano-Andrés, *Chem. Phys* **262**, 253 (2000)

[11] K. H. Hassan, J. M. Hollas, *J. Mol. Spec* **138**, 398 (1989)

[12] M. Schmitt, C. Ratzler, K. Kleinermanns, W. L. Meerts, in press

- [13] W. A. Majewski, J. F. Pfanstiel, D. F. Plusquellic, and D. W. Pratt, in *Laser Techniques in Chemistry*, edited by A.B. Myers and T. R. Rizzo (Wiley, New York, 1995), pp.101
- [14] S. Gerstenkorn and P. Luc, *Atlas du spectre d'absorption de la molecul e d'iode* (CNRS, Paris, 1978).
- [15] W. Caminati, S. D. Bernardo, A. Trombetti, *J.Mol.Struct.* **223**, 415 (1990)
- [16] M. J. Frisch, G. W. Trucks, H. B. Schlegel, P. M. W. Gill, B. G. Johnson, M. A. Robb, J.R.Cheeseman,T.Keith, G.A. Petersson, J.A.Montgomery, K. Raghavachari, M.A.Al-Laham, V.G.Zakrzewski, J.V.Ortiz, J.B.Foresman, J. Cioslowski, B.Stefanov, A.Nanyakkara, M.Challacombe,C.Y. Peng, P.Y.Ayala, W.Chen, M.W.Wong, J.L Andres, E.S.Replogle, R.Gomperts, R.L. Martin, D. J. Fox, J.S.Binkley, D.J.Defrees, J.Baker, J.P.Stewart, M.Head-Gordon, C.Gonzalez, and J.A.Pople, *Gaussian 98*, Revision A9; Gaussian, Inc.: Pittsburgh, PA, 1998..
- [17] J. K. G. Watson, *Vibrational Spectra and Structure*; Durig, J. R., Ed.; Elsevier: Amsterdam, 1977; Vol. 6, pp. 1.
- [18] C.-H. Kang, J. T. Yi, D. W. Pratt, in press
- [19] D. M. Sammeth, S. Yan, L. H. Spangler, P.R.Callis, *J.Amer.Chem.Soc.* **94**, 7340 (1990)
- [20] K. Fuke, I. Yoshiuchi, K. Kaya, *J.Phys.Chem.* **88**, 5840 (1984)
- [21] J. Kraitchman, *Am.J.Phys.* **21**, 17 (1953)
- [22] T. M. Korter, J. Küpper. D.W. Pratt, *J.Chem.Phys.* **111**, 3946 (1999)

Chapter 5.

- [1] W. Gordy and R. L. Cook, *Microwave Molecular Spectra*, 3rd ed., Wiley-Interscience: New York, 1984.

- [2] D. E. Freeman and W. Klemperer, *J. Chem. Phys.* **45**, 52 (1966)
- [3] J. R. Lombardi, *J. Chem. Phys.* **48**, 348 (1968)
- [4] C.-T. Chang, C.-Y. Wu, A. R. Muirhead and J. R. Lombardi, *Photochem. Photobiol.* **19**, 347 (1974)
- [5] W. A. Majewski and W. L. Meerts, *J. Mol. Spectrosc.* **104**, 271 (1984)
- [6] M. Okruss, B. Rosenow and A. Hese, *Chem. Phys. Lett.* **220**, 286 (1994)
- [7] M. Okruss, R. Müller and A. Hese, *J. Chem. Phys.* **110**, 10393 (1999)
- [8] T. M. Korter, D. R. Borst, C. J. Butler and D. W. Pratt, *J. Am. Chem. Soc.* **122**, 96 (2001)
- [9] D.R Borst, T. M. Korter and D. W. Pratt, *Chem.Phys.Lett.* **350**, 485 (2001)
- [10] J. A. Reese, T. V. Nguyen, T. M. Korter and D. W. Pratt, *J. Am. Chem. Soc.* **126**, 11387 (2004)
- [11] A.J. Stone, *Chem.Phys.Lett.* **83**, 233 (1981)
- [12] A.J. Stone, *Mol.Phys.* **56**,1065 (1985)
- [13] P.W. Fowler and A.J. Stone, *J.Phys.Chem.* **91**, 509 (1987)
- [14] C.R. Le Sueur and A.J. Stone, *J.Phys.Chem.* **95**, 3519 (1991)
- [15] K.C. Janda, L.S. Bernstein, J.M. Steed, S.E. Novick and W. Klemperer, *J.Am.Chem. Soc.* **100**, 8074 (1978)
- [16] R.S. Altman, M.D. Marshall, W. Klemperer and A. Krupnov, *J.Chem.Phys.* **79**, 52 (1983)
- [17] R.S. Altman, M.D. Marshall and W. Klemperer, *J.Chem.Phys.* **77**, 4344 (1982)
- [18] For a review, see P. R. Callis, in *Methods in Enzymology*, edited by L. Brand, M. L. Johnson, Academic: San Diego, 1997; Vol. 278, and references therein.
- [19] A. P. Demchenko, *Ultraviolet Spectroscopy of Proteins*, Springer-Verlag: Berlin, 1986.

- [20] R.F.Chen, in *Practical Fluorescence*, 2nd ed., edited by G.G.Guilbault (Marcel Dekker, New York, 1990), p. 575.
- [21] For a review, see: P. J. Suppan, *Photochem. Photobiol. A* **50**, 293 (1990)
- [22] a) P.R. Callis and B. K. Burgess, *J. Phys. Chem. B* **101**, 9429 (1997)
b) G. Weber, *J. Biochem.* **75**, 335 (1960)
- [23] L. Serrano-Andrés and B. O. Roos, *J. Am. Chem. Soc.* **118**, 185 (1996)
- [24] P.R. Callis, *J. Chem. Phys.* **95**, 4230 (1991)
- [25] L. S. Slater and P. R. Callis, *J. Phys. Chem.* **99**, 8572 (1995)
- [26] H. Lami and N. Glasser, *J. Chem. Phys.* **84**, 597 (1986)
- [27] J. R. Lombardi, *J. Phys. Chem. A* **102**, 2817 (1998)
- [28] W. A.Majewski, J. F. Pfanstiel, D. F. Plusquellic and D. W. Pratt, in *Laser Techniques in Chemistry*, edited by Myers, A. B.; Rizzo, T. R.; Wiley: New York, 1995; Vol. 23, p.101.
- [29] S. Gerstenkorn, and P. Luc, *Atlas du spectroscopie d'absorption de la molécule d'iode*, CNRS: Paris, 1978 and 1982.
- [30] D. G. Lister J. K. Tyler, J. H. Høg and N. W. Larsen, *J. Mol. Struct.* **23**, 253 (1974)
- [31] L. A. Philips and D. H. Levy, *J. Chem. Phys.* **85**, 1327 (1986)
- [32] G. Berden, W. L Meerts and E. Jalviste, *J. Chem. Phys.* **103**, 9596 (1995)
- [33] T. M. Korter, D. W. Pratt and J. Küpper, *J. Phys. Chem.* **102**, 7211 (1998)
- [34] D. R. Borst and D. W. Pratt, unpublished.
- [35] J. K. G. Watson, in *Vibrational Spectra and Structure*, edited by Durig, J. R.; Elsevier: Amsterdam, 1977; Vol.6, p.1.
- [36] W. Gordy, R. L. Cook, *Microwave Molecular Spectra*, 3rd ed., Wiley-Interscience: New York, 1984.

- [37] A. Held, B. B. Champagne and D. W. Pratt, *J. Chem. Phys.* **95**, 8732 (1991)
- [38] W. Caminati and S. di Bernardo, *J. Mol. Struct.* **240**, 253 (1990)
- [39] J. R. Lombardi, *J. Phys. Chem. A* **103**, 6335 (1999)
- [40] M. Cotton, C. Tian, D. D. Busath, R. B. Shirts and T. A. Cross, *Biochemistry* **38**, , 9185 (1999) ; W. Hu and T. A. Cross, *Biochemistry* **34**, 14147 (1995)
- [41] M. J. Frisch, G. W. Trucks, H. B. Schlegel, G. E. Scuseria, M. A. Robb, J. R. Cheeseman, V. G. Zakrzewski, J. A. Montgomery, R. E. Stratmann, J. C. Burant, S. Dapprich, J. M. Millam, A. D. Daniels, K. N. Kudin, M. C. Strain, O. Farkas, J. Tomasi, V. Barone, M. Cossi, R. Cammi, B. Mennucci, C. Pomelli, C. Adamo, S. Clifford, J. Ochterski, G. A. Petersson, P. Y. Ayala, Q. Cui, K. Morokuma, D. K. Malick, A. D. Rabuck, K. Raghavachari, J. B. Foresman, J. Cioslowski, J. V. Ortiz, B. B. Stefanov, G. Liu, A. Liashenko, P. Piskorz, I. Komaromi, R. Gomperts, R. L. Martin, D. J. Fox, T. Keith, M. A. Al-Laham, C. Y. Peng, A. Nanayakkara, C. Gonzalez, M. Challacombe, P. M. W. Gill, B. G. Johnson, W. Chen, M. W. Wong, J. L. Andres, M. Head-Gordon, E. S. Replogle and J. A. Pople, *Gaussian 98*, Revision A9; Gaussian, Inc.: Pittsburgh, PA, 1998.
- [42] A. L. Sobolewski and W. Domcke, *Chem. Phys. Lett.* **315**, 293 (1999)
- [43] E. H. Strickland, J. Horwitz and C. Billups, *Biochemistry* **9**, 4914 (1970)
- [44] M. Martinaud and A. Kadiri, *Chem. Phys.* **28**, 473 (1978)
- [45] A. A. Rehms and P. R. Callis, *Chem. Phys. Lett.* **140**, 83 (1987)
- [46] P. Illich, C. Haydock and F. G. Prendergast, *Chem. Phys. Lett.* **158**, 129 (1989)
- [47] D. R. Demmer, G. W. Leach, E. A. Outhouse, J. W. Hager and S. C. Wallace, *J. Phys. Chem.* **94**, 582 (1990)

- [48] M. J. Tubergen and D. H. Levy, *J. Phys. Chem.* **95**, 2175 (1991)
- [49] S. A. Clough, Y. Beers, G. P. Klein and L. S. Rothman, *J. Chem. Phys.* **59**, 2254 (1973)
- [50] C.S. Ewig, M. Waldman and J.R. Maple, *J. Phys. Chem. A* **106**, 326 (2002); J.W. Ponder, *et al.*, in press

Appendix.

- [1] D. H. Levy, NATO Advanced Study Institutes Series, Series B: Physics B57 (Quantum Dyn. Mol.), 115-42. (1980)
- [2] R. S. Fellers, L. B. Braly, R. J. Saykally, and C. Leforestier, *J. Chem. Phys.* **110**, 6306 (1999)
- [3] J. B. Paul, R. A. Provencal, C. Chapo, A. Petterson, and R. J. Saykally, *J. Chem. Phys.* **109**, 10201 (1998)
- [4] J. G. Gregory and D. C. Clary, *J. Chem. Phys.* **105**, 6626 (1996)
- [5] C.-J. Tsai and K. D. Jordan, *Chem. Phys. Lett.* **213**, 181 (1993)
- [6] J. M. Hutson, A. Ernesti, M. M. Law, C. F. Roche, and R. J. Wheatley, *J. Chem. Phys.* **105**, 9130 (1996)
- [7] W. A. Majewski, J. F. Pfanstiel, D. F. Plusquellic and D. W. Pratt, in *Laser Techniques in Chemistry*, edited by Myers, A. B.; Rizzo, T. R.; Wiley: New York, Vol. **101**, 23 (1995).
- [8] S. Gerstenkorn, and P. Luc, *Atlas du spectroscopie d'absorption de la molecule d'iode*, CNRS: Paris, (1978 and 1982).
- [9] D. G. Lister, J. K. Tyler, J. H. Høg, and N. W. Larsen, *J. Mol. Struct.* **23**, 253 (1974)
- [10] R. Sussmann, R. Neuhauser, and H. J. Neusser, *Can. J. Phys.* **72**, 1179 (1994)

- [11] J. K. G. Watson, in *Vibrational Spectra and Structure*, edited by J. R. Durig (Elsevier, Amsterdam, 1977), Vol. 6, p. 1.
- [12] Described in D. F. Plusquellic, R. D. Suenram, B. Maté, J. O. Jensen, and A. C. Samuels, *J. Chem. Phys.* **115**, 3057 (2001)
- [13] J. Kraitchman, *Am. J. Phys.* **21**, 17 (1953).
- [14] B. B. Champagne, J. F. Pfanstiel, D. W. Pratt, and R. C. Ulsh, *J. Chem. Phys.* **102**, 6432 (1995)
- [15] M. J. Frisch, G. W. Trucks, H. B. Schlegel, G. E. Scuseria, M. A. Robb, J. R. Cheeseman, V. G. Zakrzewski, J. A. Montgomery, R. E. Stratmann, J. C. Burant, S. Dapprich, J. M. Millam, A. D. Daniels, K. N. Kudin, M. C. Strain, O. Farkas, J. Tomasi, V. Barone, M. Cossi, R. Cammi, B. Mennucci, C. Pomelli, C. Adamo, S. Clifford, J. Ochterski, G. A. Petersson, P. Y. Ayala, Q. Cui, K. Morokuma, D. K. Malick, A. D. Rabuck, K. Raghavachari, J. B. Foresman, J. Cioslowski, J. V. Ortiz, B. B. Stefanov, G. Liu, A. Liashenko, P. Piskorz, I. Komaromi, R. Gomperts, R. L. Martin, D. J. Fox, T. Keith, M. A. Al-Laham, C. Y. Peng, A. Nanayakkara, C. Gonzalez, M. Challacombe, P. M. W. Gill, B. G. Johnson, W. Chen, M. W. Wong, J. L. Andres, M. Head-Gordon, E. S. Replogle and J. A. Pople, *Gaussian 98, Revision A9; Gaussian, Inc.: Pittsburgh, PA*, (1998).
- [16] T. M. Korter, J. Küpper, and D. W. Pratt, *J. Chem. Phys.* **111**, 3946 (1999).
- [17] J. T. Hougen and J. K. G. Watson, *Can. J. Phys.* **43**, 298 (1965)
- [18] A. Held, B. B. Champagne, and D. W. Pratt, *J. Chem. Phys.* **95**, 8732 (1991)
- [19] D. F. Plusquellic and D. W. Pratt, *J. Chem. Phys.* **97**, 8970 (1992)
- [20] C. -H. Kang, J. T. Yi, and D. W. Pratt, *J. Chem. Phys.* in press

- [21] C. -H. Kang, T. M. Korter, and D. W. Pratt, *J. Chem. Phys.* in press
- [22] C. -H. Kang, J. T. Yi, and D. W. Pratt, in press
- [23] W. M. van Herpen, W. L. Meerts, H. E. Hunziker, M. S. de Vries, and H. R. Wendt, *Chem. Phys.* **163**, 209 (1992)
- [24] B. B. Champagne, D. F. Plusquellic, J. F. Pfanstiel, D. W. Pratt, W. M. van Herpen, and W. L. Meerts, *Chem. Phys.* **156**, 251 (1991)
- [25] G. Meijer, G. Berden, W. L. Meerts, H. E. Hunziker, M. S. de Vries, and H. R. Wendt, *Chem. Phys.* **163**, 209 (1992)
- [26] B. B. Champagne, D. F. Plusquellic, J. F. Pfanstiel, D. W. Pratt, and R. C. Ulsh, *J. Chem. Phys.* **102**, 6432 (1995)
- [27] W. E. Sinclair, and D. W. Pratt, *J. Chem. Phys.* **105**, 7942 (1996)
- [28] M. Becucci, G. Pietraperzia, N. M. Lakin, E. Castellucci, and Ph. Bréchnignac, *Chem. Phys. Lett.* **260**, 87 (1996)
- [29] N. M. Lakin, G. Pietraperzia, M. Becucci, E. Castellucci, M. Coreno, A. Giardini-Guidoni, and A. van der Avoird, *J. Chem. Phys.* **108**, 1836 (1998)
- [30] K. Remmers, R. G. Satink, G. van Helden, W. L. Meerts, H. E. Hunziker, M. S. de Vries, and H. R. Wendt, *Chem. Phys.* **163**, 209 (1992)
- [31] T. M. Korter, D. W. Pratt, *J. Phys. Chem. B* **105**, 4010 (2001)
- [32] I. Szydłowska, G. Myszkiewicz, and W. L. Meerts, *Chem. Phys.* **371**, 283 (2002)
- [33] D. R. Herschbach, *J. Chem. Phys.* **27**, 975 (1957)
- [34] W. Gordy, and R. L. Cook, *Microwave Molecular Spectra*, 3rd ed. (Wiley-Interscience, New York, 1984).
- [35] A. Lofthus, and P. H. Krupenie, *J. Phys. Chem. Ref. Data* **113**, 6 (1977)

- [36] S. Lee, J. Romascan, P. M. Felker, T. B. Pedersen, B. Fernández, and H. Koch, *J. Chem. Phys.* **118**, 1230 (2003)
- [37] M. Schaefer, C.-H. Kang, and D.W. Pratt, *J. Phys. Chem. A* **107**, 10753 (2003)
- [38] D. R. Herschbach, *J. Chem. Phys.* **31**, 91 (1959)
- [39] M. Schäfer, and D. W. Pratt, *J. Chem. Phys.* **115**, 11147 (2001)
- [40] T. M. Korter, D. R. Borst, C. J. Butler, and D. W. Pratt, *J. Am. Chem. Soc.* **123**, 96 (2001)
- [41] B. Brutschy, *Chem. Rev.* **100**, 3891 (2000)
- [42] Kim, K. S.; Tarakeshwar, P.; Lee, J. Y. *Chem. Rev.* **2000**, *100*, 4145.
- [43] M. Gerhards, M. Schmitt, K. Kleinermanns, and W. Stahl, *J. Chem. Phys.* **104**, 967 (1996)
- [44] G. Berden, W. L. Meerts, M. Schmitt, and K. Kleinermanns, *J. Chem. Phys.* **104**, 972 (1996)
- [45] S. Melandri, A. Maris, P. G. Favero, and W. Caminati, *Chem. Phys.* **283**, 185 (2002)
- [46] H.-D. Barth, K. Buchhold, S. Djafari, B. Reimann, U. Lommatzsch, and B. Brutschy, *Chem. Phys.* **239**, 49 (1998)
- [47] M. Becucci, G. Pietraperzia, M. Pasquini, G. Piani, A. Zoppi, R. Chelli, E. Castellucci, and W. Demtröder, *J. Chem. Phys.* **120**, 5601 (2004)
- [48] J. W. Ribblett, W. E. Sinclair, D. R. Borst, J. T. Yi, and D.W. Pratt, submitted.
- [49] U. Spoerel, and W. Stahl, *J. Mol. Spectrosc.* **190**, 278 (1998)
- [50] M. J. Tubergen, A. M. Andrews, and R. L. Kuczkowski, *J. Phys. Chem.* **97**, 7451 (1993)
- [51] T. M. Korter, D. W. Pratt, and J. Küpper, *J. Phys. Chem. A* **102**, 7211 (1998)
- [52] J. R. Carney, F. C. Hagemester, and T. S. Zwier, *J. Chem. Phys.* **108**, 3379 (1998)
- [53] A. J. Gotch, and T. S. Zwier, *J. Chem. Phys.* **96**, 3388 (1992)

- [54] S. Suzuki, P. G. Green, R. E. Bumgarner, S. Dasgupta, W. A., III Goddard, and G. A. Blake, *Science* **257**, 942 (1992)
- [55] H. S. Gutowsky, T. Emilsson, and E. Arunan, *J. Chem. Phys.*, **99**, 4883 (1993)
- [56] R. N. Pribble, A. W. Garrett, K. Haber, and T. S. Zwier, *J. Chem. Phys.* **103**, 531 (1995)
- [57] T. Emilsson, H. S. Gutowsky, G. de Oliveira, and C. E. Dykstra, *J. Chem. Phys.* **112**, 1287 (2000)
- [58] A. W. Garrett, and T. S. Zwier, *J. Chem. Phys.* **96**, 3402 (1992)
- [59] R. N. Pribble, and T. S. Zwier, *Faraday Discuss. Chem. Soc.* **97**, 229 (1994)
- [60] N. Solcà, and O. Dopfer, *Chem. Phys. Lett.* **347**, 59 (2001)
- [61] C.-H. Kang, D.W. Pratt, and M. Schäfer, *J. Phys. Chem. A* **109**, 767 (2005)
- [62] R. M. Helm, H. Vogel, H. J. Neusser, V. Storm, D. Consalvo, and H. Dreizler, *Z. Naturforsch. Teil A*, **52**, 655 (1997)
- [63] V. Storm, H. Dreizler, and D. Consalvo, *Chem. Phys.* **239**, 109 (1998)
- [64] S. Melandri, D. Consalvo, W. Caminati, and P. G. Favero, *J. Chem. Phys.* **111**, 3874 (1999)
- [65] M. Schäfer, D. R. Borst, D. W. Pratt, and K. Brendel, *Mol. Phys.* **100**, 3553 (2002)
- [66] X. Q. Tan, W. A. Majewski, D. F. Plusquellic, and D. W. Pratt, *J. Chem. Phys.* **94**, 7721 (1991)
- [67] A. Bauder, E. Mathier, R. Meyer, M. Ribeaud, and H. H. Günthard, *Mol. Phys.* **15**, 597 (1968)
- [68] M. Schäfer *J. Chem. Phys.* **115**, 11139 (2001)
- [69] F. C. DeLucia, P. Helminger, R. L. Cook, and W. Gordy, *Phys. Rev.* **A5**, 487 (1972)

[70] Actually, because of electron repulsion between the lone pairs of the fluorine and oxygen atoms, the water molecule does not freely rotate about the axis of the H---O-H hydrogen bond. The two hydroxyl hydrogens experience a simultaneous inversion in the course of its internal rotation motion.

[71] P. Tarakeshwar, K. S. Kim, and B. Brutschy, *J. Chem. Phys.* **110**, 8501 (1999)

[72] W. Caminati, S. Melandri, I. Rossi, and P. G. Favero, *J. Am. Chem. Soc.* **121**, 10098 (1999)

[73] D. R. Borst, T. M. Korter, and D. W. Pratt, *Chem. Phys. Lett.* **350**, 485 (2001)

[74] The -132 cm^{-1} complex exhibits a short Franck-Condon progression along at least one mode, with a frequency of 24 cm^{-1} . Presumably, this mode is related to the structural changes reported here. See: P. L. Muiño, P. R. Callis, *Chem. Phys. Lett.* **222**, 156 (1994)

[75] S. A. Clough, Y. Beers, G. P. Klein, and L. S. Rothman, *J. Chem. Phys.* **59**, 2254

(1973)

[76] K.C. Janda, L.S. Bernstein, J.M. Steed, S.E. Novick, and W. Klemperer,

J. Am. Chem. Soc. **100**, 8074 (1978)

[77] R.S. Altman, M.D. Marshall, W. Klemperer, and A. Krupnov, *J. Chem. Phys.* **79**, 52

(1983)

[78] R.S. Altman, M.D. Marshall and W. Klemperer, *J. Chem. Phys.* **77**, 4344 (1982)

[79] C. S. Ewig, M. Waldman and J. R. Maple, *J. Phys. Chem. A* **106**, 326 (2002);

J.W. Ponder, *et al.*, in press.